The Dynamic History of Kamb Ice Stream, West Antarctica: Controls on streaming behavior and ice stream shutdown

Ginny A. Catania

A dissertation submitted in partial fulfillment of
the requirements for the degree of

Doctor of Philosophy

University of Washington

2004

Program Authorized to Offer Degree: Earth & Space Sciences

University of Washington

Graduate School

This is to certify that I have examined this copy of a doctoral dissertation by

Ginny A. Catania

and have found that it is complete and satisfactory in all respects,
and that any and all revisions required by the final
examining committee have been made.

Chair of Supervisory Committee:

_____

Professor Charles F. Raymond

Reading Committee:

_____

Charles F. Raymond

_____

Howard Conway

_____

Kenneth Creager

Date: _____

University of Washington

Abstract

The Dynamic History of Kamb Ice Stream, West Antarctica: Controls on streaming behavior and ice stream shutdown

by Ginny A. Catania

Chair of Supervisory Committee:

Professor Charles F. Raymond
Department of Earth and Space Sciences

The present flow regime of Kamb Ice Stream (KIS) is unique amongst ice streams draining West Antarctica. Its trunk region has stagnated despite the fact that fast flowing tributaries continue to supply ice. This recent stagnation has contributed to changing the overall mass balance of the Ross Sea Sector. This pattern of short-term variability may be embodied in all ice streams, making calculations of short-term mass balance more complex.

The history of past motion is evident by complex features on the surface around KIS. These features have alignment, internal layer and bed characteristics indicating they are relict shear margins of KIS. Dating of these margins provides constraints on timing of changes in the speed and configuration of ice motion. Other features outside of the margins have internal structure different from margins. These are characterized by strongly down-warped syncline-shaped isochrones over deep diffractors. I show that the origin of these features involves some component of basal melt. No simple scenario explains all available observations but the emerging hypothesis is that a large portion of the lower part of KIS was once floating with bottom melting at the edge of the grounding zone. The period of melting was short (<300 years) and could have ended ∼350 years ago.

The ice flow history of KIS is re-examined in light of this hypothesis; the ice stream was once thin enough to float but regional changes in thickness caused localized grounding over time. Furthermore, the through-going subglacial drainage system was likely destroyed after grounding thus prohibiting the supply of water to the lower reaches of the ice stream from the melting tributaries. Continued grounding eventually led to ice stream shutdown, possibly due to basal freezing. The short-term variability and interconnectedness embodied by at least Kamb and Whillans Ice Streams may be characteristic of the entire ice stream system. The shutdown of KIS may represent one part of its cycle and may not signal the adjustment of the Siple Coast ice streams to the end of the last glacial maximum, ~14,000 years ago.

TABLE OF CONTENTS

LIST OF FIGURES

LIST OF TABLES

ACKNOWLEDGEMENTS

"Glaciers are delicate and individual things, like humans. Instability is built into them." -Will Harrison

Despite the fact that only one name appears on the front of this dissertation, I have a long list of people to thank for their time and support since I began this work. At the top of that list is Charlie Raymond who propelled me through the last five years with his inquisitive nature and endless enthusiasm for science. Charlie gave generously of his time and provided many opportunities for learning and research along the way. I also had the amazing fortune of spending many field seasons with Twit who eventually became, not only a good friend but an excellent role model for how field work is conducted. Twit's amiable personality and optimistic spirit made it easy to get things done and have fun at the same time. I'd like to thank him for always having his door open and a willing ear to listen to my crazy ideas. Special thanks to Kari Cooper for extending her support and advice to me during my last summer here and for convincing me that strong women have a place in academics. And to Ed Waddington who never chased me out of his office and could be consistently counted on for late night conversations. Thanks also to my committee members Darrel Cowan, David Kaplan and especially Ken Creager for reading and listening to my ideas.

I'd also like to thank the larger "WAIS" community for many stimulating discussions about the work I've presented over the last few years and for their camaraderie both in and out of the field. In particular, this includes my co-authors; Ted Scambos, Dale Winebrenner, Hermann Engelhardt, but also Tina Hulbe, Slawek Tulaczyk, Sridhar Anandakrishnan, Bob Jacobel, Brian Welch and Mark Fahnestock for the many thoughts on my work and enthusiasm that I continue in research.

Closer to home, the UW Glaciology Group, made up of students, faculty, post-docs and several visitors have provided me with many new research avenues as well as a friendly forum to eat lunch. Several students within the Glaciology Group provided invaluable support, both technical and emotional through the years. In particular I benefited greatly from following in the footsteps of Tony Gades and Nadine Nereson who taught me a lot about radar and left a great paper trail of Matlab code to follow. Also many, many thanks (and several beers) to Bob Hawley and Tom Neumann. Their camaraderie kept me in stitches

and continuing in graduate school ever since I first arrived. Thanks to Steve Price and Ben Smith who were always happy to discuss the specific modeling and radar parts of my work.

Crucial to this dissertation are the numerous field seasons that have been conducted in the Antarctic where logistical planning is difficult. RPSC continues to provide everything we have ever needed to have successful field seasons year after year. In particular I'd like to thank Leslie Blank, Karla College, Melissa Ryder, Bjorn Johns and Chuck Kurnik for making everything go so smoothly. Also, special thanks to Maurice Conway who was an inspiration for both his people skills, mechanical know-how and general attitude toward life.

I can't say that I would have gotten through the last five years without the warmth and affection of the many friends I've met here in Seattle and abroad. There seems to be a particular breed of person who thrives in Antarctica and I've been fortunate enough to become great friends with several of them. I'd like to thank Charlee, Andrea, Craige, Mel, Bruce, Jen, Phil, Beth, Burmie, Anna, Naked John, Sandwich and Keri for reminding me of the goofiness in life! And in Seattle, where I know I'll always leave a piece of my heart, thanks to Wendy, Pete, Claire, Michelle, Michele, Ben, Jenny, Kimiora, Jane, Alison, Ruth, Elizabeth, Ursula, Chris, Lisa, Sarah, Anya, Marc, Dara, Markus, Lora, Julia, and Ryan. And there's more: Andrea, Dyanna and Shul, some of my longest friends and diehard supporters.

And even though they probably thought they'd never see the day, I'd like to give great thanks to my two families. In Canada thanks to Jeff, Char, Jamie, Lori, Mom and Dad for your support ever since I came into the world. And in Seattle thanks to Kir, Pim and especially to Maude who brought us together. Namaste to those at Samadhi Yoga who rejuvenated me numerous times over the last year while frantically writing: Darlene, Steve, Veronica and especially Bret.

Finally, I'd like to thank David McPike for constantly reminding me of the joy in life and the value that I can add to the world.

This project was funded by the National Science Foundation through an Office of Polar Programs Grant: OPP-9909469, OPP-9615347 and OPP-9615420. Cover image provided by Ian Joughin (JPL).

Chapter 1

INTRODUCTION

1.1 Background

Concern about the collapse of the marine-based West Antarctic Ice Sheet (WAIS), which has the potential to raise sea level by roughly 6 m, has directed recent and ongoing research in the Siple Coast region (Figure 1.1). Fast flowing ice streams are of particular interest because they are the primary pathways for drainage of ice from the WAIS and so partially regulate its mass balance. Since the end of the last glacial maximum (LGM) ∼14,000 years ago the WAIS has shown significant retreat manifested in both grounding line recession (Conway and others, 1999) and mass loss (Bindschadler, 1998). While the ice streams likely respond to the influence of such long-term environmental changes, they also exhibit profound variability in discharge, flow direction and position over much shorter (century) time scales (Retzlaff and Bentley, 1993; Jacobel and others, 2000; Conway and others, 2002).

The mass balance for the Siple Coast area has recently shifted positive due to the stagnation of Kamb Ice Stream about 150 years ago and slowing of Whillans Ice Stream (Joughin and Tulaczyk, 2002; Retzlaff and Bentley, 1993). Such ice stream fluctuations make it difficult to determine how long the present positive mass balance can be maintained and as a result, an accurate measure of mass balance for the entire WAIS is inherently tied to our understanding of ice stream behavior and our ability to predict ice stream behavior into the future.

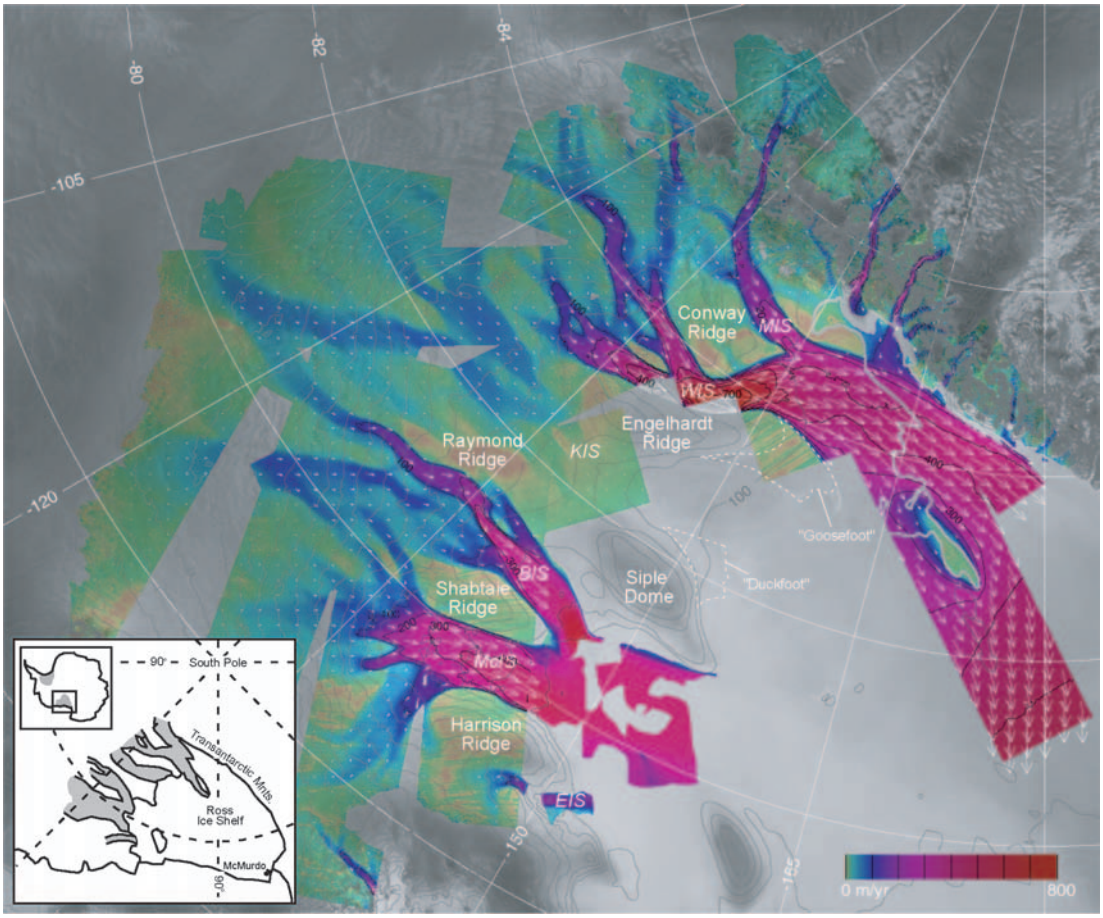

Figure 1.1: Present-day surface speeds of the Siple Coast ice streams overlying a RAMP SAR mosaic (Joughin and others, 2003); Mercer (MIS), Whillans (WIS), Kamb (KIS), Bindschadler (BIS), MacAyeal (McIS) and Echelmeyer (EIS). Velocity is indicated in color with 100 m a^{-1}contours in black. Velocity vectors are shown in white. The RAMP DEM is shown with 100 m contours (grey). Areas enclosed by the white dashed lines are the "Duckfoot" and "Goosefoot" flat-ice terrains. Inset shows Siple Coast ice streams and the Ross Sea Embayment, in context of West Antarctica.

1.2 Thesis Goals and Contributions

This thesis comprises two specific goals. The first is to examine the dynamic history of Kamb Ice Stream (KIS) using information recorded in the internal stratigraphy of the ice. It is important because profound changes are known to have occurred over the past millennia in this area, but the timing and type of events are largely unknown. Such information can provide insight into the mechanisms governing ice stream shutdown. The second goal is to contribute to understanding the controls on ice stream behavior and how these controls affect short-term variability in position and discharge. It is an essential step toward prediction of ice stream behavior through physically based modelling. Both goals are crucial for understanding the regional mass balance of the Siple Coast Sector of the WAIS.

1.2.1 History of ice flow prior to KIS shutdown

Kamb Ice Stream has been studied in detail because of its anomalous flow situation; the trunk region stagnated ∼150 years ago (Retzlaff and Bentley, 1993) but active tributaries continue to supply ice to the central portions of the ice stream, altering topography and driving stress there (Price and others, 2001). Satellite images of KIS show many curvilinear "scar" features aligned sub-parallel to the ice flow direction located in the terrains surrounding the lower end of the ice stream (called the "Duckfoot" and "Goosefoot" in Figure 1.1). Radio echo-sounding (RES) profiles across these features indicate that some of these "scars" are coincident with changes in layer stratigraphy that reveal the locations of several relict ice stream margins and thus ice stream configuration in the past (Jacobel and others, 2000). No accurate timing exists for the changes in margin position, but it is likely that margins in the trunk of KIS migrated inwards over large distances (∼20 km) prior to the stagnation of KIS (Nereson, 2000). Such unstable behavior in the downstream end of KIS may have contributed to the shutdown of the ice stream a few centuries later. Since the nature of the KIS shutdown is still under debate, information regarding the ice flow changes prior to shutdown of KIS can reveal important controls on streaming behavior.

1.2.2 Controls on Streaming Flow and Variability

Ice stream shear margins mark the location where horizontal surface velocities change by more than two orders of magnitude over a few kilometers causing chaotic crevasses (Echelmeyer and Harrison, 1999). Shear stress in the margins exceeds the basal shear stress due to the presence of a well lubricated, deforming bed (Kamb, 2001). As a result, the relatively narrow margins support as much (and often more) of the driving stress as the bed (Raymond and others, 2001). The positions of ice stream margins appear to be sensitively tied to the energy balance of the ice stream bed with fast margin migration possible through switching from a melting to a freezing basal environment (Jacobson and Raymond, 1998).

The shutdown of KIS has been examined with regard to these thermal processes. Since a small reduction in the water content of the underlying till through basal freezing can lead to significant strengthening (Tulaczyk and others, 2000b), the ice stream can slow as basal resistance increases at a rate faster than can be compensated for through increased driving stress. Such a process implies that ice streams are thermally regulated and may exhibit oscillatory flow behavior that includes quiescent periods as one stage of the entire ice stream life cycle. This suggests that the future behavior of the ice streams could be predicted with a greater understanding of these thermodynamic principles (Bougamont and others, 2003). This is an important step in improving predictability of ice sheet response to climate change.

1.3 Measurements and Analysis Techniques

This work makes use of ground-based ice-penetrating radar and GPS data that has been acquired over several field seasons in Antarctica involving a number of scientists. Tony Gades, Charlie Raymond (University of Washington) and Bob Jacobel (St. Olaf College) collected radar data across Siple Dome and the margin of Siple Ice Stream in 1994 and 1996. Data across Engelhardt Ridge and Shabtaie Ridge were collected by Nadine Nereson and Charlie Raymond in 1998/99. Data across Kamb Ice Stream and Roosevelt Island were collected by Tony Gades and Howard Conway in 1997/98. Data across the "scar" features

of KIS were acquired by myself with the help of Tony Gades, Howard Conway, Charlie Raymond and Ted Scambos (National Snow and Ice Data Center) in 2001/02. Significant re-design of the UW radar system was accomplished with the help of John Chin and Bob Hawley. Matlab scripts for processing radar data come from Tom Neumann, Bob Hawley, Ben Smith, Nadine Nereson and Tony Gades. The kinematic ice-flow model in Chapter 5 is adapted from a model developed by Ed Waddington and Tom Neumann. Satellite images used in this study were provided by both Ted Scambos and Ian Joughin (Jet Propulsion Laboratory).

1.4 Nomenclature

In 2003, several prominent features in the Siple Coast region were renamed. The nomenclature changed as follows: ice streams previously labelled A through F (from south to north) are now known as Mercer, Whillans, Kamb, Bindschadler, MacAyeal and Echelmeyer Ice Streams respectively. Names of inter-ice stream ridges, once based on the ice streams that surround them (e.g. Ridge BC is surrounded by Ice Streams B and C) are now Conway, Engelhardt, Siple Dome, Shabtaie, Raymond and Harrison Ridge respectively (Figure 1.1).

1.5 Synopsis

This thesis is composed of five stand-alone manuscripts. Because of this, some figures and descriptions of measurements are repeated. Chapter 2 has been published in its present form while Chapters 3 to 6 will be submitted for publication in the near future.

I have used ice-penetrating radar data to characterize the sub-glacial bed properties across ice stream margins (Chapter 2) and inter-ice stream ridges (Chapter 3) in order to understand how bed conditions limit/permit streaming flow. Both chapters follow from the work of Gades and others (2000) who examine the reflection amplitude of radar signals from the bed to elucidate spatial changes in bed properties across ice stream margins. Chapter 2 re-examines some of the data presented by Gades and others (2000) (as well as data from additional relict margins) in light of a radar profile calibrated to known bed conditions

obtained from borehole observations. In Chapter 3, I compile a set of radar profiles from several inter-ice stream ridges in West Antarctica to examine the consistency of bed and internal reflectivity across ridges. A new approach is used, which allows for comparison of data collected with different instruments and center frequencies.

Chapters 4 and 5 contain radar data analyses and geophysical models that are used to constrain a detailed ice flow history for the KIS area, presented in Chapter 6. In Chapter 4, I use radar-detected internal stratigraphy to classify several different surface features that are visible in satellite images. In particular, I describe a new dynamic terrain (flat-ice) that has not previously been defined. The results presented here challenge previous assumptions that these terrains were once part of the active ice stream. In Chapter 5, the internal layer characteristics of these terrains are examined in greater detail using an ice flow model that predicts the expected morphology of internal layers for a variety of boundary conditions. Modelled layers are compared to radar-detected layers in order to test several hypotheses concerning the origin of flat-ice terrains that bound the downstream end of KIS. Model results indicate that basal melting plays a key role in shaping the internal layers. An emerging hypothesis to describe the character of the melting, in conjunction with other internal layer features, is that these terrains represent relict ice shelf terrain and that floatation occurred in the mouth of KIS several hundred years ago. The ice flow history presented in Chapter 6 is derived from the previous chapters and from other published sources. This synthesis shows that short-term variability in the ice stream system is common and that the shutdown of KIS occurred subsequent to the grounding of a large portion of its trunk. The ongoing changes that occur in the KIS area are indicative of a system that is in constant flux due to changes in ice thickness and basal conditions, each affecting ice flow on different time scales.

Chapter 2

BED-REFLECTIVITY BENEATH INACTIVE ICE STREAMS IN WEST ANTARCTICA

This chapter was published under the same title in Annals of Glaciology 36, 287-291 with co-authors H. Conway, A. Gades, C. Raymond at the University of Washington and H. Engelhardt at California Institute of Technology. Helpful review comments were provided by D.G. Vaughan and L. Copeland.

2.1 Summary

Radio-echo sounding (RES) techniques are used to examine spatial changes in bed reflectivity across relict ice streams in West Antarctica. Measurements from adjacent inter-stream ridges are used to correct the measured power returned from the bed for attenuation and losses due to geometric spreading, scattering and absorption. RES measurements near boreholes drilled on Kamb Ice Stream (KIS) indicate high coefficients of bed reflectivity ($R > 0.1$) in locations where the bed was thawed and boreholes connected to the basal water system, and low reflectivity coefficients ($R < 0.02$) at locations that were frozen and not connected. Intermediate values of bed reflectivity were measured at locations where the connection to the basal water system was weak. Measurements across four relict margins show that bed reflectivity usually jumps from low to high values several kilometers inside the outermost buried crevasses. We interpret this to be a transition from frozen to thawed basal conditions and discuss implications of these observations.

2.2 Introduction

Horizontal surface velocities typically change by more than two orders of magnitude across the margins of active ice streams in West Antarctica, and chaotic surface crevasses

form where the shear strain rate exceeds $\sim 0.12\ a^{-1}$ (Echelmeyer and Harrison, 1999). Such changes at the surface require a switch from locked to lubricated conditions at the bed.

Theory suggests that the positions of ice stream margins are probably not stable if position is controlled only by a transition between frozen and thawed bed (Raymond and others, 2001). Jacobson and Raymond (1998) discussed processes that might affect the migration of ice stream margins. One (the so-called "edge-deficit" process) occurs because drag from the sides causes a decrease in basal slip, basal shear stress and production of frictional energy toward the margin, which would favor freezing and inward migration of the margin. In contrast, heat generated by side shearing within the ice column effectively reduces the basal heating necessary to maintain a thawed bed. This "edge-shield" process might promote basal melting outside the margin and allow an ice stream to expand sideways into the surrounding slow-moving ice.

Knowledge of the position of the thawed zone relative to the outermost chaotic crevasses provides insight into the relative importance of these two competing processes. Switches from frozen to thawed conditions at the bed should be detectable using RES, and the aim of this paper is to interpret RES measurements of bed reflection power across several relict ice stream margins in West Antarctica (Fig. 2.1). Our ground-based studies focus on inactive ice streams because crevasses have been buried by accumulation subsequent to stagnation, which simplifies the logistics of travel across the surface.

We use observations and measurements from boreholes that have been drilled to the bed of both active and inactive ice streams to help interpret the RES measurements. Boreholes within ice streams reveal thick (>1 m) layers of water-saturated, dilated till at the base of the ice (Engelhardt and others, 1990b; Engelhardt and Kamb, 1997; Kamb, 2001). In contrast, slow-moving inter-stream ridges are frozen at the bed; ridges with a history of streaming (e.g. the Unicorn between the two limbs of Whillans Ice Stream) have beds of frozen till while others with no prior history of streaming (e.g. Siple Dome) are frozen to bedrock (Kamb, 2001).

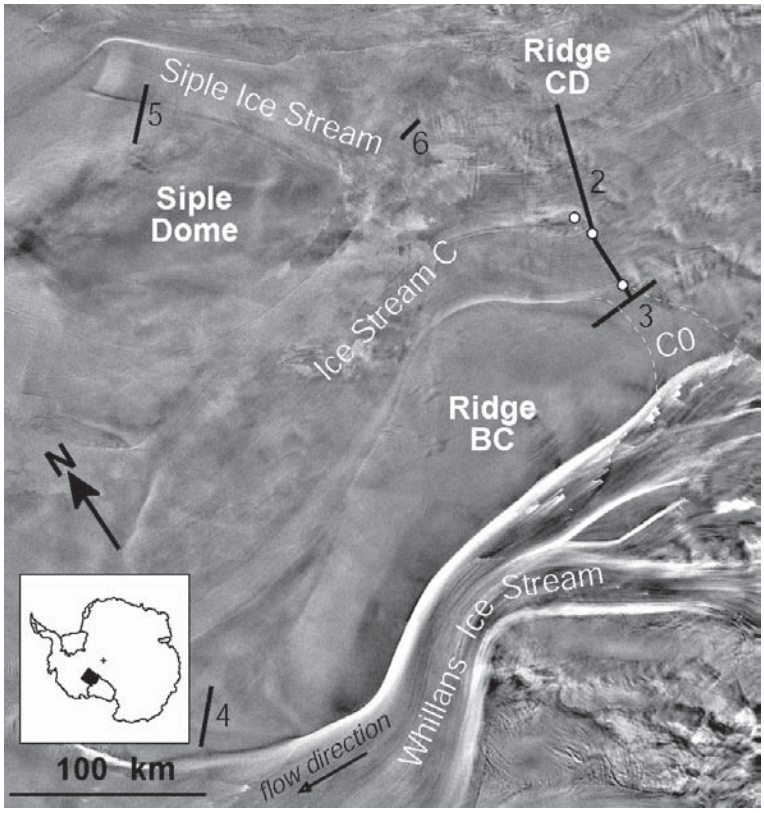

Figure 2.1: RADARSAT image of the Siple Coast Ice Streams in West Antarctica. Numbers next to each radar line (shown as black lines) correspond to the figure number that shows data from that line. Dashed white lines indicate the boundaries of Ice Stream C0. Boreholes discussed in the text are indic+ated as black circles with white fill. Image courtesy of T. Scambos.

2.3 Calculation of Bed Reflectivity

The power returned from a particular time window in a RES trace is defined following Gades (1998) and Gades and others (2000) to be one-half the sum-of-squared voltage amplitudes divided by the number of samples in the window. The measured power reflected from the bed (BRP) is calculated by centering a hand-selected time window around the reflected bed pulse. BRP is affected by the properties of the system (coupling to surface, antenna frequency), the overlying ice (thickness, temperature, chemistry, presence of crevasses and layer stratigraphy) as well as the properties of the bed (presence liquid water, water chemistry, type of bed material, bed slope and roughness).

We assume that the coupling between the radar system and the snow surface remains constant across the profiles. This is reasonable since there were no observed changes in snow properties across these areas. Furthermore, we calculate the internal power reflected from the ice column (IRP) within a time window that spans from 2 μs (just below the air wave) to 0.5 μs before the shallowest point on the bed. Since changes in BRP might arise from variations in the ice or instrument properties, variations in BRP must be examined in light of any changes in IRP over the same area (Gades and others, 2000).

Radar profiles were collected at frequencies of $\backsim$ 2 MHz and $\backsim$ 5 MHz and we expect both attenuation and bed reflectivity to be frequency dependent. To account for this we simply scale the 2 MHz data to match the 5 MHz data using the ratio of the mean bed reflection amplitudes at locations where data were collected at both frequencies.

To correct for the effects of changes in path length we derive an empirical relationship $F(H)$ between the measured BRP and ice thickness (H) using measurements from Ridge BC and Siple Dome. Ice thickness across the two ridges ranges from 600 to 1500 m, and the ice and bed reflection properties are relatively constant, as indicated by the goodness of the fit to F(H) (Gades and others, 2000; Winebrenner and others, 2003). BRP at a particular location and frequency is then normalized to yield a depth-corrected relative bed reflectivity BRP_R = BRP/F(H) (Gades and others, 2000). For ease of comparison to BRP_R, IRP is

normalized to the mean IRP to calculate IRP_N = IPR/<IRP>.

RES techniques have been used by others to infer basal conditions beneath glaciers and ice sheets (Bentley and others, 1998; Gades and others, 2000; Copeland and Sharp, 2001). Here we examine RES measurements near boreholes that have been drilled to the bed of Kamb Ice Stream and interpret changes in bed reflectivity in context of measurements and observations from the boreholes. We then use these relationships to infer basal conditions from RES profiles across other relict margins where borehole data are not available.

2.4 Measurements

2.4.1 Kamb Ice Stream

The lower reaches of Kamb Ice Stream (KIS) (Fig. 2.1) stopped streaming $\backsim$ 150 years ago (Retzlaff and Bentley, 1993), while a tributary to the ice stream (ISC0) slowed $\backsim$ 250 years ago (Conway and others, 2002). Fig. 2.2 a shows a radar profile across KIS that starts in the region of ISC0 (0 km), crosses a bedrock ridge (between km 35 and km 50) and ends on Ridge CD (km 97). Many boreholes were drilled during the 1996/97 and 2000/01 seasons, however only a few of these are located exactly along the RES profile across KIS (96-12 and 96-01 are two of these) (Kamb, 2001).

All of the boreholes drilled within the relict ice stream (within 10km of borehole 96-01 at km 30) connected to a sub-glacial drainage system (Kamb, 2001). A video camera lowered down one hole in the area revealed a large (1.4 m) water-filled cavity at the base of the ice with water pressure near the overburden pressure (unpublished data, H. Engelhardt, 2001). Thinner water cavities ($\backsim$ 0.05 m) were observed at the bottom of several other boreholes in the vicinity. Ice frozen on to the base of the ice column has been detected in several (but not all) boreholes (Kamb, 2001). This freeze-on ice, which ranges from $\backsim$ 12 to 25 m thick, consists of stratified dirty and clean ice layers. Measurements indicate that the BRP_R in this region is very high ($\backsim$ 20 to 30) and variable (Fig. 2.2b); it is likely that both the freeze-on ice and variations in the subglacial water content contribute to cause variability

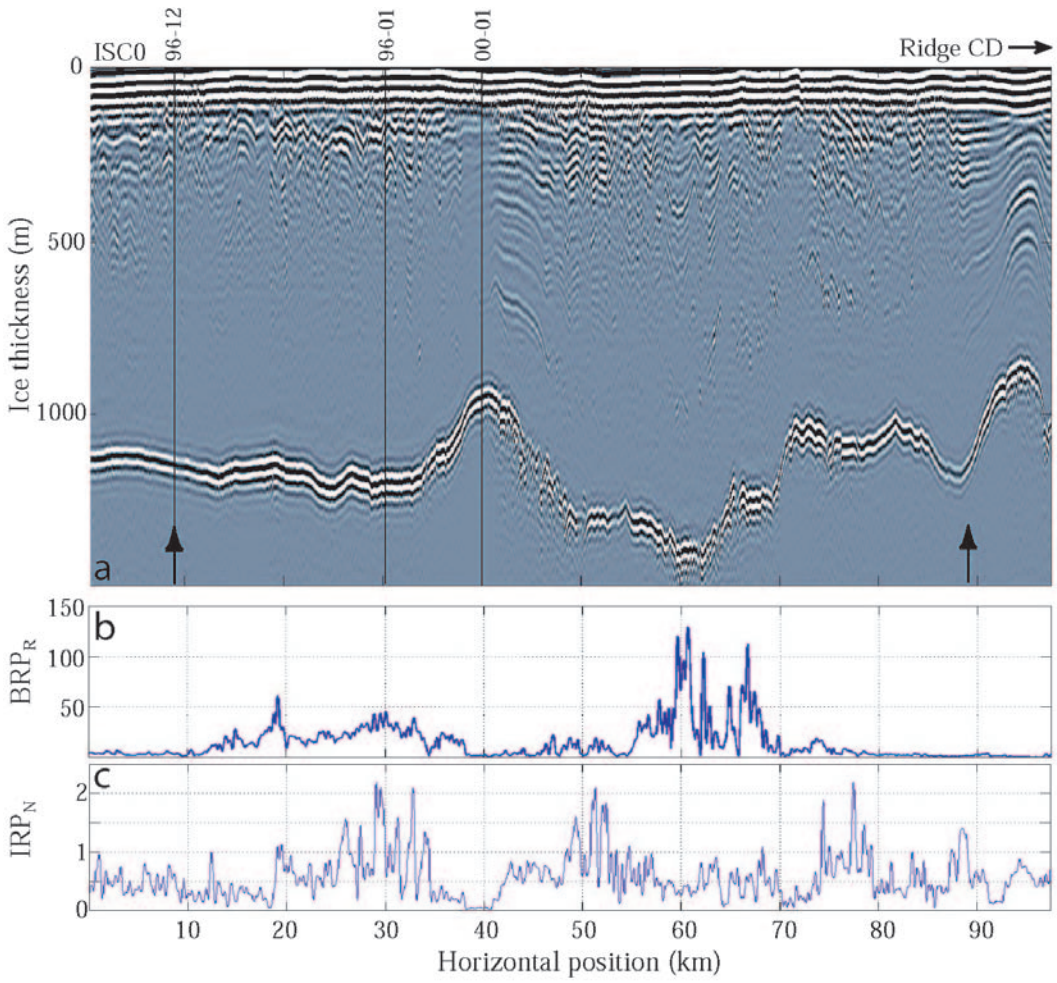

Figure 2.2: (a) 2 MHz RES profile across Kamb Ice Stream starting at 82.76^{o}S, 135.77^{o}W and ending at 81.83^{o}S, 136.00^{o}W. Ridge CD is located at km 90 and the relict tributary ISC0 is to the south (near km 0). Outer limits of buried near-surface crevasses are indicated by black arrows on Figures 2-6. (b) BRP$_R$ (c) IRP$_N$

in the values of BRP_R across the ice stream.

The bedrock bump that rises $\backsim$ 270 m above the surrounding bed (Fig. 2.2a) is part of a ridge that extends $\backsim$ 50 km downstream. Borehole 00-01, drilled through the center of the ridge revealed a frozen bed (unpublished data, H. Engelhardt, 2001). This is consistent with measurements of BRP_R that yield relatively low values (< 2.0) across the ridge (Fig. 2.2b).

Borehole 96-12 (near km 9 in Fig. 2.2a) was drilled outside the most recent margin of KIS but within ISC0. Connection to the subglacial drainage system at this borehole was weak (Kamb, 2001). Values of BRP_R calculated in this region ($\backsim$ 6.0 -see Fig. 2.3) are intermediate between regions that are thought to be totally frozen and those that are thawed.

Fig. 2.3 shows a radar profile across ISC0 that starts and ends in undisturbed ridge ice. The outer limits of buried surface crevasses, detected by high frequency (100 MHz) radar, are at km 4.9 and km 27. BRP_R across this inactive tributary are generally much lower than those across KIS (discussed above) although intermediate values ($\backsim$ 6.0) in the deepest section of the bedrock trough located near the eastern margin of the ice stream (Fig. 2.3b) suggest that the bed there is still partly thawed.

2.4.2 Whillans Ice Stream

Whillans Ice Stream (WIS - formerly known as Ice Stream B) is still actively streaming, but radar profiles (Fig. 2.4) across visible scar features near the present grounding line on Ridge BC (Fig. 2.1) show that the active margin has migrated inward in recent times. Buried crevasses detected by high frequency (100 MHz) radar indicate at least two distinct paleo-margins: one at km 4.8 where the tops of crevasses are buried $\backsim$70 m below the surface, and another at km 17, where crevasses are $\backsim$ 30 m below the surface. The more recent margin (at km 17) was probably abandoned at about the same time as KIS stagnated ($\backsim$ 150 years ago), while the older margin must be more than 600 years old (assuming typical accumulation rates for the area). It is possible that the ice stream was even wider in the

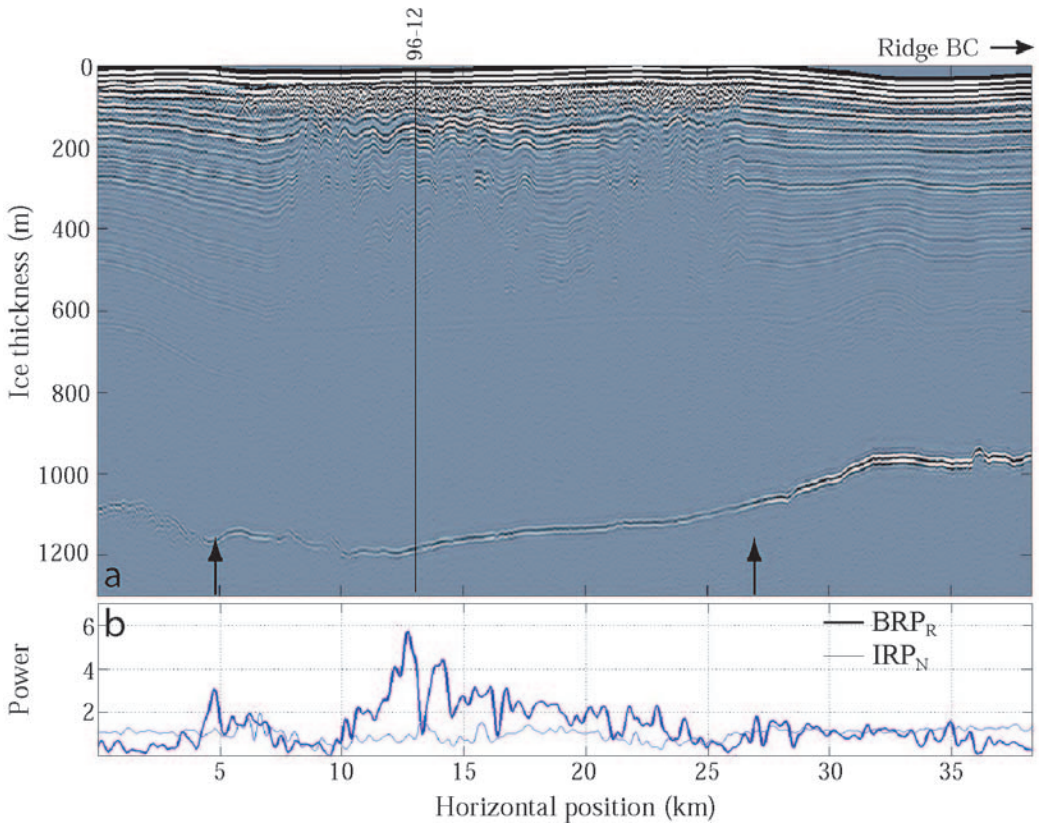

Figure 2.3: (a) 5 MHz RES profile across KIS tributary C0, which used to stream across Ridge BC into KIS. This profile starts at 82.79^{o}S, 136.84^{o}W and ends at 82.68^{o}S, 134.33^{o}W. Ridge BC is on the right. (b) IRP$_N$ (thin line) and BRP$_R$ (thick line) across the profile.

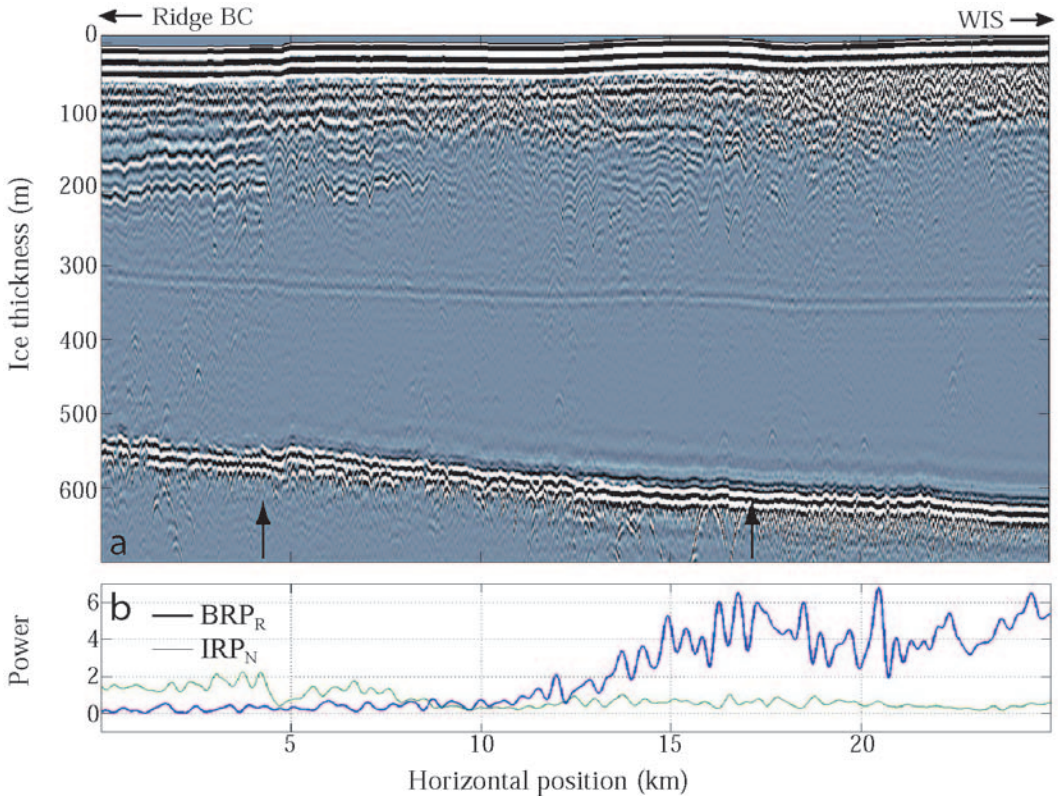

Figure 2.4: (a) 5 MHz RES profile across two relict margins of Whillans Ice Stream starting at 83.47^{o}S, 155.21^{o}W and ending at 83.65^{o}S, 156.94^{o}W. The active northern margin of WIS is farther east (at $\sim$ km 40). Note the prominent return about $\backsim$ 300 m below the surface is a glitch in the radar system. (b) IRP$_N$ (thin line) and BRP$_R$ (thick line) across the profile.

more distant past because the internal layers in the flat ice region outside of the former margins also show evidence of disturbance (Fig. 2.4).

Measurements indicate that the BRP_R remains relatively low until km 13, which is about 8 km within the oldest paleo-margin (defined by the outer buried crevasses at km 4.8). BRP_R increases to $\backsim$ 5.0 but remains variable. Variability may be a result of bed roughness as evidenced by the point diffractors visible at the bed (Fig. 2.4). Using the observations and measurements from KIS as a guide to interpret values of BRP_R, we infer a frozen bed between km 0 and km 11, and an intermediate condition (similar to those at BH 96-12 where the connection to the bed was weak) between km 11 to km 25.

2.4.3 Siple Ice Stream

Siple Ice Stream(SIS) slowed about 450 years ago (Smith, 2000); Figs. 2.5 and 2.6 show radar profiles across the western and eastern margins of the former ice stream. Fig. 2.5 shows an abrupt increase in BRP_R (to $\backsim$ 6.0) across the western margin about 4 km into the ice stream (beyond the outer limit of chaotic crevasses); again we interpret this to indicate a transition from frozen to partly frozen conditions at the bed. The transition is not so obvious across the eastern margin (Fig. 2.6) where, although the BRP_R does increase about 4 km into the ice stream, the maximum value is only $\backsim$ 2.0, suggesting that the bed here is probably more frozen.

2.5 Discussion

Tulaczyk and others (2000a,b) believe that KIS stagnated when the basal energy gradient switched from a melting to freezing environment because even small amounts of freezing can reduce the till porosity and this can have a large impact on its strength. Hence an ice stream might slow long before its bed is completely frozen, and liquid water remaining at the bed would keep it highly reflective. With on-going freezing, the spatial extent of the basal water is expected to decrease and high bed reflectivity might occur only in regions where water has ponded, such as beneath deep sections of an ice stream (as observed near

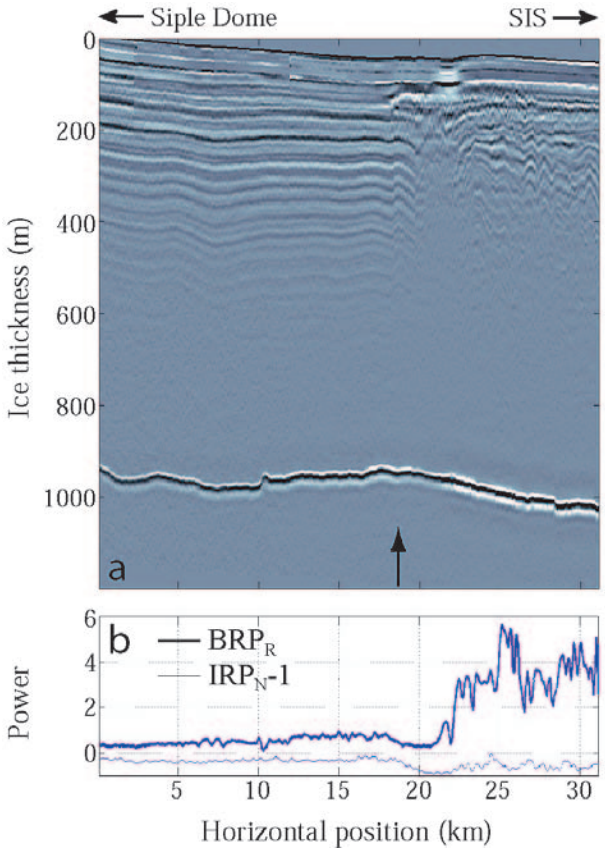

Figure 2.5: (a) 2 MHz RES profile across the western margin of Siple Ice Stream from 81.29^{o}S, 148.09^{o}W and ending at 81.08^{o}S, 147.01^{o}W. The flank of Siple Dome is to the left. (b) IRP$_N$ (thin line) and BRP$_R$ (thick line) across the profile; note that IRP$_N$ has been shifted down by 1 for display purposes in Figures 2.6 and 2.5. These data were also previously examined by Gades and others (2000)

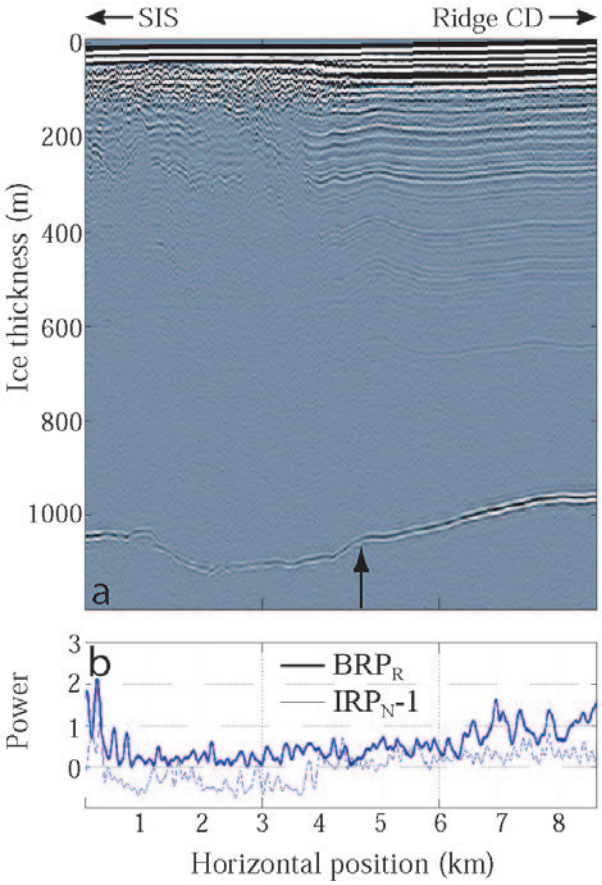

Figure 2.6: (a) 5 MHz RES profile across the eastern margin of Siple Ice Stream starting at 81.70^{o}S, 140.12^{o}W and ending at 81.75^{o}S, 140.84^{o}W. Ridge CD is on the right. (b) IRP$_N$ (thin line) and BRP$_R$ (thick line) across the profile.

km 65 in Fig. 2.2).

RES profiles, together with measurements and observations from boreholes on KIS, strongly support the notion that much of the measured increase in BRP_R beneath the inactive ice streams is caused by the presence of sub-glacial water systems with various degrees of connectivity. We interpret regions of low bed reflectivity ($\mathrm{BRP}_R < 2.0$) to be frozen at the bed, and high reflectivity ($\mathrm{BRP}_R > 6.0$) to be distinctly wet. Intermediate values of bed reflectivity indicate basal conditions that lie between these two regimes.

Measurements by Echelmeyer and others (1994) and Echelmeyer and Harrison (1999) across an active margin of WIS show surface velocities increasing from near zero to more than 10^2 m a^{-1} within a few kilometers. The outer edge of chaotic crevassing corresponds to the position where transverse velocity gradients reach values of $\backsim 0.12\ \mathrm{a}^{-1}$. This location is about 1 km from where the velocity first starts to increase. The structure of the velocity profile across a margin depends both on the spatial distribution of basal shear stress and the stiffness of the overlying ice column, but model results suggest that basal slip resistance likely changes within a few kilometers of the outermost chaotic crevasses (Raymond, 1996; Echelmeyer and others, 1994). If their results are typical for active margins, we expect to observe a jump in BRP_R within about 2 km of the outer edge of the chaotic crevasses.

The jump in bed reflectivity from low values ($\mathrm{BRP}_R \leqslant 1$) beneath ridges to high values ($\mathrm{BRP}_R > 2$) beneath the relict ice streams presumably delineates the transition from frozen to thawed conditions at the bed. In most cases studied here (the profile across the eastern margin of ISC0 is an exception) the thawed/frozen transition occurred 4-10 kilometers *inside* the outer edge of chaotic crevasses.

It is possible that the frozen/thawed boundary has migrated inward subsequent to the shut-down of the ice streams studied here. It is also possible that the margins migrated inward prior to shut-down thus contributing to the slowing, and eventual stoppage of the ice stream. Freezing at a margin is expected if the frictional energy produced by sliding is not sufficient to maintain thawed conditions at the bed (Jacobson and Raymond, 1998). For conditions typical of West Antarctica, energy production reaches a critical value when

an ice stream slows to $\sim 10^2$ m a^{-1} (sooner if cold ice is advected across the margin into the ice stream).

It is not clear why the BRP_R beneath the trunk region of KIS is so bright (up to two orders of magnitude higher than the ridges in the deep trough near km 60 in Fig. 2.2). The power reflection coefficient R from a perfect reflector is 1.0, although physically we expect a maximum value of $R = 0.8$ (Gades, 1998). Assuming that values of BRP_R beneath KIS are a maximum, at Siple Dome (with BRP_R roughly 0.01 of KIS) R must be less than 0.008, which is about 0.1 that estimated by Gades and others (2000).

It is possible that such low BRP_R values are a result of over-estimating the attenuation and losses associated with the travel path. However measurements from airborne RES also indicate high bed reflectivity beneath KIS - in fact values are significantly higher than beneath WIS (Bentley and others, 1998), which is still actively streaming. Another possibility is that the overlying ice column is relatively transparent to radar waves, although calculations of IRP_N across the ice stream (Fig. 2.2c) do not exhibit anomalous values. A third possibility is that the water beneath KIS is either much more conductive and/or thicker than that beneath WIS. The conductivity of basal water beneath WIS ($\sim$ 0.025 Sm^{-1} Engelhardt and others (1990a)) would yield values of $R \sim 0.1$ to 0.2 for physically reasonable values of water thickness (Gades, 1998). Water of higher conductivity such as that for sea water ($\sim$ 3-4 Sm^{-1}) would be necessary to yield $R \sim 0.8$. It is possible that the conductivity of water beneath KIS is very high because the solutes are not being flushed out by a through-flowing basal water system.

The inferred presence of liquid water across more than 75% of the bed of KIS raises the possibility that the ice stream system is metastable. The time scale for freezing all of the water at the bed might be such that an inactive ice stream can exist for hundreds of years in a sub-critical state, during which relatively small perturbations in driving stress or lubrication could reactivate fast flow.

Chapter 3

RADAR REFLECTIVITY BENEATH ICE STREAM RIDGES

3.1 Summary

Inter-ice stream ridges are features that appear to have long-term resistance to fast flow. Radar and borehole investigations on Siple Dome, an inter-ice stream ridge between Kamb and Bindschadler Ice Streams, indicate that this ridge is frozen to bedrock. Radar measurements from several inter-ice stream ridges are corrected for instrumentation and operational differences and compared to the coherent and homogenous bed and ice reflectivity measurements of Siple Dome. Results show that most ridges have reflectivity similar to that of Siple Dome. Some differences include Roosevelt Island where ice reflectivity is more variable and possibly larger, Shabtaie Ridge where bed reflectivity is more variable, and Engelhardt Ridge where reflectivity of the internal layers may be brighter and the bed dimmer than other ridges.

3.2 Radar Derived Bed Conditions

Radio-echo sounding (RES) of ice sheets is often used to measure ice thickness, internal layer geometry and bed topography derived from the arrival times of radar echoes. In addition, the amplitude of the bed reflection is sensitive to basal water, because of the large dielectric contrast between water and most geologic materials. This makes RES well-suited for profiling and mapping bed conditions (e.g. Bentley and others, 1998; Gades and others, 2000; Catania and others, 2003). In general, these studies demonstrate that ice stream beds have high and spatially variable bed reflectivity (interpreted as wet till and larger basal roughness) and ridges have low and spatially homogenous bed reflectivity (interpreted as frozen till or bedrock).

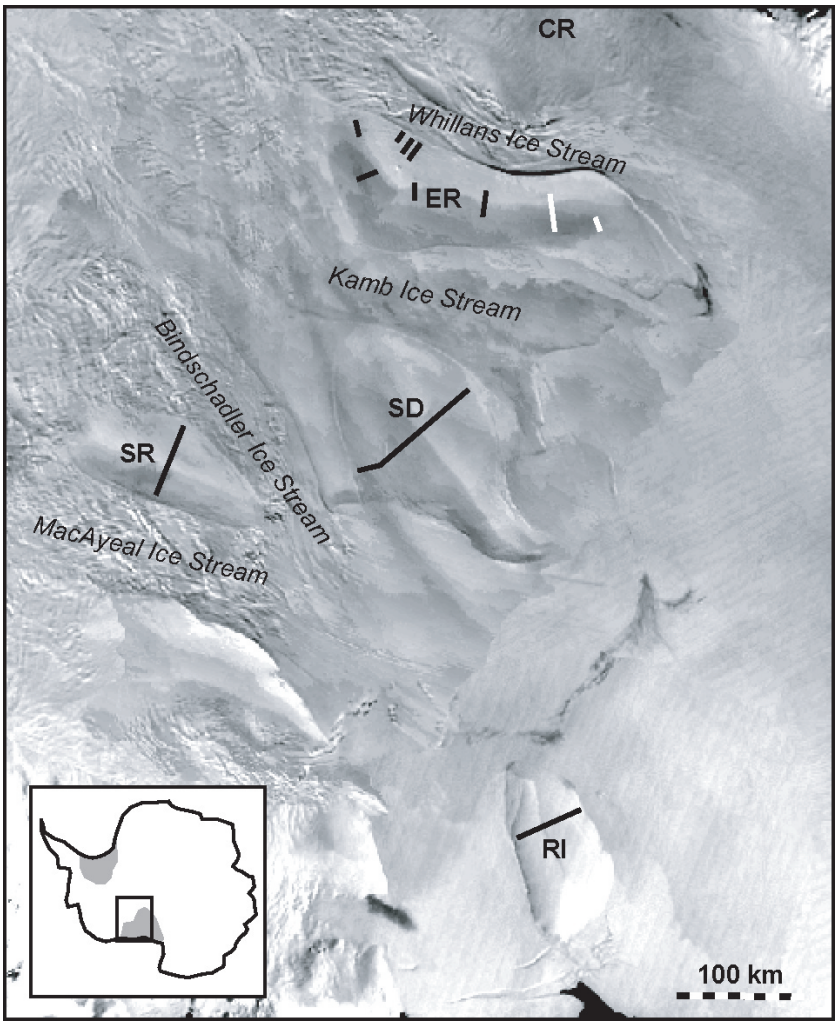

Figure 3.1: AVHRR image of Siple Coast ice streams and ridges; Roosevelt Island (RI), Siple Dome (SD), Shabtaie Ridge (SR), Engelhardt Ridge (ER) and Conway Ridge (CR). Heavy black lines are the locations of ice-penetrating radar profiles. Downstream Engelhardt Ridge data (described in text) are shown as white lines. Inset shows the Siple Coast in context with Antarctica.

Here we examine the nature of bed reflectivity beneath several inter-ice stream ridges in the Siple Coast region (Figure 3.1). With the exception of Conway Ridge, internal layers within ridges are often undisturbed to great depths suggesting that the ridges have not been overrun by streaming flow for at least the last 10^4 years (Nereson and others, 2000). This is likely because their frozen beds rise 200-400 m above that of the intervening ice streams effectively guiding the flow of ice. Boreholes drilled to the bed of Siple Dome, a ridge between Kamb and Bindschadler Ice Streams (Figure 3.1), reveal that the ice here is frozen to solid bedrock with little or no overlying till (Kamb, 2001). Because of this, the bed reflectivity of Siple Dome is low (Gades and others, 2000). Bed reflectivity here is also spatially invariant (Winebrenner and others, 2003; Gades and others, 2000) which makes it particularly useful for comparison with other ridges.

3.3 Reflectivity Measurements

A low-frequency (2-7 MHz) monopulse ice-penetrating radar system, designed and built at the University of Washington, has been used to collect bed and internal layer echoes across several inter-ice stream ridges in West Antarctica; Engelhardt Ridge, Siple Dome, Shabtaie Ridge and Roosevelt Island (Figure 3.1). The radar system consists of a transmitter and receiver mounted on separate sleds and pulled in-line by a snowmobile (Figure 3.2). The receiver consists of a dipole antenna (resistively-loaded to prevent ringing), a signal amplifier, a digital oscilloscope and a computer where stacked waveforms are downloaded and stored. The transmitter delivers a single voltage step to its antenna which is radiated in broad-band with a center frequency determined by the length of the antenna.

In this paper we compile several sets of radar data collected over a 10 year period during which the radar system has been modified to improve performance and data resolution. Such changes might alter the bed reflection amplitude. Two different transmitters have been used to collect the data presented here, but both transmitters output a stable ± 2 kV voltage step with a 15 ns rise time. Several other factors can alter the reflection amplitude. Known factors include; antenna center frequency, attenuation through the ice column, oscilloscope

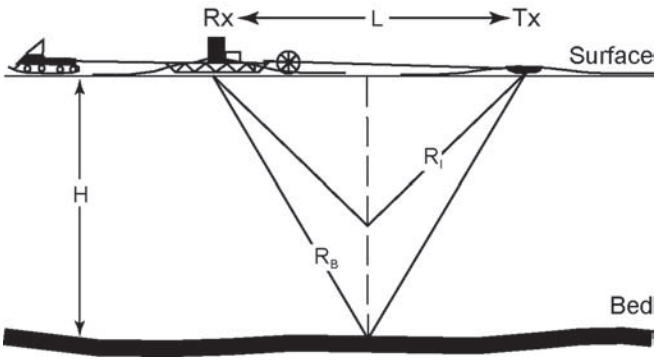

Figure 3.2: RES field setup and sounding geometry. Ice thickness is H, the distance between the receiver (Rx) and transmitter (Tx) is L, and the range to the bed and internal layers from either the transmitter or receiver is R_B and R_I respectively.

settings, antenna spacing, and post-collection filtering (Table 3.1). Unknown factors that might affect reflectivity can come from changes in the signal amplification used in the field, and coupling to the snow surface which are not necessarily consistent between data sets. Multiple radar profiles were collected on Siple Dome and Engelhardt Ridge using different instrumentation set-ups and antenna frequencies. Two repeated data sets were collected at Siple Dome separated by a period of roughly 6 years and using different instrumentation (SD-94 and SD-00). Because of regional differences in reflectivity, the data from Engelhardt Ridge are grouped into "upstream" and "downstream" ridge data (Figure 3.1). Each group contains data collected with multiple frequencies but otherwise similar instrumentation.

The data sets are bandpass filtered and the amplitude of the bed reflection is obtained with an automated bed-picking routine developed by Gades (1998). The returned power within a time window $t_1 - t_2$ is calculated following Gades and others (2000)

$$P_r^* = \frac{1}{2(Nt_2 - Nt_1 + 1)} \sum_{i=Nt_1}^{Nt_2} \left(Y_{inc}\Omega_i\right)^2 . \tag{3.1}$$

where Ω_i is the reflection amplitude, $(Nt_2 - Nt_1 + 1)$ is the number of samples in the time window and Y_{inc} (in units of Volts per bit) is an oscilloscope setting that changes the scale of the recorded waveform and is set to avoid clipping the bed reflection (Table 3.1). To calculate the bed reflection power BRP, Equation 3.1 is used with a time window $(t_2 - t_1)$ that is twice the time interval between the maximum and minimum values in the amplitude and is centered on the reflected pulse. The returned power from the ice column (IRP) is calculated in a similar manner but with a time window (t_1=2 μs to t_2=5.24 μs) that begins just below the air-wave and ends just before the shortest bed travel-time found in Table 3.1. In this way IRP is an estimate of the integrated power returned from the packet of internal layers that lie within a constant ice thickness for each ridge.

Table 3.1: Properties of radar data sets; location (Engelhardt Ridge - upstream end (ER-Up), Engelhardt Ridge - downstream end (ER-Dn), Siple Dome (SD), Shabtaie Ridge (SR) and Roosevelt Island (RI)), antenna center frequency (MHz), waveform amplification, antenna spacing (m), minimum travel-time to the bed (μs) , maximum travel-time to the bed (μs), corner frequencies (MHz) used in bandpass filtering.

Data set	f	Y_{inc}	L	tt_{min}	tt_{max}	corner f	
ER-Dn-1	2	2	103	6.98	7.36	2	10
ER-Dn-2	7	1	85	6.26	9.00	4	9
ER-Up-1	5	1	85	10.16	15.50	4	9
ER-Up-2	2	2	103	11.92	12.56	2	10
ER-Up-3	2	5	118	9.37	10.9	2	10
SD-96	2	1	100	7.46	11.56	1	10
SD-00	5	2	85	7.2	8.48	4	9
SR	2	5	118	8.8	12.25	2	10
RI	7	2	66	5.74	8.19	4	9

Correcting for frequency differences

Our observations indicate that there is a frequency dependence to the power received, P_r; lower frequency antennas have longer wavelengths and less propagation loss in the firn column. Coupling of the antennas to the snow surface is also important and we make the assumption that coupling is constant between all data sets. Differences in antenna frequency between data sets are corrected using a modified version of the radar equation from Winebrenner and others (2003) in which the effective area A of the transmitting and receiving antennas is independent of the antenna wavelength λ. This equation neglects the effects of refraction and focussing in the firn:

$$P_r = \frac{AP_t}{\lambda^2}\frac{1}{(2R)^2}\mathcal{R}\exp(-2\kappa_H R) \tag{3.2}$$

where P_t is the transmitted power, $\mathcal{R}$ is the reflectivity of the bed or internal layers, κ_H is the depth-averaged attenuation, H is the ice thickness, and R is the range to the bed (R_B) or internal layer packet (R_I) from either the transmitter to the receiver or vice versa. For BRP, $R = \sqrt{\frac{L^2}{4} + H^2}$ and for IRP $R = \sqrt{\frac{L^2}{4} + h^2}$ where h is the average distance over the depth-converted time window that defines the IRP calculation. Increasing the separation distance between transmitter and receiver (L) has the effect of lessening the returned reflection amplitude however, since L is typically much smaller than H and h, changes in L by up to $\sim$30% (observed for 7 MHz data) produce only a 0.1% change in R. For this reason we consider a constant L, and thus R for all data sets.

The reflectivity for any given travel time in each data set is scaled to match the expected "2 MHz" reflectivity at that travel time by assuming $P_t, \mathcal{R}, A, \kappa_H$, and R in Equation 3.2 are independent of frequency and then taking the ratio between the measured power received and the (2 MHz) expected power received:

$$P_{r2\mathrm{MHz}} = P_{r\mathrm{f}}\frac{\lambda_{2\mathrm{MHz}}^2}{\lambda_f^2} \tag{3.3}$$

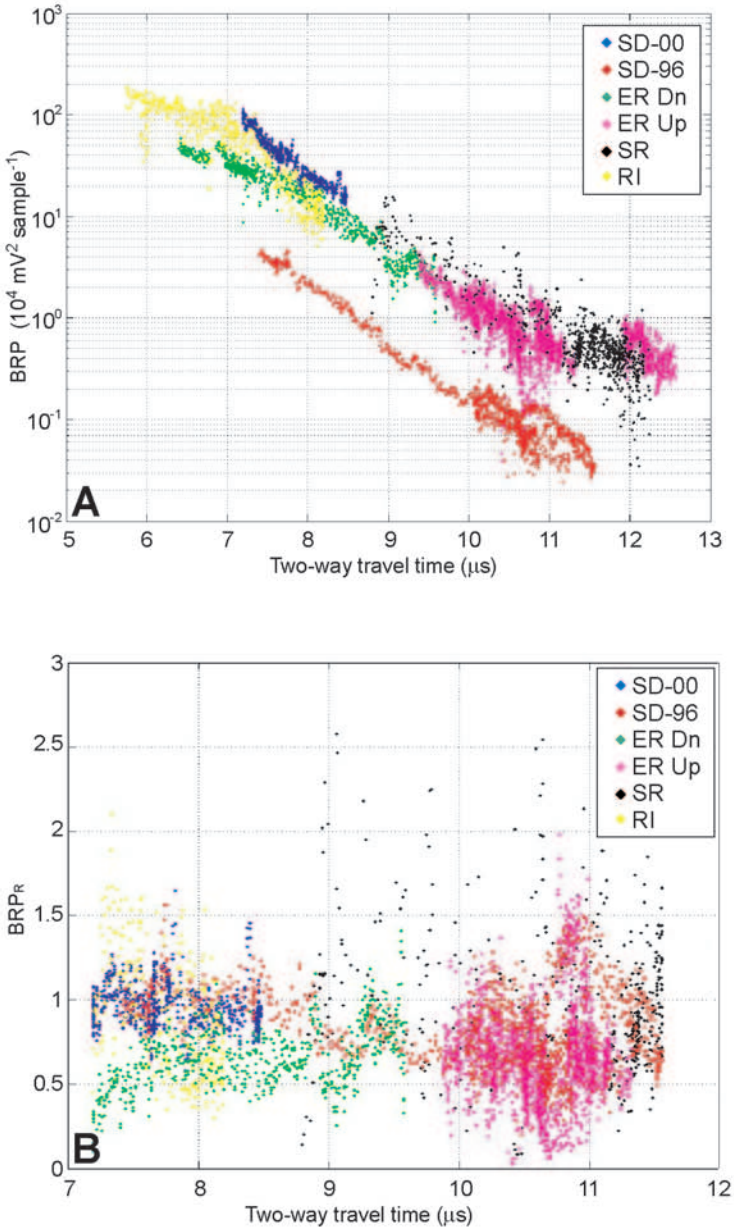

Figure 3.3: BRP versus two-way travel time for all available inter-ice stream ridge profiles. Different colors indicate data set group; Siple Dome (SD); Shabtaie Ridge (SR); downstream Engelhardt Ridge (ER Dn); upstream Engelhardt Ridge (ER Up) and; Roosevelt Island (RI). Multiple data sets in one general location are plotted as one color. A. BRP corrected for frequency differences. B. BRP corrected for frequency and attenuation.

where $\lambda = \frac{v_i}{f}$, v_i is the speed of radio-wave propagation in ice (168 m μs^{-1}) and f is either 5 MHz or 7 MHz, the other antenna frequencies used. Equation 3.3 gives a scaling factor of 6.3 for 5 MHz data and 12.3 for 7 MHz data. Both BRP and IRP are corrected for frequency differences in this way and are plotted against travel time (Figure 3.3A and Figure 3.4).

We can compare our results to an empirical correction for frequency differences made by Gades and others (2000) who measured the difference in mean bed reflection amplitude from repeated radar profiles collected with different frequency antennas. Their results from Siple Dome (using similar instrumentation as discussed here) indicate that 3 MHz data produced a mean bed reflection amplitude that was 1.76 times that of 4 MHz data. To compare their results with our theoretical approach we take the square of 1.76 (to reflect the power received) as in Equation 3.1 to get a scaling factor of 3. In comparison, Equation 3.3 gives a scaling factor of 1.8 for comparing 3 and 4 MHz antennas. While this is a reasonable match a better one might be obtained by lifting our stated assumptions and further examining the frequency dependence on A and κ_H. Little is known about these relationships but reasonable estimates of their dependence on frequency could be made using a similar empirical approach as Gades and others (2000).

One way to overcome frequency differences between data sets is to take the ratio of BRP to IRP which removes the effects caused by using different instrumentation and post-collection processing techniques in data acquisition. Using Equation 3.2, the ratio between BRP and IRP is

$$\frac{\mathrm{BRP}}{\mathrm{IRP}} = \frac{R_I^2}{R_B^2}\frac{\mathcal{R}_B}{\mathcal{R}_I}\frac{\exp(2\kappa_h R_I)}{\exp(2\kappa_H R_B)} \tag{3.4}$$

which demonstrates that the ratio between BRP and IRP is dependent only on the signal attenuation, $\mathcal{R}$ and range R.

Correcting for attenuation

The relationship between BRP and travel time for each ridge is relatively similar, with the exception of SD-96 which is ∼13 times dimmer than other 2MHz data (Figure 3.3).

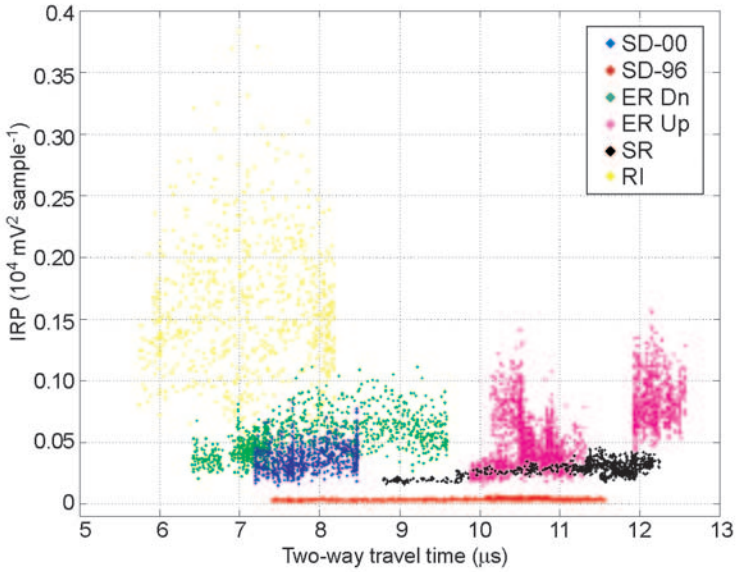

Figure 3.4: Frequency corrected-IRP versus two-way travel time for all available inter-ice stream ridge profiles. Different colors indicate location of profiles; Siple Dome (SD); Shabtaie Ridge (SR); downstream Engelhardt Ridge (ER Dn); upstream Engelhardt Ridge (ER Up) and; Roosevelt Island (RI). Multiple data sets in one general location are plotted as one color.

Since the SD-00 data align well with BRP measured on other ridges, the offset between SD-96 and these other data sets is likely from assuming constant gain (Equation 3.3) for all data sets and implies that the SD-96 data set was collected with different instrumentation characteristics than all other data sets. This was likely due to the use of a different signal amplifier on the SD-96 data compared to later data sets.

The exponential relationship between BRP and travel time is a result of attenuation losses in the ice column. BRP can be corrected for attenuation by dividing by an empirical relationship between ice thickness and BRP following from Gades and others (2000) to obtain BRP_R (Figure 3.3B). Since the SD-96 and SD-00 data cover a large range of travel times (although not the entire range of travel times seen in the ridges examined here) and because Siple Dome is known to have a nearly invariant bed-reflected waveform (Gades and others, 2000; Winebrenner and others, 2003), these data make a good benchmark for comparison to other ridges. An empirical fit of travel time versus BRP is obtained by combining these two data sets (with SD-96 data multiplied by 13 to correct for instrumentation differences as discussed earlier). Data with corresponding travel times that fall outside of the range of travel times in the empirical fit cannot be corrected for attenuation in this way. For this reason, these data points (including the entire ER-Up-2 data set) are not plotted in Figure 3.3B.

Discussion: Variability within and between ridges

The mean, standard deviation and coefficient of variation of IRP and BRP_R (BRP corrected for attenuation) for each data set are calculated to examine the variability of reflectivity measurements for any particular travel time (Table 3.2). Since a small number of measurements in a data set can result in an unusually low standard deviation, the results for ER-Dn-1 (100 data points) are ignored here. Furthermore, the calculation of mean BRP and IRP does not take into account instrumentation differences, and therefore, can not be directly compared. For instance, the $\overline{IRP}$ for Roosevelt Island data is much larger than the

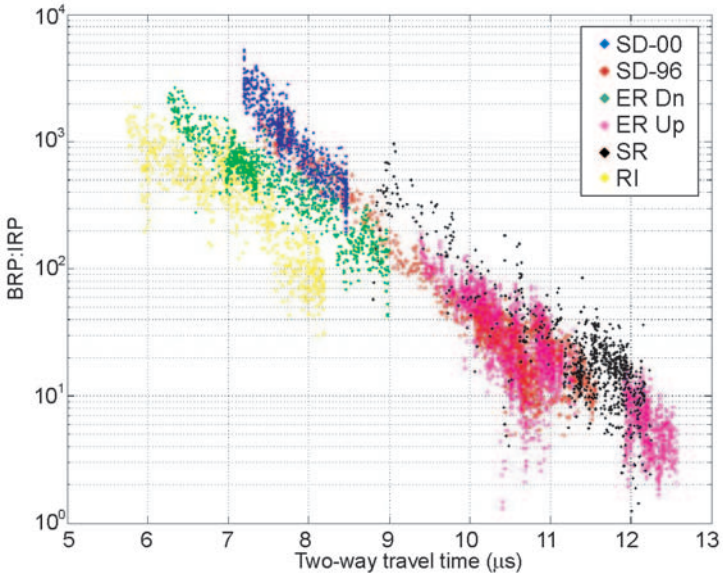

Figure 3.5: BRP:IRP versus two-way travel time for all available inter-ice stream ridge profiles. Different colors indicate location of profiles; Siple Dome (SD); Shabtaie Ridge (SR); downstream Engelhardt Ridge (ER Dn); upstream Engelhardt Ridge (ER Up) and; Roosevelt Island (RI). Multiple data sets in one general location are plotted as one color.

$\overline{\text{IRP}}$ from other data sets however, $\overline{\text{BRP}}_{\text{R}}$ for Roosevelt Island is not. This may be because internal layers at Roosevelt Island are brighter than on other ridges but could also mean that Roosevelt Island has a dimmer bed than other inter-ice stream ridges.

Unlike the means of IRP or BRP, the variability in IRP or BRP and travel time can be more meaningfully compared between ridges (Table 3.2). Roosevelt Island (RI) has greater variability in measured IRP than other ridges, nearly three times larger than the next highest σ_{I}. Variability in BRP is greatest for Shabtaie Ridge, nearly three times more variable than Siple Dome. Roosevelt Island also has a relatively large σ_{B} compared to Siple Dome. In contrast, the downstream end of Engelhardt Ridge has a relatively low σ_{B} similar to that of Siple Dome.

As travel time increases, the incoming radar signal becomes weaker due to attenuation. At large enough travel times, the expected error in bed amplitude can become as large as the measurement itself resulting in greater variability of returned power for very large travel times. This may explain some component of the increased variability with travel time observed in Figure 3.5 and why SD-96 has a higher σ_{B} than SD-00. High variability at smaller travel times is more likely a result of actual variability in the layers or bed material. Figure 3.5 shows that for any given travel time, most ridges collapse to a similar BRP:IRP with the exception of Roosevelt Island and ER-Dn. Three possibilities exist to explain this; either these regions have dimmer beds than the other ridges, brighter internal layers, or a different relationship between signal attenuation and travel time than the other ridges.

Both Roosevelt Island and ER-Dn have low BRP:IRP compared to the other ridges (Figure 3.5). Low BRP:IRP on Roosevelt Island might be due to brighter than average internal layers since BRP here appears to be similar to other ridges (for any given travel time). Because ER-Dn data were collected in the same field season as SD-00 data there are no instrumentation differences between these two data sets. $\overline{\text{BRP}}_{\text{R}}$ and $\overline{\text{IRP}}$ for these areas indicates that the low BRP:IRP for ER-Dn may be due to a combination of both brighter internal layers and a dimmer bed at the downstream end of Engelhardt Ridge.

Table 3.2: Mean, standard deviation, and coefficient of variation of IRP and BRP for selected inter-ice stream ridges taken from Figures 3.3B and 3.4. Values for Siple Dome have been multiplied by 13 to account for instrumentation differences.

Location	$\overline{\text{IRP}}$	σ_{I}	CV_{I}	$\overline{\text{BRP}}_{\text{R}}$	σ_{B}	CV_{B}
ER-Dn-1	0.0458	0.0096	20.96	0.4556	0.0407	8.933
ER-Dn-2	0.0595	0.0158	26.55	0.6759	0.1723	25.49
ER-Up-1	0.0578	0.0185	32.01	0.6168	0.2020	32.75
ER-Up-2	0.0829	0.0187	22.56	N/A	N/A	N/A
ER-Up-3	0.0332	0.0058	17.47	0.7091	0.3003	42.35
SD-96	0.0507	0.0117	23.08	1.0538	0.2349	22.29
SD-00	0.0369	0.0104	28.18	0.9637	0.1311	13.60
SR	0.0291	0.0057	19.59	1.0628	0.5240	49.30
RI	0.1597	0.0541	33.87	0.8822	0.3256	36.91

3.4 Conclusions

Our results substantiate the idea that Siple Dome is well suited as a calibration point for other ridges since IRP and BRP are generally not as variable here as on other ridges. Most ridges have a highly consistent travel time versus BRP:IRP relationship indicating relatively homogenous bed and ice conditions between the ridges over large distances. However, differences in BRP:IRP do exist and may highlight subtle differences in ice and/or bed properties between ridges. In particular, Roosevelt Island has a much larger and more variable IRP than other ridges indicating that the ice here may be affected by processes that are atypical. One possible explanation is that the proximity of Roosevelt Island to the open ocean permits the accumulation of wind blown salts on the ice surface which can greatly increase IRP in a non-uniform way.

The large variability in BRP seen for Shabtaie Ridge compared to other ridges may be a result of relatively high roughness; radar profiles there show slightly more irregular bed topography compared to both Engelhardt Ridge and Siple Dome (Nereson and Raymond, 2001).

Chapter 4

SURFACE MORPHOLOGY AND INTERNAL LAYER STRATIGRAPHY IN THE DOWNSTREAM END OF KAMB ICE STREAM, WEST ANTARCTICA

4.1 Summary

Satellite images of the terrain in the downstream end of Kamb Ice Stream (KIS, formerly Ice Stream C), West Antarctica reveal several long, curved linear features (lineations) oriented sub-parallel to the ice-flow direction. We use ground-based radar and satellite images to characterize the surface morphology and internal layer stratigraphy of these lineations and the terrains that they bound. Some lineations are relict ice stream shear margins, identified by the onset-of or change-in-depth of hyperbolic diffractors near the surface (interpreted to be buried crevasses) and highly disturbed internal layers at depth. Relict margins are aligned roughly parallel with the paleo-flow direction and bound paleo-ice stream terrain, which is characterized by continuous deep layers and near-surface crevasses. Satellite images show another set of lineations outside of the relict ice stream margins that wrap around the ends of the surrounding inter-ice stream ridges. Internal layers beneath these lineations are downwarped strongly into a syncline-shape. The internal stratigraphy of the terrain between these lineations and the relict margins is characterized by deep hyperbolic line-diffractors. Our preferred hypothesis for the origin of this terrain is that it was floating sometime in the past; the deep hyperbolas are interpreted to be basal crevasses and the strongly downwarped internal layers mark the position of a relict grounding line. Our study shows that lineations and intervening terrains have different internal layer characteristics implying different origins. Differentiation between these features is not possible using satellite images alone. Ground-based radar measurements are necessary to identify the origin of

these features.

4.2 Introduction

Satellite images provide information about changes in ice flow history through interpretation of the arrangement of visible flow features including crevasses, rifts, flowstripes and relict shear margins (Fahnestock and others, 2000; Bindschadler and Vornberger, 1998; Scambos and Bindschadler, 1993). Such features are associated with subtle topography (amplitudes of a few meters and wavelengths of several kilometers) not easily seen on the ground. Some flow-features have a clear origin, such as crevasses and rifts, but the dynamic causes of the subtle topographic signatures associated with flowstripes and relict margins are often unclear. Supplementary information about the genesis and evolution of these features is necessary to characterize them and fully interpret their glacial origin.

We present results from ground-based, ice-penetrating radar profiles across satellite-detected lineations and terrains in the downstream end of Kamb Ice Stream (formerly Ice Stream C) during the 2001-02 and 2002-03 field seasons (Figure 4.1A). Kamb Ice Stream (KIS) stagnated about 150 years ago (Retzlaff and Bentley, 1993); most of the lineations that are visible in satellite images of this region likely formed prior to stagnation. We distinguish three types of terrains and three types of lineations based on their surface morphology and their radar-detected internal stratigraphy. Figure 4.1A shows the location of acquired radar profiles (labelled A through I) and visible lineations (L1 to L8). The north side of KIS includes an area called the "Duckfoot", named for the splayed pattern of lineations that mark its surface (Jacobel and others, 2000). A similar area exists on the south side of KIS and in the same spirit we call this the "Goosefoot". These two regions consist of several different types of ice terrains, each with distinct characteristics. Our goal in this paper is to illustrate the differences in dynamic origin of the terrains and lineations in these two regions in order to aid in interpretation of the recent ($\sim$1000 year) ice flow history.

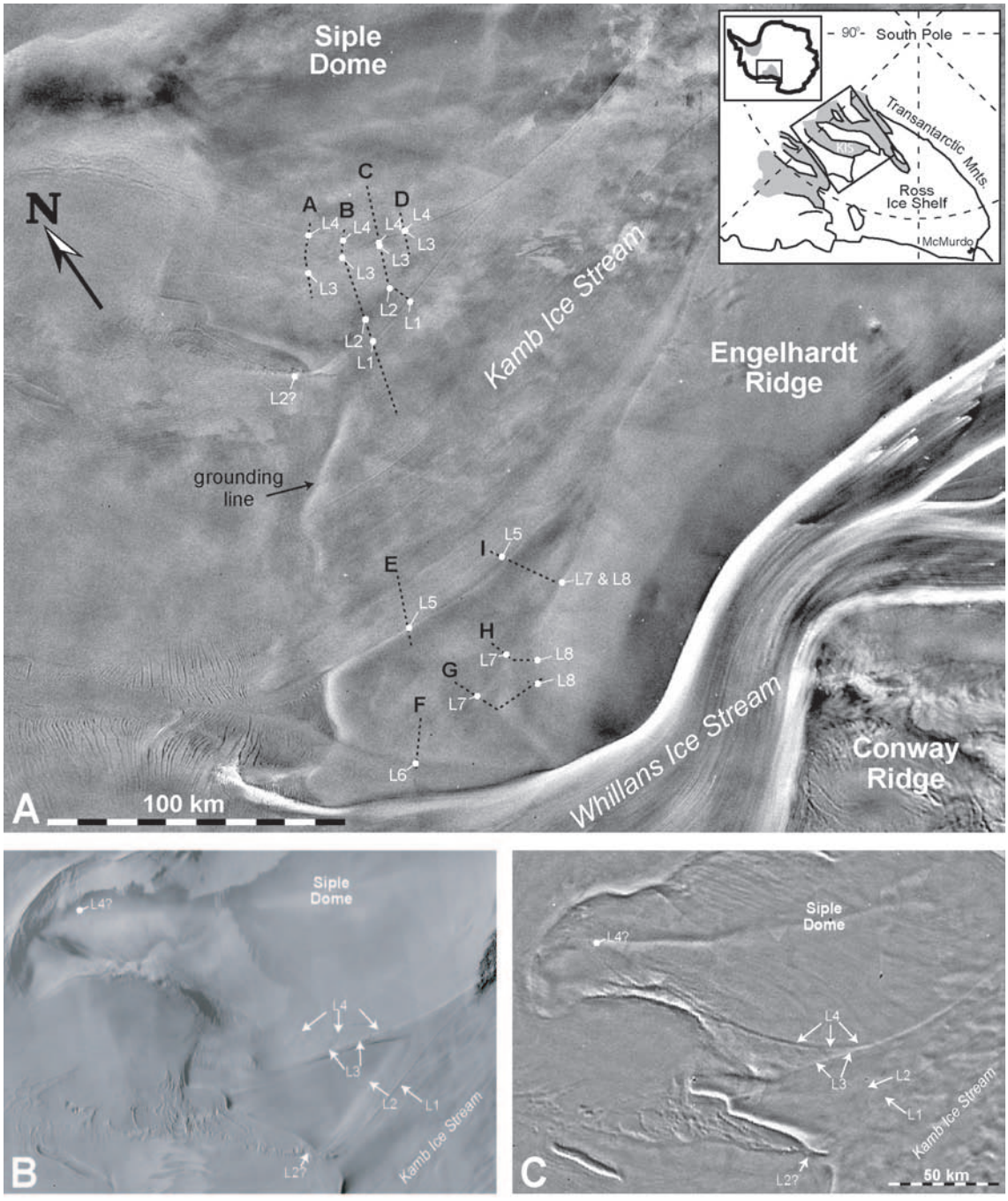

Figure 4.1: A. RADARSAT image of the KIS and WIS area. Flow direction is generally from the right to the left. Black dotted lines (labelled A-I) show the location of radar profiles across lineations (L1 to L8). Inset shows our study area in West Antarctica. B. MODIS and C. AVHRR images of the Duckfoot area and south flank of Siple Dome.

4.3 Radar and Satellite Data

BEDMAP data (bed and surface elevations Lythe and others (2001)) provide information regarding the bed topography and elevation above floatation for the downstream KIS area (Figure 4.2). Bed topography is relatively high beneath the inter-ice stream ridges and terrains surrounding KIS, and a ∼300 m deep overdeepening exists in the mouth of KIS just upstream from the modern grounding line. Also, most of the ice in the mouth of Whillans Ice Stream (WIS) and KIS is within 50-100 m of floatation. The height above floatation is remarkably constant in the mouth of KIS but begins to increase toward the middle of the ice stream approaching the old UpC Camp (82.4 S, 136.6 W).

Several sources of satellite data are used to map lineations. Variations in brightness of a feature depend not only on its morphology but also on the satellite source and/or the illumination angle. We use data from two moderate resolution (250-1100 m) satellites that provide information about the surface topography and albedo through variations in brightness: Advanced Very High Resolution Radiometer (AVHRR) imagery from U.S. National Oceanic and Atmospheric Administration polar-orbiting weather satellites (Figure 4.1C) and Moderate Resolution Imaging Spectroradiometer (MODIS) imagery from NASA (Figure 4.1B). We also use high-resolution (25m) synthetic aperture radar satellite (RADARSAT-1) data to derive a 125 m mosaic of our field site. Brightness in RADARSAT data comes from a combination of radar backscatter from both the surface and subsurface (up to ∼2 m on exposed ice and up to ∼10 m on dry, cold firn (Rignot and others, 2001)), which permits detection of crevasses that are thinly covered by accumulation. Active crevasse regions such as the north margin of WIS are bright in backscatter (Figure 4.1A).

Two ground-based radar systems are used to study internal layer structure and bed characteristics. Of particular interest are changes in internal structure across the satellite detected lineations. In most cases, these lineations mark boundaries between terrains with different origin. Continuous layers are classified as either smooth or distorted, a qualitative distinction that is based on changes in layer shape relative to changes in bed topography.

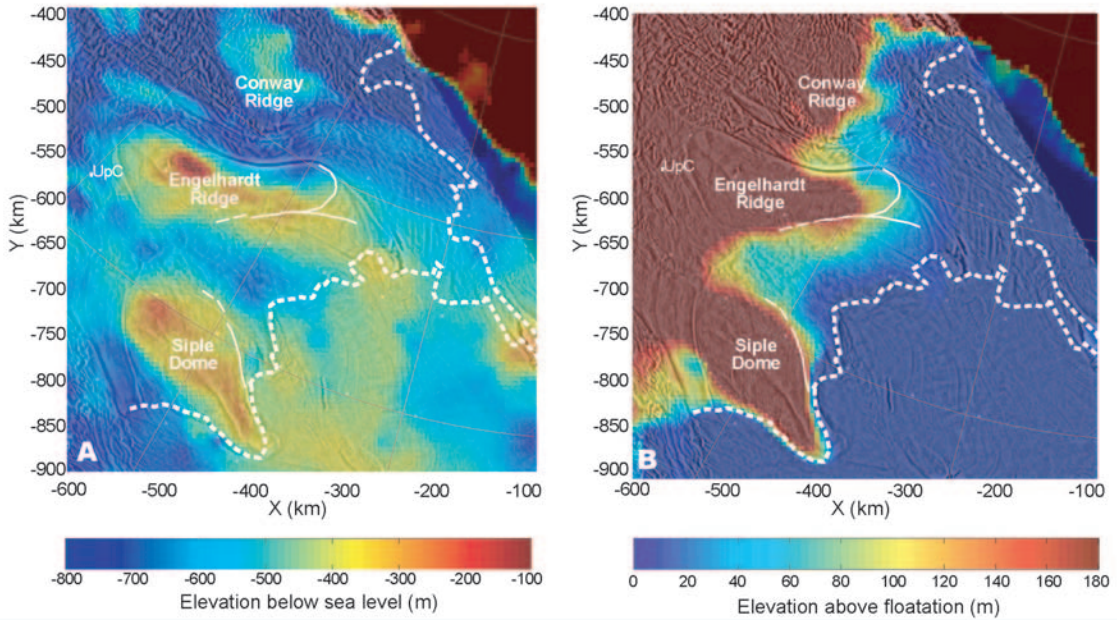

Figure 4.2: A. Bed elevation and B. Elevation above floatation for the KIS area. Data has a 5 km grid spacing, 1-5% vertical accuracy and the vertical datum is corrected to the OSU91 geopotential model which deviates from mean sea level by an average of 1.5 m (Lythe and others, 2001). Active margins and flowlines of WIS are visible in the underlying AVHRR image. The present-day grounding line position is shown as a thick dashed white line. Positions of the syncline features (see text) are indicated by thin white solid lines. The dashed white line shows the possible extrapolation of syncline features across KIS. The color bars saturate at values outside of their limits.

We used a low frequency (2-5 MHz) short-pulse radar system (described by Gades (1998)) to image deep internal layers ($\backsim$100-1000 m) and the bed. A pressure transducer and a geodetic quality global positioning system (GPS) receiver were used to measure surface topography and elevations relative to the WGS84 ellipsoid; here the ellipsoid is $\sim$45 m above present-day sea level. To map the near-surface stratigraphy we used a commercial high frequency (50-200 MHz) radar system (RAMAC) with a corresponding resolution of 1 and 0.25 m respectively. To improve the signal to noise ratio, we recorded radar waveforms that consist of several hundred stacked (averaged) waveforms acquired continuously over horizontal spacing that ranged from 1.5-5 m for high-frequency radar and 10-25 m for low-frequency radar. As a result, steeply dipping internal layers may be aliased. Depth-density profiles from snow pits and a 17 m firn core are used to convert radar wave travel-time to depth (Gades, 1998).

4.4 Character and Origin of Lineations

4.4.1 Lineations Associated with Near-surface Diffractors

Radar profiles across four of the lineations (L2, L3, L5 and L6) reveal near-surface diffractors and distorted, often discontinuous deep internal layers (Figure 4.3). GPS measurements across these features show broad topographic troughs that are 10-50 m deep over 3-10 km (e.g. Figure 4.1A). MODIS and AVHRR images of the Duckfoot (Figures 4.1B and C) both show L2 and L3 as bright, narrow lines (likely due to these troughs) aligned respectively parallel and sub-parallel to the most recent flow direction of KIS (as indicated by flowstripes in the main body of KIS). Radar data show that the near-surface diffractors are closer to the surface at L2 than L3. Because diffractors here are not distinct, we pick the depth of the deepest continuous internal layer: 30 m for L3, and 18 m for L2 (Figures 4.3C and 4.3B respectively). Two sets of near-surface diffractors are detected beneath the lineations on the Goosefoot; one at L5 (22 m below the surface) and another at L6 (17 m below the surface) (Figure 4.1A).

We interpret these four lineations to be relict ice stream shear margins now buried under

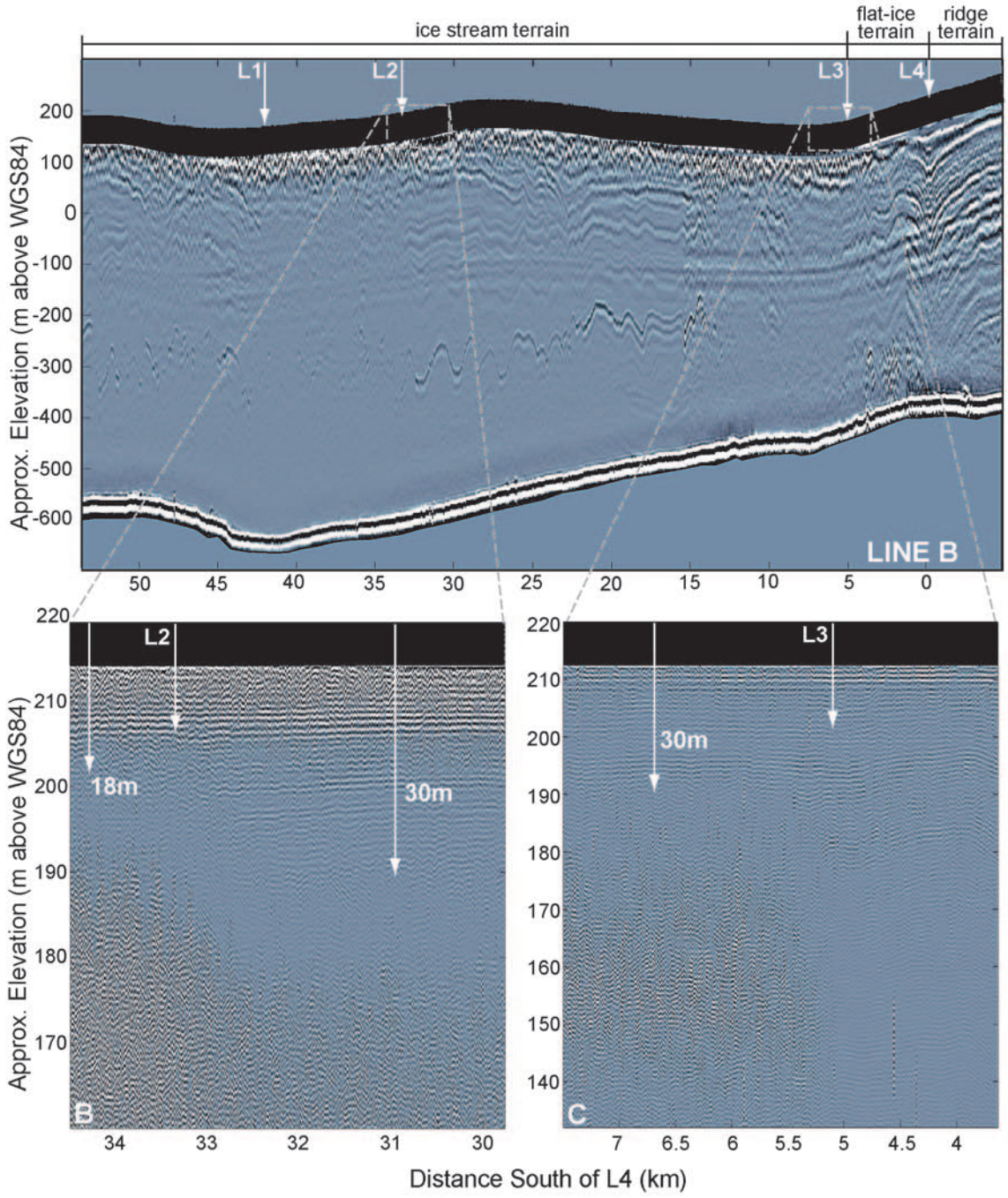

Figure 4.3: A. 2 MHz radar profile across L1-L4 along Line B (Figure 4.1A). The prominent return at ∼-100 m depth is a glitch in the transmitter. Stratigraphy in the upper ∼80 m (shown as a black band) is not resolved by the radar system. B. 100 MHz radar profile across L2. Arrows indicate the depth to the deepest continuous layer. C. 100 MHz radar profile across L3. Continuous layers are visible as deep as 140 m north of km 5.

more than 100 years of accumulation. The numerous near-surface diffractors associated with the lineations are interpreted to be buried crevasses that formed at the surface within a margin of an active ice stream. This interpretation is not new; Retzlaff and Bentley (1993) identified L5 as a relict margin of KIS and Jacobel and others (2000) identified L3 as a relict margin. The deep internal layer stratigraphy is consistent with conditions in an active ice stream where large cumulative strains can deform layers. Layer continuity here is lost from some combination of high strain causing steeply sloping layers and signal loss from scattering within the near-surface diffractors. Deeper layers regain continuity about 10 km inside the ice stream margin (towards the middle of the ice stream). The discontinuous layers are probably related to the chaotic zones observed in active shear margins where strain rates are largest and crevassing does not conform to a particular pattern (Echelmeyer and Harrison, 1999).

Several characteristics of margins are apparent; the presence of near-surface point diffractors, deep discontinuous layers and the coincidence of these margins with broad topographic troughs, which are present across other active and relict ice stream margins (Whillans and others, 1993; Gades and others, 2000; Conway and others, 2002; Catania and others, 2003). One possible explanation for trough formation is that focussed strain heating in margins allows for localized melting (Jacobson and Raymond, 1998). Thorsteinsson and others (2003) show that ice advected across an ice stream margin undergoes rapid changes in the stress pattern such that the direction of maximum compression becomes horizontal. They argue that ice expands vertically as it traverses an ice stream margin but indicate that recrystallization and crevasse formation may counter this. The troughs that we observe across ice stream margins likely represent some combination of these processes.

4.4.2 Lineations Associated with No Change in Internal Layers

L1 is a distinct, narrow lineation parallel to the most recent flow direction of KIS. It appears to originate at the junction between the southern edge of Siple Dome and the innermost margin of KIS and fades out about 20 km before the KIS grounding line. Our

measurements show that L1 is a low-amplitude (⌣2 m), long wavelength (⌣2 km) undulation in surface topography, which appears as an alternating light and dark pattern in Figure 4.1A and 4.1B. Both high and low frequency radar profiles across L1 show deep disturbed layers and near-surface diffractors beneath the surface undulation.

The depth to near-surface diffractors does not change across L1, and so we do not think that this is a relict margin of KIS, as hypothesized by Jacobel and others (2000). Instead we believe that it is a relict flowstripe that originated from within an active shear margin. Merry and Whillans (1993, Figs. 5 and 7) show several examples where flowstripes originate from margins of active ice streams, and Gudmundsson and others (1998) show flowstripes with similar geometry to that of L1 in satellite images.

4.4.3 Lineations Associated with Syncline Layers

Three of the eight lineations examined (L4, L7 and L8) are associated with shallow topographic troughs (∼1-3 m deep) that span only a few kilometers. On the surface, such small-scale topographic changes are not easily discernable but they are visible in satellite images especially when taken at low sun angles. These lineations are found at the boundaries between inter-ice stream ridges and the flat-ice terrains in the mouth of KIS. In the Duckfoot, L4 wraps alongside the southern edge of Siple Dome diverging away from the paleo-flow direction of KIS towards the grounding line (Figure 4.1C). On the south side of KIS in the Goosefoot, L7 also wraps around the western end of Engelhardt Ridge away from the paleo-flow direction of KIS (Figure 4.1A). L7 branches away from the edge of the ridge (where it merges with L8) and cuts across the Goosefoot towards the grounding line (Figure 4.1A).

Internal layers beneath these troughs are warped downwards as much as 200 m, forming a syncline that is unrelated to bed topography (Figures 4.4, 4.5 and 4.6); this distinctive pattern does not change when the data are migrated to adjust for geometric artifacts. The fold amplitude of these synclines increases with depth and the deepest layers are truncated at the bed. The fold axis of the syncline in the Duckfoot is tilted away from Siple Dome such that the minimum elevation of the uppermost isochrone is offset by ∼150 m from the

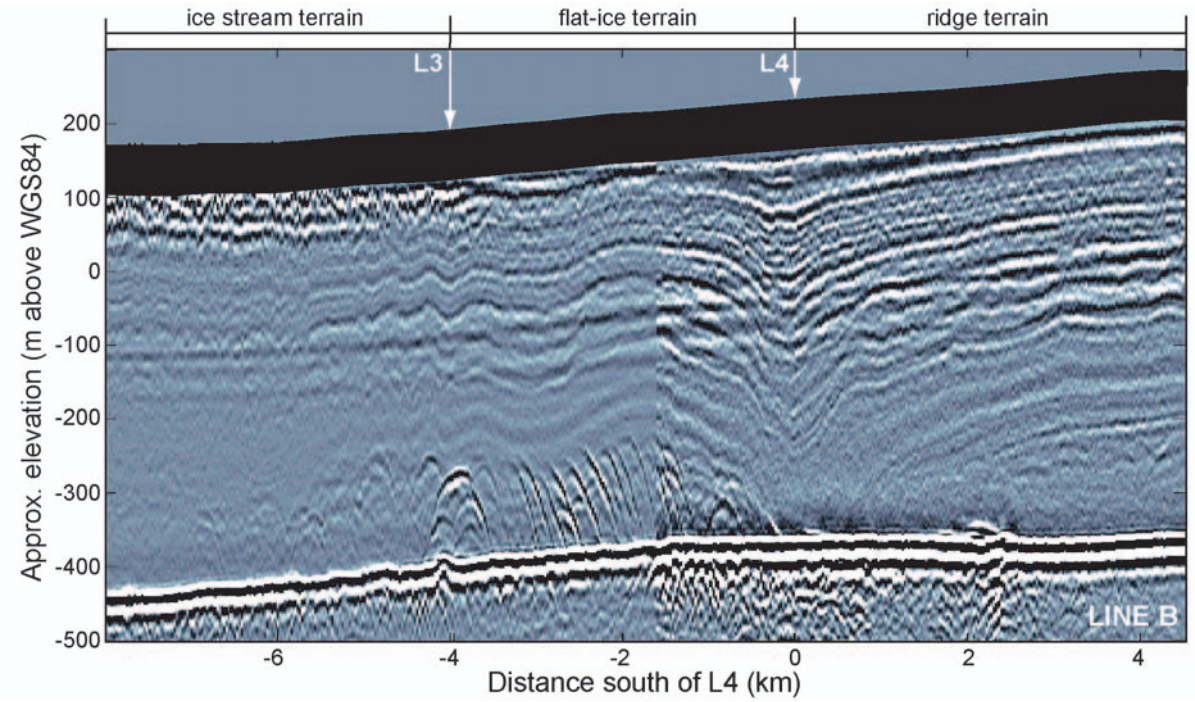

Figure 4.4: 2MHz radar profile along Line B (Figure 4.1A) crossing L4 and the northernmost KIS margin (L3). The prominent return at ∼ -100 m elevation is a glitch in the transmitter. Stratigraphy in the upper ∼80 m (shown as a black band) is not resolved by the radar system.

minimum elevation of the deepest isochrone (Figure 4.4). Assuming that the mechanism causing the downwarp maintained a consistent spatial pattern over time, this offset is likely caused by flow off Siple Dome after the syncline formed. If the present-day surface velocities (0.9 m a^{-1}; Jacobel and others (2000)) have been constant over the past few hundred years, we estimate that the processes forming the syncline stopped about 170 years ago. Synclines in the Goosefoot (L7 and L8) have vertical fold axes (Figure 4.5) implying that the processes causing these synclines may still be active or only recently ceased, although slope-driven flow across L7 might be too low to cause a noticeable tilt in the syncline axis. The most distinct characteristic of L7 is that it marks the location where the depth of deep diffractors changes (Figure 4.6). We note that the H-line profile across L7 does not show downwarped layers (Figure 4.6), but the G-line profile (not shown) does.

Several mechanisms could cause downwarping of internal layers. For example, Vaughan and others (1999) attribute near-surface downwarped internal layers across the boundary between Carlson Inlet and Fletcher Promontory to a localized accumulation high. Their data show that the amplitude of the layer syncline increases with depth in the upper 100 m of ice and they attribute this to a 33% increase in accumulation at the slope break between the ridge (Fletcher Promontory) and the area of flat ice adjacent to it (Carlson Inlet). Picked layers across the upper 30 m ($\sim$350 years) of the Goosefoot and Duckfoot syncline-layer boundaries do not show changes in layer thickness that might suggest an accumulation anomaly here for at least the past few hundred years.

Localized basal melting can also downwarp internal layers over a narrow region. Basal melting can occur through several processes including melt beneath an ice shelf at the grounding line (Smith, 2000; Rignot and Jacobs, 2002; Gill, 1973), melt from a localized high geothermal flux (Fahnestock and others, 2001) and, melting due to strain heating within shear margins (Jacobson and Raymond, 1998). We do not think that the observed stratigraphy is consistent with that of typical relict ice stream margins for several reasons: (1) high-frequency radar data across L4, L7 and L8 do not show near-surface point diffractors while relict ice streams (e.g. Siple Ice Stream) as old as 420 years $\pm$ 60 years (personal

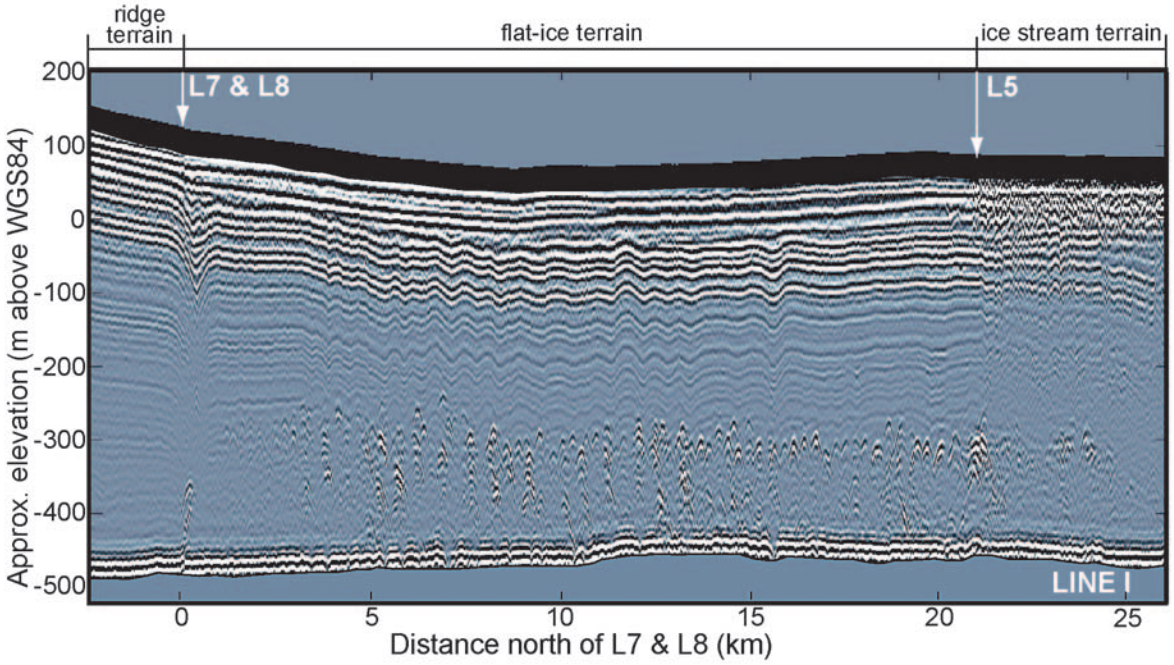

Figure 4.5: 5MHz radar profile along Line I in the Goosefoot crossing L5, L7, and L8. Stratigraphy in the upper ∼80 m (shown as a black band) is not resolved by the radar system.

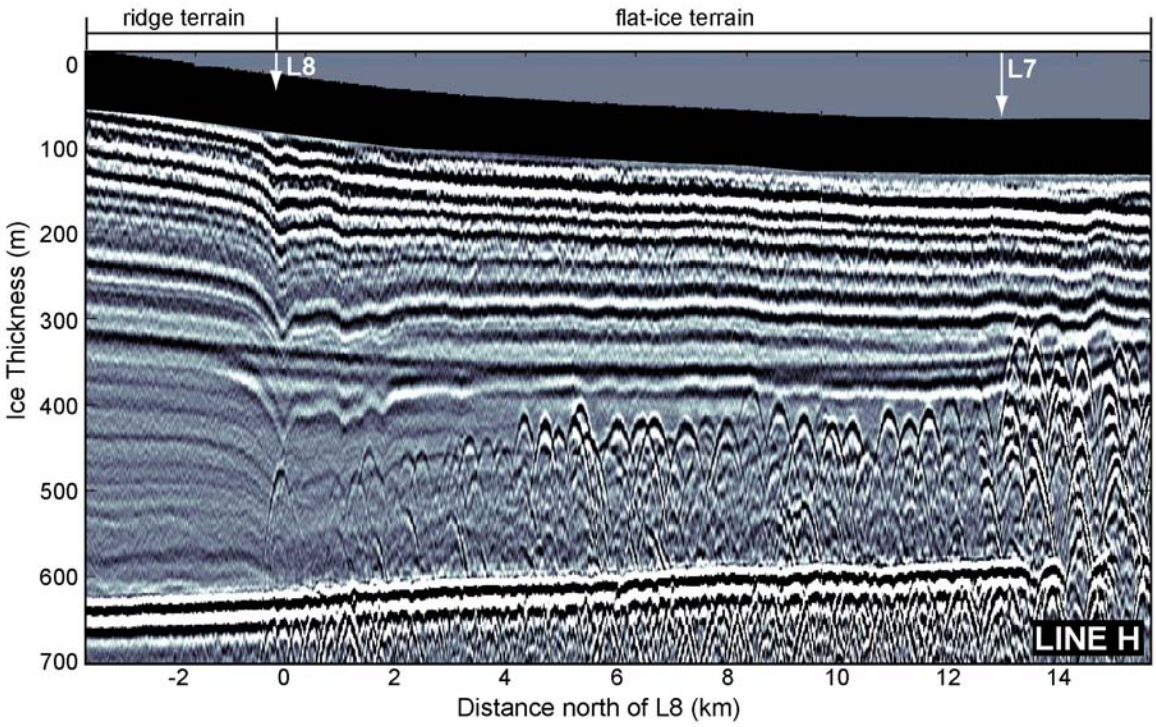

Figure 4.6: 2MHz data along Line H in the Goosefoot crossing L7 and L8 (Figure 4.1A). Note the prominent return at ∼300 m depth is a glitch in the transmitter. Stratigraphy in the upper ∼80 m (shown as a black band) is not resolved by the radar system.

communication, B. Smith, 2000) still show evidence of near-surface point diffractors; (2) both L4 and L8 wrap around the edges of inter-ice stream ridges away from the paleo-flow direction of KIS; (3) deep layers are preserved across these features indicating that strain rates were not as high as those observed in present-day margins; (4) there is no evidence of flowstripes (indicative of sliding) on the surface in the areas adjacent to the syncline lineations; (5) radar profiles across known relict and active shear margins do not show localized downwarping to this degree. Rather, the pattern of deeper layers across ice stream margins appears to be disorganized (Catania and others, 2003; Gades and others, 2000, e.g.).

A locally elevated geothermal heat source could produce the observed melt signature since localized fault slip can raise temperature in the underlying material by several hundred degrees (Fialko, 2004). The syncline-layer boundaries appear to be associated with the edges of the inter-ice stream ridges which may represent geologic as well as topographic boundaries. Geomagnetic data are not available for this region to determine whether local anomalous heat sources are a possibility in these locations (Sweeney and others, 1999). Because of this, we are not able to rule out that these syncline-layer boundaries result from a geothermal anomaly. However, this mechanism gives no explanation for the deep line-diffractors seen in adjacent terrains. It is possible that the diffractors and the synclines are unrelated but we search for a hypothesis that can simply explain all observations.

Our preferred hypothesis is that the melting occurred near a grounding line when the region was once floating. Grounding line melt occurs at the back of a sub-ice-shelf cavity through the circulation of high-salinity shelf-water (HSSW) which is produced when salt is rejected during the formation of sea ice (MacAyeal, 1985). HSSW is delivered along the seabed to the grounding line and can remain up to 0.5 $^{\circ}$C warmer than the in-situ freezing point of water beneath the ice shelf base (Gill, 1973). HSSW can induce basal melting but strong stratification often prevents its contact with the ice shelf base. MacAyeal (1984) shows that large tidal currents, developed in areas with a small water column thickness (such as at grounding lines), can stir the water column and promote localized basal melting. The

pattern of grounding line melt is not clear; some modelling predicts that melt would be spread over wide (∼100 km) areas downstream of the grounding line (Jenkins and Doake, 1991) although limited observational evidence indicates that it could be more focussed (< 10 km) near the grounding line (Smith, 2000).

4.5 Character and Origin of Terrains

4.5.1 Ridge Terrain

Inter-ice stream ridges (e.g. Siple Dome and Engelhardt Ridge in Figure 4.7) rise several hundred meters above the surrounding ice streams, but have a smooth surface topography over scales of 100's of meters (Figure 4.1). Surface velocities are slow (<8 m a^{-1} Whillans and van der Veen (1993)) and radar profiles generally reveal continuous internal layers with undulations that appear as smoothed versions of the bed topography (Nereson and others, 2000).

4.5.2 Ice Stream Terrain

Rose (1979) deduced that Ice Stream C (here called KIS) had stagnated based on a lack of visible surface crevasses compared to other ice streams. Satellite images confirm this observation but also show that the surface topography of KIS is complex and more undulating than the surrounding inter-ice stream ridges and flat-ice terrains (Figure 4.1). Typical slopes of ice stream terrain are $\sim 10^{-3}$ and although KIS is now slow moving (0.1-10 m a^{-1}), numerous flow stripes still visible on the surface and buried marginal crevasses provide evidence of fast flow in the past. Typical internal structure within ice stream terrain includes near-surface diffractors and deeper layers that are often continuous but highly distorted due to the large cumulative strain. Relict and active ice stream terrains are indicated in Figure 4.7.

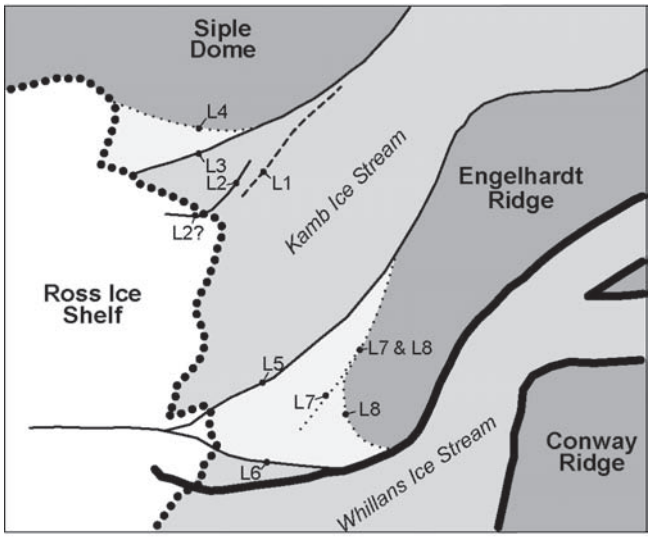

Figure 4.7: Lineations and terrains of lower KIS and WIS mapped from Figure 4.1. Flat-ice terrains are light grey, inter-ice stream ridges are dark grey, ice stream terrains are medium-grey. The active grounding line is a thick dotted line and the hypothesized relict grounding lines are thin dotted lines. Active ice stream margins are shown as thick black lines while relict margins are thin black lines.

4.5.3 Flat Ice Terrain

Flat-ice terrain is a distinctive, previously undefined terrain type that lies between the inter-ice stream ridges and the main body of relict KIS. Surface slope (10^{-4}) and velocities ($<$0.3 m a^{-1}) are small (Jacobel and others, 2000) and the surface topography across these regions is smoother than ice stream terrain but rougher than ridge terrain (Figure 4.1).

Radar-detected stratigraphy across these areas shows layers that are continuous and lightly disturbed in the upper half of the ice but discontinuous with numerous diffractors in the lower half of the ice (Figure 4.5). These diffractors extend throughout the flat-ice terrains from their boundary with the inter-ice stream ridges (at the location of L4 and L8) to several kilometers (up to 10 km in Goosefoot) into the relict shear margins of KIS. The diffractors occur in distinct sets with uniform heights. In the Duckfoot there is one set $\sim$150 m above the bed (Figure 4.4) while in the Goosefoot there are two sets of diffractors; one $\sim$200 m above the bed and another $\sim$250 m above the bed (Figures 4.5 and 4.6). The transition between the two sets of diffractors in the Goosefoot occurs at L7.

Although the pattern of layer distortion above these diffractors appears to be random in the Duckfoot, it is partly organized in the Goosefoot. Figure 4.5 shows the upper layers in the Goosefoot undulate with a wavelength of $\sim$1 km; peaks in the layers roughly align with the tops of diffractors below them. Other profiles in the Goosefoot (Figure 4.6) show flat layers overlying diffractors implying that this organized pattern may not be widespread.

Grid and star patterns of radar data from across deep diffractors in the Goosefoot and Duckfoot reveal more information about diffractor geometry and orientation. Radar profiles across diffractors (in directions perpendicular to L4 and L8) show diffraction hyperbolas, and migration of radar data along Line I (Figure 4.5) reduces these hyperbolas to point sources. In contrast, radar profiles in directions parallel to L4 and L8 show a line diffractor at the same depth as the top of the hyperbolas. This pattern is indicative of a source of contrasting permittivity along a line oriented parallel to L4 and L8.

We are not certain of the origin of the deep diffractors in these terrains. We rule out the possibility that they are buried surface crevasses because at such depths crevasses would be

closed, reducing the permittivity contrast necessary to produce a diffractor.

Clarke and others (2000) found similar deep diffractors in the small inter-ice stream ridge between the two limbs of Whillans Ice Stream (the Unicorn). They proposed several possible causes for the diffractors including the presence of basal crevasses, englacial morainal debris, or a residual zone of temperate ice produced within the high strain rate environment of an active shear margin. Unlike the Clarke-diffractors, diffractors in these flat-ice terrains occur up to 20 km away from relict shear margins and so we discount that they originated as temperate ice zones within shear margins.

Debris-rich ice can be accreted to the base of the ice column as seen beneath parts of KIS (personal communication, H. Engelhardt, 2001). Kamb (2001) calculated freeze-on at the UpC camp of 0.0045 m a^{-1} from borehole data and rates of up to 0.1 m a^{-1} have been reported beneath Matanuska Glacier in Alaska (Lawson and others, 1998). Even using this large rate, accretion of 250-300 m of basal ice (the height of the point diffractors above the bed) would take at least 2500 years. Although we do not rule out basal freeze-on, we suspect that other processes dominate.

Similar diffractor features have been detected in airborne-radar profiles over ice shelves (Jezek and Bentley, 1983; Jezek and others, 1979). These are usually interpreted to be basal crevasses formed in floating ice. Tops of basal crevasses are likely to produce a strong reflection, especially if pockets of brine are trapped within them prior to crevasses closure. For a free floating ice shelf of thickness H, Weertman (1980) calculated that a single bottom crevasse could penetrate up to $\frac{\pi H}{4}$. In the case of multiple basal crevasses, penetration height is expected to be lower ($\sim \frac{H}{2}$) because the stress causing crevasse formation is spread over multiple crevasse tips (Van der Veen, 1998). The remarkably constant height of these diffractors above the bed across large regions of these terrains might suggest that large areas were susceptible to a similar stress environment. The height of basal crevasses can be increased through tidal flexing of the ice shelf. Diffractor orientation supports the idea that, if these features are basal crevasses, they formed from increased tensile stress as ice flowed from the ridges into floating and/or faster moving ice.

If these diffractors were caused by basal crevasses, an implication is that these terrains were once floating, which is consistent with the hypothesis that the syncline features described above formed through basal melting at relict grounding lines (marking the outermost boundary of these terrains). However, the ice in these terrains is presently grounded (Figure 4.2B); in order for these regions to be floating they would have to have been 50-100 m thinner or sea level must have been much higher than present (Figure 4.2).

4.6 Synopsis

Although satellite images clearly illuminate the three types of lineations, their different origins are difficult to distinguish from the satellite data alone. Relict margins are associated with the greatest topographic relief (10-50 m vertically over 3-10 km) while topographic changes across syncline lineations and flowstripes are much smaller (1-2 m over 1-2 km). Supplementary ground-based radar measurements are needed to differentiate the characteristics and possible origins of these features. This is crucial to an accurate interpretation of ice flow history.

Jacobel and others (2000) were the first to complete ground-based radar surveys in the Duckfoot region. They acquired 5 MHz data along profile C (Figure 4.1) and showed that the northern margin of KIS had shifted inward prior to complete shutdown of the ice stream. However, without the advantage of high-frequency radar to image the near-surface structure, they mistakenly identified L1 as the most recent margin of KIS. Our data show that the depth to buried crevasses does not change from L2 to L1 and into the main body of KIS for several kilometers, indicating that L2 is the most recent margin and that L1 is likely a flowstripe originating from within this margin.

Radar profiles discussed by Jacobel and others (2000) cross L3 and L4 where they are nearly coincident (Figure 4.1) which hampers interpretation of these two lineations. Our profiles farther downstream show clearly that the internal stratigraphy of L4 is quite distinct from L3, and it is not a relict ice stream shear margin.

Our radar investigations reveal three different types of terrains in the mouth of KIS, in-

cluding a newly defined flat-ice terrain (Figure 4.7). These terrains, located between inter-ice stream ridges and relict ice-streams, is characterized by numerous mid-depth line diffractors. The simplest explanation is that these diffractors are caused by bottom crevasses, and we suggest that these terrains were once part of a relict ice shelf that occupied the mouth of KIS. Consistent with this hypothesis are internal layer-synclines that mark the boundary of the flat-ice terrains with the inter-ice stream ridges. These synclines may have been created through focussed basal melting, which can occur at grounding lines (Smith, 2000; Rignot and Jacobs, 2002; Gill, 1973). Further, the surface lineations wrap around the ends of inter-ice stream ridges, suggestive of a relict grounding line rather than relict flow features of KIS. This interpretation implies retreat and re-advance of the grounding line by $\sim$100 km. Our hypothesis suggests that the large-scale, pattern of grounding line retreat over the past 7,500 years (e.g. Conway and others, 1999) may have been periodically interrupted by re-advance some time during the past millennium.

Chapter 5

DYNAMIC SIGNIFICANCE OF FLAT-ICE TERRAINS IN THE MOUTH OF KAMB ICE STREAM, ANTARCTICA

5.1 Summary

Ice-penetrating radar reveals several distinctive characteristics in the internal layers of the flat-ice terrains that bound the lower end of Kamb Ice Stream, Antarctica; continuous and slightly disturbed upper layers overlie numerous line-diffractors located several hundreds of meters below the surface. At the boundary between these terrains and the inter-ice stream ridges, internal layers are strongly downwarped and deep layers are truncated by the bed. A simple kinematic ice-flow model is used to predict the shapes of internal layers at these boundaries, and we test several potential causes of layer downwarping. Results indicate that the observed layer pattern can be matched only with some component of basal melting. We interpret the deep line-diffractors to be basal crevasses based on their orientation and morphology. Our emerging hypothesis to explain these terrains is that they represent areas that were once floating. Model results and estimates of recent ice thickness change suggest that floatation lasted for up to 300 years and occurred up to 200 years prior to stagnation of Kamb Ice Stream.

5.2 Introduction

Fast-moving ice streams transport most of the grounded ice in the interior of the West Antarctic Ice Sheet (WAIS) out to the floating ice shelves. Weertman (1974) proposed that marine ice sheets (such as the WAIS) are inherently unstable during times of high sea level when the grounding line (representing the transition between grounded and floating ice) could retreat unstably into the central portions of the ice sheet causing it to float. The

stability of the WAIS is still in debate largely because of a lack of understanding of the affects of ice streams on ice sheet behavior.

Although ice streams transition from grounded to ungrounded conditions at their grounding lines, grounding can be ephemeral and/or "patchy" far upstream in the ice stream during high tides (Corr and others, 2001; Bindschadler and others, 2003). This is especially true where the bed is flat or sloping inland near the grounding line (Schmeltz and others, 2001; Corr and others, 2001). This zone of ephemeral grounding has been named an "ice plain" by several authors because of low surface slopes, but here we use the name "grounding zone".

In this paper we focus on the flat-ice terrains in the downstream end of Kamb Ice Stream (KIS, formerly Ice Stream C) which shutdown ∼150 years ago (Retzlaff and Bentley, 1993). Several authors have suggested that mouth of KIS was once a grounding zone that may have floated briefly prior to stagnation as a result of thinning (Joughin and others, 2003b; Thomas and others, 1988). There are contrasting views about the cause and pattern of the shutdown of Kamb Ice Stream (see review by Anandakrishnan and others, 2001). One view is that shutdown began in the mouth of the ice stream when the ice thickness was insufficient to maintain melting at the bed (Joughin and others, 2003b; Bougamont and others, 2003). De-watering of the till through freezing on to the ice base would strengthen the till and cause a negative feedback between slower speeds and decreased melting at the bed (because of reduced frictional heating) (Tulaczyk and others, 2000b).

Catania and others (2005) use ice-penetrating radar measurements in this area to identify and characterize a possible relict grounding line ∼100 km upstream from the present grounding line position (Features B1, B2 and B3 in Figure 5.1). Here we present a more detailed analysis of the internal layer shapes in these flat ice terrains using a simple two-dimensional ice flow model. Our goals are to determine the origin and significance of the flat-ice terrains and to test the hypothesis that they represent a grounding zone that existed in the mouth of KIS prior to its shutdown.

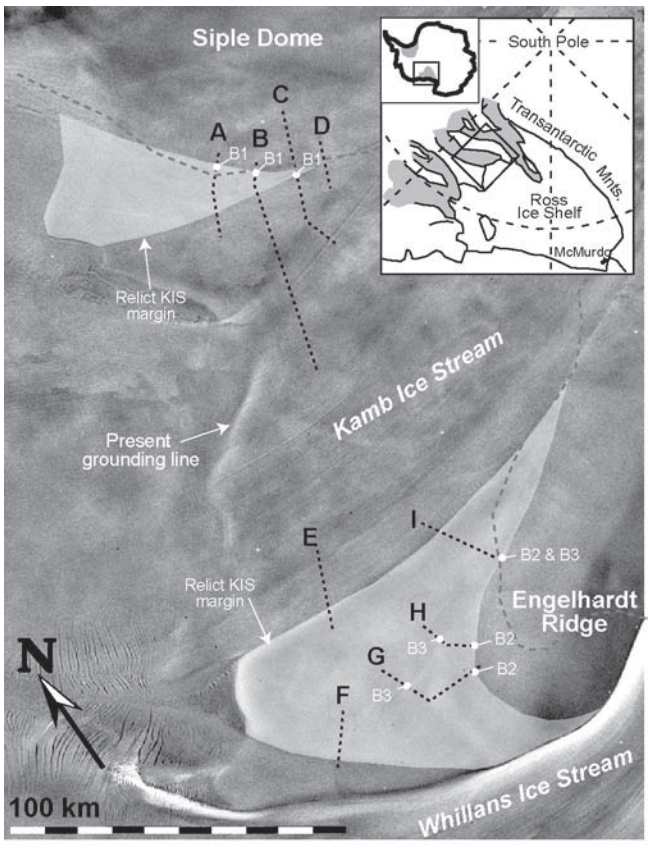

Figure 5.1: .

RADARSAT image of the mouth of KIS. The flat-ice terrains are identified by light shading and are bounded by B1 and B2 and relict KIS margins identified in Chapter 4. Black dotted lines show locations of ice-penetrating radar profiles labelled A-I. Grey dashed line defines the 200 m contour interval of surface elevation as determined by the RAMP DEM (Joughin and others, 2003b) defined as the approximate upstream boundary of the relict grounding zone. Inset shows our field site in context of West Antarctica.

5.3 Internal Layers in Flat-Ice Terrains

Flat-ice terrains bound the downstream end of Kamb Ice Stream (KIS) and separate the ice stream from the inter-ice stream ridges of Siple Dome and Engelhardt Ridge (Figure 5.1). These terrains are distinguished from other surrounding terrains (ice stream and inter-ice stream ridge) based on the unique pattern of radar-detected internal features found within them ((Catania and others, 2005)). The most unusual internal layer features are found at the boundaries of the flat-ice terrains with adjacent inter-ice stream ridges (B1, B2 and B3 in Figure 5.1). Layers at these boundaries are strongly downwarped over a narrow region forming a "syncline" shape; similar stratigraphy occurs on both sides of KIS (Figure 5.2). On the surface, these boundaries are curvi-linear and wrap around the downstream ends of the inter-ice stream ridges. The salient characteristics of these syncline-layers and the flat-ice terrains that they bound (described in detail in Catania and others (2005)) are listed below. Some of these characteristics are related.

1. Geometry and topography of flat-ice terrains (Figure 5.1):

   (a) B1 and B2 wrap around ridges and possibly connect through the main body of KIS.

   (b) Surface topography is rougher than ridges, smoother than ice streams.

   (c) Flat-ice terrains and related synclines exist on both sides of KIS, outside of ice stream terrain.

2. Internal layers across syncline-layer features B1 and B2 (Figure 5.2):

   (a) Syncline amplitude increases with depth.

   (b) Deep layers are truncated at the bed.

   (c) Downwarping is narrow in width (∼4km).

   (d) Layer shapes are unrelated to bed topography.

(e) Syncline axis of B1 is tilted slightly away from Siple Dome.

3. Internal structure within flat-ice terrains (Figure 5.3):

   (a) Near-surface layers are continuous but distorted; sometimes distortion has a regular pattern.

   (b) Mid-depth, line-type diffractors occur throughout.

   (c) Diffractors are aligned perpendicular to flow off of the inter-ice stream ridges.

   (d) Sets of diffractors have uniform depth.

   (e) Two sets of deep diffractors are found on the south side of KIS.

   (f) Deep diffractors are located within relict margins but not the main body of KIS.

Our goal is to identify possible processes that could produce the syncline-layer boundaries observed at B1 and B2. We focus on the synclines because they are widespread, detected on both sides of KIS, and because they may be diagnostic of once-active processes that could help determine the origin of the flat-ice terrains.

5.4 Ice-Flow Models

We use a kinematic model of the two-dimensional flow field across the syncline-layer boundaries to model the shape of isochronal layers. We examine three cases; Case 1, a local maximum in the spatial accumulation pattern (e.g. Vaughan and others, 1999); Case 2, a change in the basal slip conditions (e.g. Weertman, 1976; Barcilon and MacAyeal, 1993); and Case 3, a local maximum in basal melt (e.g. Fahnestock and others, 2001).

The flow field is adjusted to accommodate the velocity changes that arise from each of these cases. The model is time-dependent allowing these velocity changes to turn on and off. Isochrone layers are found by tracking particles from the surface of the ice sheet through this time-dependent flow field. Modelled layers are then compared with the layers picked from ice-penetrating radar data crossing B1 (Figure 5.2A). The model includes the following assumptions:

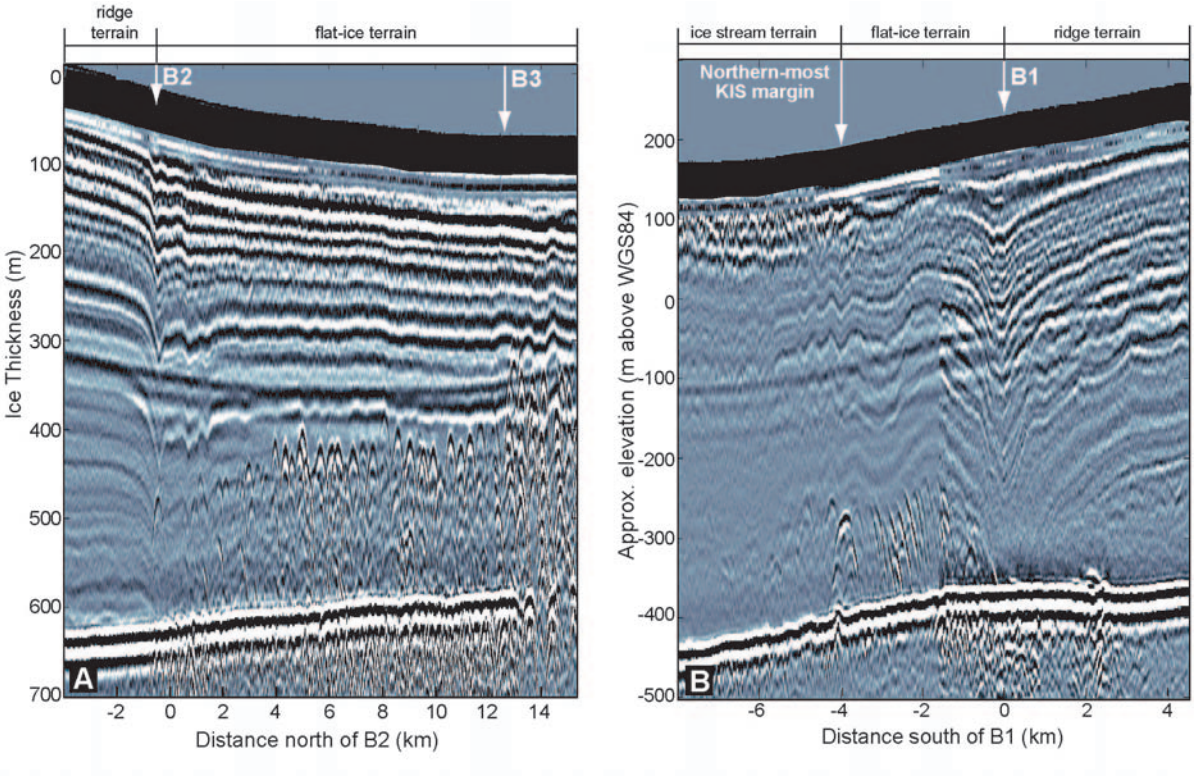

Figure 5.2: A. 2MHz radar profile along Line H (Figure 5.1) crossing B3 and B2. B. 2MHz radar profile along Line B crossing the northernmost margin of KIS and B1 (Figure 5.1). Data in the upper ∼50 m (shown as a black band) are not resolved by the radar system. Note the strong reflector at roughly 300 m depth in both profiles is a system glitch.

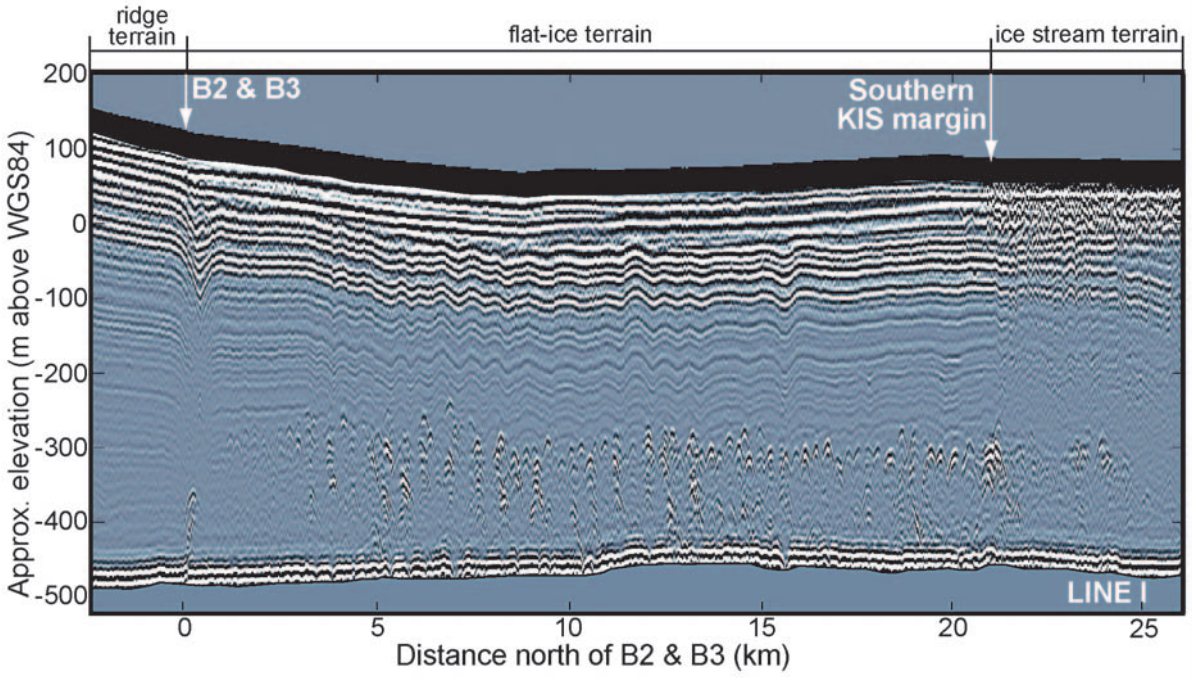

Figure 5.3: 5MHz radar profile along Line I showing the flat-ice terrain and its boundaries. Data in the upper ∼50 m (shown as a black band) are not resolved by the radar system.

1. Ice sheet geometry is steady state and two-dimensional.

2. Ice deforms according to Glen's non-linear flow law, $\dot{\epsilon} = A(T)\tau^n$, which relates the effective shear strain rate $\dot{\epsilon}$ to the effective shear stress τ with the degree of non-linearity described by $n = 3$ (Glen, 1958).

3. We use a depth-averaged value for $A(T)$, the temperature-dependent flow parameter, of 2.0×10^{-15} kPa^{-3}s^{-1}, for temperatures of roughly -4°C (Paterson, 1994, p. 97).

4. The background accumulation rate is assumed to be constant at 0.05 m a^{-1} ice equivalent based on an average of local measurements by Nereson and others (2000) and Giovinetto and Zwally (2000).

5. Where the basal melt rate is zero, ice is frozen to the bed.

We specify bed $B(x)$ and surface $S(x)$ elevations from our radar profiles and assume a constant flowband width, $W(x) = 1$ where x follows the flow direction from the ice divide and z is the vertical coordinate. Since our radar data do not extend up to the ice divide, we provide an input flux $q_{\rm in}$ and age-depth profile at $x = x_{\rm in}$.

The depth-averaged horizontal velocity is

$$\overline{u}(x) = \frac{q(x)}{H(x)\,W(x)} \tag{5.1}$$

where $H(x)$ is the ice thickness, $q(x)$ is the steady-state horizontal ice flux

$$q(x) = q_{\rm in} + \int_{x_{\rm in}}^{x} \dot{b}(x)\,W(x)dx\ . \tag{5.2}$$

and $\dot{b}(x)$ is the accumulation rate. Following Reeh (1988), we define the horizontal velocity $u(x, z)$ in terms of a depth-averaged horizontal velocity $\overline{u}(x)$ and a non-dimensional

horizontal velocity shape function $\phi(x, \hat{z})$

$$u(x, z) = \overline{u}(x)\phi(x, \hat{z}) \tag{5.3}$$

where

$$\hat{z} = \frac{z - B(x)}{H(x)}. \tag{5.4}$$

The vertical velocity follows from incompressibility,

$$\frac{\partial w}{\partial z} = -\frac{\partial u}{\partial x}, \tag{5.5}$$

and vertical integration from the bed gives:

$$\begin{aligned} w(x, z) = -\dot{b}(x)\psi(x, \hat{z}) + u(x, z)\left((1 - \hat{z})\frac{dB}{dx} + \hat{z}\frac{dS}{dx}\right) \\ -\overline{u}(x)H(x)\int_0^{\hat{z}} \frac{\partial \phi(x, \hat{z})}{\partial x} d\hat{z} \end{aligned} \tag{5.6}$$

where

$$\psi(x, \hat{z}) = \int_0^{\hat{z}} \phi(x, \hat{z}) d\hat{z}. \tag{5.7}$$

is the non-dimensional vertical velocity shape function (Waddington and others, 2004).

Following Dansgaard and Johnsen (1969) the horizontal shape function $\phi(x, \hat{z})$ is:

$$\frac{\partial u}{\partial z} = 2A\left(\rho g \frac{dS(x)}{dx}\right)^n H(x)^n \,, \tag{5.8}$$

where ρ is ice density, g is gravitational acceleration, and $n = 3$ is the flow-law exponent. Integration of Equation (5.8) gives

$$\overline{u}(x) = \frac{2A}{n+2}\left(\rho g \frac{dS}{dx}\right)^n H(x)^{n+1} \tag{5.9}$$

$$\phi(x, \hat{z}) = \frac{n+2}{n+1}(1 - (1 - \hat{z})^{n+1}). \tag{5.10}$$

assuming that A is independent of depth. Equations 5.3 and 5.6 describe the two-dimensional flow field. Particle trajectories through this flow field are linked at common ages to calculate the shape of the internal layers.

5.4.1 Case 1: Accumulation Anomaly

A local maximum in the spatial accumulation pattern can occur from changes in slope where windblown snow accumulates. Such a spatial pattern in accumulation can produce downwarped layers (Vaughan and others, 1999). To test if the synclines formed from a high local accumulation anomaly we choose a spatial pattern of accumulation described by a Gaussian distribution with a peak centered over the maximum dip in the syncline layers such that:

$$\dot{b}(x) = \dot{b}_0 + \dot{b}_p e^{-c_1(x-x_0)^2} \tag{5.11}$$

where $\dot{b}_0$ is the background accumulation rate, x_0 is the position of the maximum accumulation rate, $\dot{b}_p$ is the maximum excess accumulation over the syncline-layers and c_1 is a constant that defines the width of the accumulation spike. For each model run we keep $x_0 = 4.5$ km, $\dot{b}_0 = 0.05$ m a^{-1} and adjust c_1 and $\dot{b}_p$. We do not impose temporal change to the anomaly because we expect that spatial changes in accumulation (tied to changes in slope) would be constant over time.

5.4.2 Case 2: Basal Sliding Anomaly

It is also possible that these terrains were once influenced by nearby ice stream behavior and so we impose a horizontal velocity increase similar to ice stream onset regions where surface velocities increase in response to changes in basal slip (Bindschadler and others, 2001). The flow field is modified to accommodate plug flow ($\phi(x, \hat{z}) = \hat{z}$ and $\psi(x, \hat{z}) = 1$) where sliding occurs. Horizontal velocity becomes:

$$u(x, z) = u(x, z) + u_b(x) \tag{5.12}$$

where u_b is the basal sliding velocity. We describe u_b by an arc-tangent function to allow gradation from stuck to sliding over a few kilometers.

Present surface velocities in the flat-ice terrains are low and so we suspect $u_b = 0$ m a-1 today. However, basal sliding could have occurred here in the past since the bed between the flat-ice terrains and the ice streams is flat and it is possible to have melting at the base of the ice outside of an ice stream margin (Jacobson and Raymond, 1998). There are no fast-flow features (buried crevasses and/or flowstripes) in the flat-ice terrains to indicate streaming speeds ($\geq$120 m a^{-1}) and so we investigate conditions of u_b =6 m a^{-1}. Similar velocities have been measured on the flank of Engelhardt Ridge close to the Whillans Ice Stream margin (Whillans and van der Veen, 1993). We note that in order to maintain the balance flux of ice flowing from the ridge (u=3 m a^{-1}) to the flat-ice area (u=6 m a^{-1}), surface velocity off the ridge would need to be $\sim$6 m a^{-1}. Under present day conditions for steady state, a more realistic sliding velocity would be u_b=3 m a^{-1} in the flat ice terrain and our choice of u_b=6 m a^{-1} therefore represents an upper limit. Smaller rates of sliding would tend to have less effect on the deformation of internal layers.

Sliding is made time-dependent as follows:

$$u_b(x,t) = \begin{cases} 0 & \text{for } t \leq T_1 \\ u_b(x) & \text{for } T_1 < t \leq T_2 \\ 0 & \text{for } t > T_2 \end{cases} \tag{5.13}$$

where T_1 and T_2 are fractional times of the maximum model time span t. From time $t = 0$ to $t = T_1$ the model is run with no special dynamics. Sliding occurs from time T_1 to T_2 and subsequently the flow field returns to one of no special dynamics.

5.4.3 Case 3: Basal Melting Anomaly

Our final test is to impose spatial and temporal variation in the basal melt rate which increases vertical velocity at the base of the ice. An example of this condition is given by Fahnestock and others (2001) who argue that downwarped layers observed in Greenland are

linked to locally elevated geothermal flux.

We use an equation similar to Equation 5.11 to describe a local spatial pattern of basal melt:

$$\dot{m}(x) = \dot{m}_0 + \dot{m}_p e^{-c_2(x-x_0)^2} \tag{5.14}$$

where we vary $\dot{m}_p$, the peak melt rate, but keep x_0 =4.2 km, $c_2 = 6{\times}10^{-7}$ m^{-2}, and $\dot{m}_0 = 0$ m a^{-1}.

Following from Equation 5.13 we make the melt rate time dependent as follows:

$$\dot{m}(x,t) = \begin{cases} 0 & \text{for } t \leq T_1 \\ \dot{m}(x) & \text{for } T_1 < t \leq T_2 \\ 0 & \text{for } t > T_2 \end{cases} \tag{5.15}$$

with melting during time $T_m = T_1 - T_2$. We alter the flow field to reflect both basal melting and basal sliding by using the shape functions for plug flow and combining Equations 5.3 and 5.6:

$$u(x,z,t) = u(x,z) + u_b(x,t) \tag{5.16}$$

$$w(x,z,t) = w(x,z) - \dot{m}(x,t)(1-\hat{z}) \tag{5.17}$$

5.5 Model Results

Modelled results are first qualitatively compared to the layers picked from Figure 5.2B. This is accomplished by examining how well the predicted layers match the entire packet of picked layers. We also examine the ability of predicted layers to reproduce the salient characteristics of the syncline-layer features that were listed in an earlier section.

Case 1 has greatest effect on the near-surface internal layers because of the large near-surface vertical velocity changes associated with an accumulation anomaly. With $\dot{b}_p$=0.085 m a^{-1} spread over ∼4 km it is possible to reproduce the top picked layer, but the rest of the layers are not well matched (Figure 5.4A). Similarly, we can match the bottom layer using

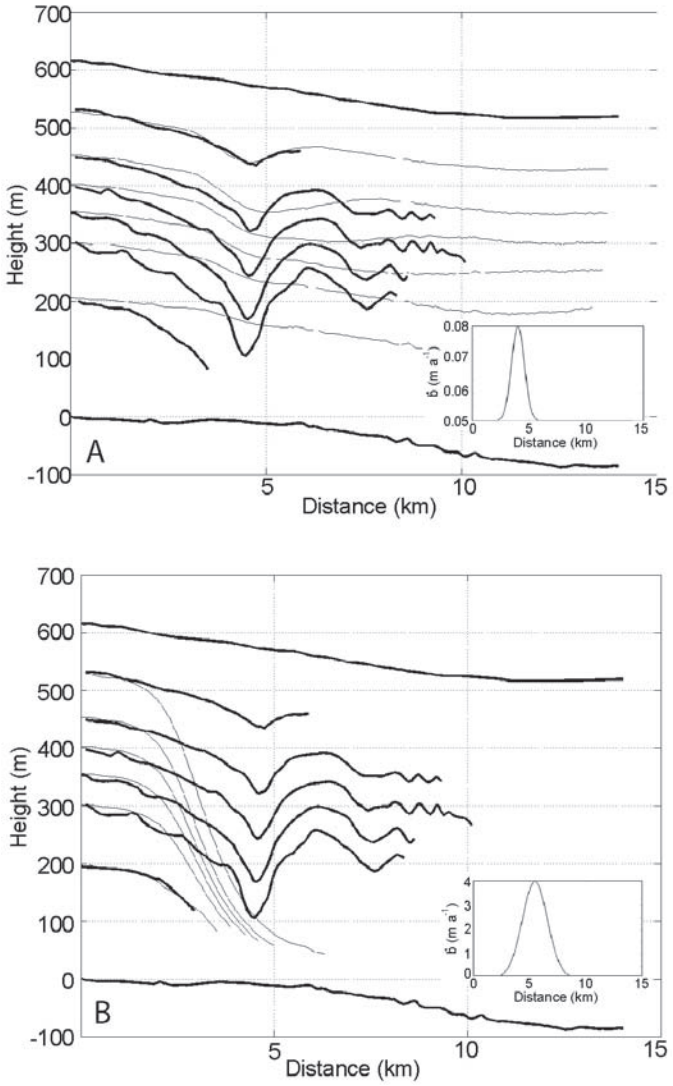

Figure 5.4: Modelled internal layers (thin black lines) for Case 1, a local accumulation maximum. Observed layers (thick black lines) are picked from radar Line B (Figure 5.2B). Insets show accumulation rate (ice equivalent) across the model domain. A. Accumulation case for modelled layers matching the topmost picked layer; $\dot{b}_p$=0.085 m a^{-1}spread over 4 km. B. Accumulation case for modelled layers matching the bottom picked layer; $\dot{b}_p$=4 m a^{-1}, spread over 6.5 km.

an unrealistically high accumulation anomaly ($\dot{b}_p$=4 m a^{-1}, spread over 6.5 km) but the match with upper layers is poor (Figure 5.4B). In addition, Case 1 does not explain many of the characteristics of the syncline-layer features listed earlier; (observation 2i) syncline amplitude grows with depth; (2ii) deep layers are truncated by the bed. This is in contrast to the observations of Vaughan and others (1999) who see spatial changes in layer thickness across their features.

It is also difficult to develop a hypothesis that can link the formation of deep diffractors to an accumulation spike (observation 3). It is possible that a local high in accumulation can contribute some amount of layer downwarping (especially in the uppermost layers) but this mechanism acting alone cannot produce the observed characteristics in these terrains.

For Case 2 we first tested the scenario of a spatial change in sliding velocity across the domain with no time dependence. Results (not shown) indicate that the formation of a layer syncline is impossible because layers become downwarped at the no slip/slip transition and remain downwarped across the domain.

Temporal changes in basal sliding are examined using Equation **??**. In this scenario, the spatial pattern in basal sliding is prescribed and sliding is turned on and off during the model time as described by Equation 5.13. Results from this indicate that as in Case 1, we are unable to match the entire packet of observed layers. The top picked layer can be matched with 6 m a^{-1} sliding rate for 30 years but this does not produce acceptable fits to the bottom layers (Figure 5.5A). Using the same sliding velocity we are able to match the bottom layer by increasing the amount of sliding time to 650 years but this tends to downwarp the upper layers too much (Figure 5.5B).

Furthermore, a scenario involving basal sliding cannot explain several of the characteristics of the syncline-layer boundaries including (2i) syncline amplitude grows with depth and (2ii) deep layers are truncated by the bed. We conclude from this that basal sliding alone cannot reproduce the observed layers. However, as with the accumulation case, we cannot rule out that some component of the layer shape could be attributed to sliding.

We tested Case 3 (localized basal melting) in which melting occurs for the total model

time (results not shown). As with the case of basal sliding, modelled layers become downwarped and remain downwarped across the domain and so we do not believe that melting was long lived. Case 3 was also tested with a temporal variation in basal melt (Figure 5.6). Qualitatively this case best fits the picked internal layers as the entire layer packet can be matched and several key layer characteristics are replicated; (2iii) focussed downwarping; (2i) increasing syncline amplitude with depth and (2ii) the truncation of deeper layers (Figure 5.6). Hence we explore Case 3 in more detail by adjusting model parameters to best fit the observed layer pattern.

5.6 Calculation of Model Performance

Our goal is to match layers of the same age. To do this, we trace layers of known age from the core site at the summit of Siple Dome to the edge of our model domain using an established age-depth scale for Siple Dome (Taylor and others, 2004). This gives an age-depth profile for the six internal layers picked from Figure 5.2B. Each picked layer is denoted by the index j with points along the layer in the x direction denoted by i, the total number of points along a layer being n_j. The shape of each layer is obtained by measuring its elevation S_{ij} at each position i along each layer j. We define a chi-square performance index J in terms of observed and modelled layers (S^o_{ij} and S^m_{ij}):

$$J = \frac{1}{N-p} \sum_{j=1}^{6} \sum_{i=1}^{n_j} \omega_{ij} \frac{(S^m_{ij} - S^o_{ij})^2}{\sigma_j^2} \tag{5.18}$$

where $N = \sum_j n_j$ is the total number of points sampled in the domain, and p is the number of free parameters in the model less one. We use a weighting function ω_{ij} to give increased weight to the residual in the syncline area.

The expected combined error σ_j consists of uncertainties in the model and the data. Following Nereson and others (1998) we assume a total error of 3-6 m which includes error from simplifications made with the model, picking precision, processing errors and errors from converting the travel-time to depth. Models within the $J < 1$ contour fit the data to

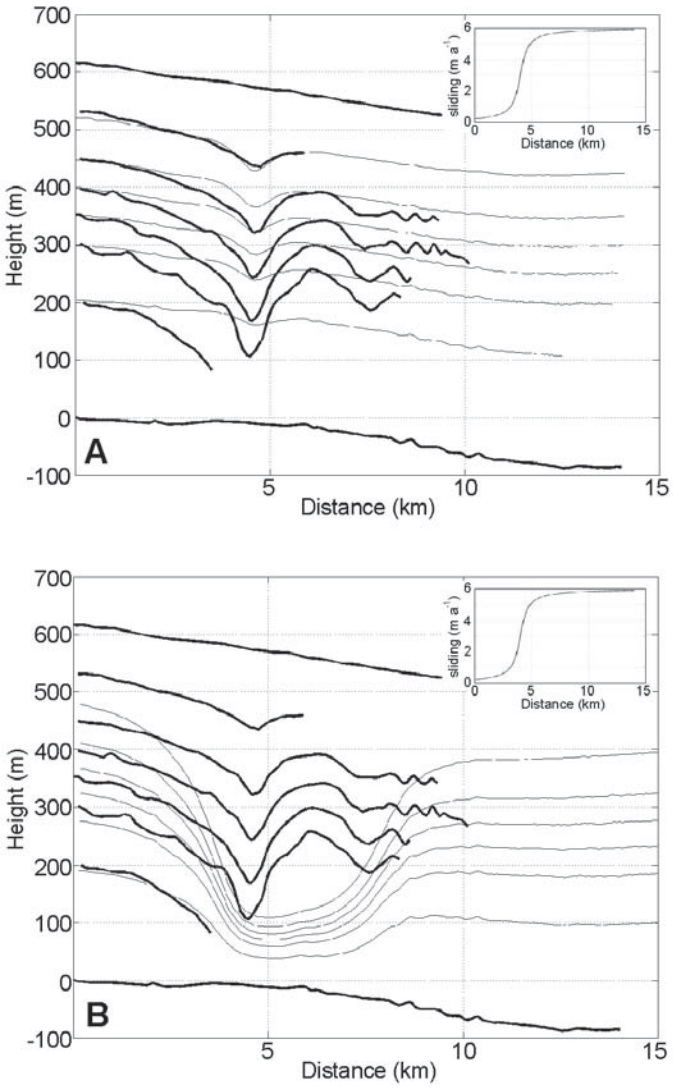

Figure 5.5: Modelled internal layers (thin black lines) for Case 2, change in slip condition with a 6 m a^{-1} sliding rate. Observed layers (thick black lines) are picked from radar Line B (Figure 5.2B). Insets show sliding velocity across the model domain. A. Sliding case for modelled layers matching the topmost picked layer; sliding time of 30 years. B. Sliding case for modelled layers matching the bottom picked layer; sliding time of 650 years.

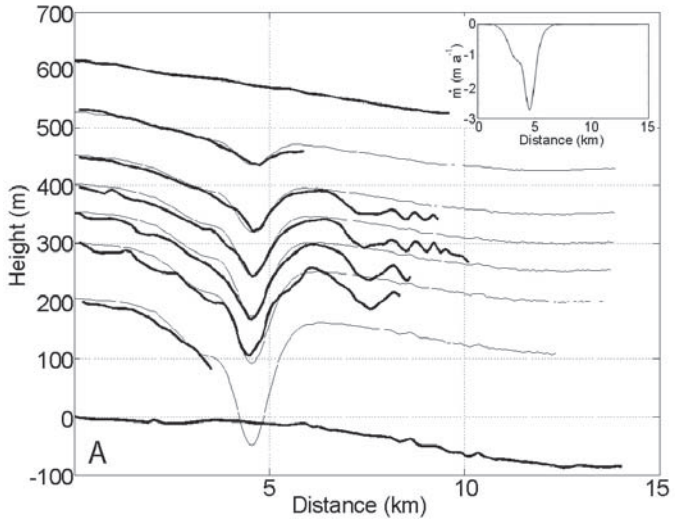

Figure 5.6: Modelled internal layers for one best-fit solution of Case 3 (basal melt) with T_m =100 years and $\dot{m}_p$=2.5 m a^{-1}. Observed layers (thick black lines) are picked from radar Line B (Figure 5.2B). Inset shows melt rate across the model domain.

within the expected errors.

5.6.1 Best-fit Melting Solution

We choose to vary the peak melt rate $\dot{m}_p$ and the length of melt time T_m because in combination these parameters determine the total amount of bottom melting. The highest rates of basal melt (up to 45 m a^{-1}) have been estimated at the grounding lines of several Antarctic glaciers (Rignot and Jacobs, 2002). For simplicity we choose not to vary the location of melt maximum (x_0=4.2 km) or the shape of the Gaussian melt-curve (c_2=6×10^{-7} km^{-2}). Our results show that the two-dimensional parameter space that defines the best fit (minimum J) is not entirely enclosed by a contour indicating an unbounded degree of non-uniqueness (Figure 5.7A).

We can reduce the range of acceptable solutions by imposing a reasonable limit to the peak melt rate based on physical grounds. Analysis of the observed layer pattern suggests that a maximum of 150-200 m of basal ice has been melted. Furthermore, we expect some effects from basal sliding due to the availability of water at the bed and perform a second misfit analysis using the same range in melt rates as above but with u_b =6 m a^{-1}. This further limits the range of acceptable solutions to those with T_m between 8-130 years (Figure 5.7B).

5.7 Discussion: Mechanisms of Basal Melt

Based on these results, we believe that the syncline features formed through basal melting over a short time (<300 years) and over a short distance (∼2 km). We now search for a process involving basal melt with this temporal and spatial pattern. We prefer a hypothesis that is consistent with the internal layer characteristics listed in an earlier section, namely the presence of deep diffractors and the geometry and orientation of the syncline-layer boundaries on the surface. We consider several hypotheses; focussed melting within an ice stream shear margin; basal melting from increased geothermal heat; melting above a subglacial water channel and focussed basal melting at the grounding line.

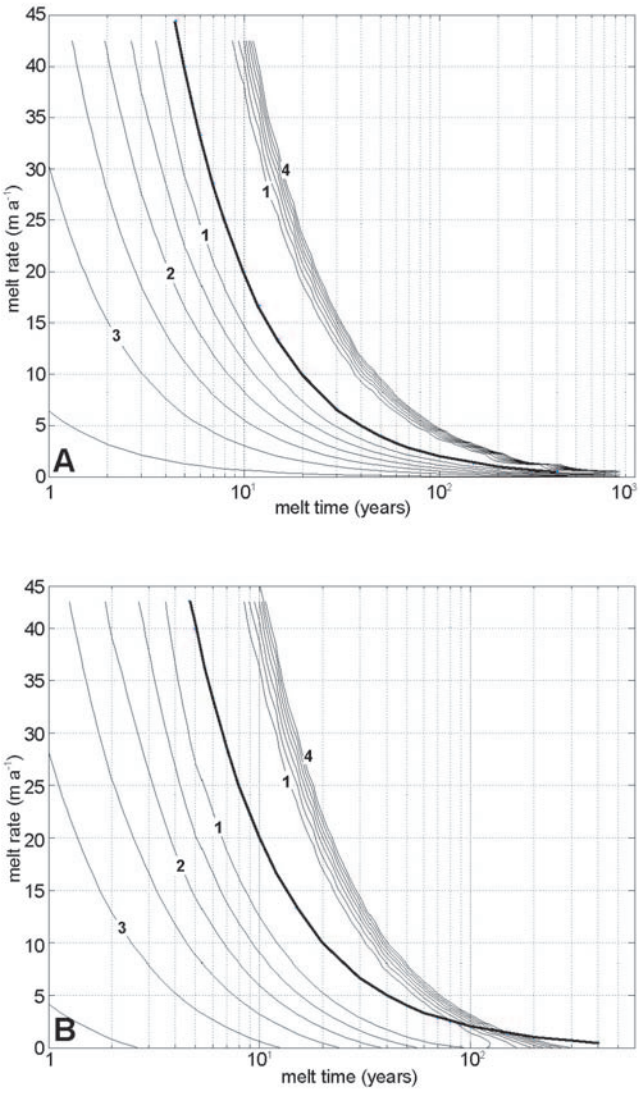

Figure 5.7: Semi-log plot of the model misfit for Case 3, local melt maximum with varying melt time T_m and melt rate $\dot{m}_p$. Contours for J are shown with a 0.5 interval. Thick black line indicates the 200 meters of melt contour. A. Case 3 with no sliding. B. Case 3 with u_b =6 m a^{-1}.

Shear deformation in ice stream margins could be large enough to locally elevate temperatures and focus melting possibly causing layer downwarping (Harrison and others, 1998; Jacobson and Raymond, 1998). However, Catania and others (2005) argue that the synclines are not related to ice stream margins (and thus the flat-ice terrains are not relict ice stream terrains) for several reasons; (1) many typical internal layer characteristics found in ice stream margins (near-surface diffraction from buried crevasses and highly distorted, discontinuous deeper layers), are not observed in the flat-ice terrains; (2) internal layer synclines and deep diffractors are features not typical of radar profiles across both active and relict margins; (3) the trend of the syncline-layer boundaries on the surface deviates substantially from the paleo-flow direction of the ice stream; (4) large distances exist (up to 30 km) between syncline-layer boundaries and the locations of established relict margins. For these reasons we dismiss the hypothesis that the syncline features originated as ice stream margins.

Focussed basal melting can also occur at a geological boundary with active rifting (e.g. Fahnestock and others, 2001). Unlike in ice stream margins, this could cause a internal layer syncline to develop in otherwise undisturbed isochrones. Furthermore, a geologic boundary might be aligned with the topographic boundary of the ridges explaining the orientation of the syncline-layer boundaries on the surface. However, several features related to the synclines and terrains cannot be easily reconciled with this hypothesis; (1) localized geothermal heating provides no mechanism to cause the pervasive deep diffractors seen in the adjacent flat-ice terrains; (2) we expect that geologic sources of heat would be much more constant over time and not appear to turn on or off as we have deduced; (3) most aeromagnetic anomaly sources at the base of the ice have low bed relief (60-600 m) (Behrendt and others, 2004) while no bed relief is seen here and; (4) we expect that melting from increased geothermal heat would be more widely distributed than the narrow region of basal melt observed, unless the heat source is very shallow. Aerogeophysical surveys have been completed for parts of the Siple Coast (Behrendt and others, 2004) however, no data exists for the downstream end of KIS. This makes it difficult to completely rule out the possibility

that increased geothermal heat in these areas may be responsible for the observed basal melting.

Water moving through a conduit at the base of the ice releases viscous energy which can focus melting in the region above the conduit. While this may provide a mechanism for localized layer downwarping, it does not explain the presence of the numerous deep diffractors within the adjacent flat ice terrains. Furthermore, we believe that surface gradients (which dominate the hydraulic gradient) are too low in these regions to focus subglacial melt water so highly. More likely (if meltwater did indeed exist beneath these regions), are the interconnected channel networks described by Kamb (2001) and Catania and Paola (2001).

Focussed basal melting is also possible at the grounding line beneath ice shelves through one mode of ice shelf melting known as thermohaline circulation (Gill, 1973). This process occurs when salt is concentrated in seawater during sea ice formation producing dense, high-salinity shelf-water HSSW which could be up to 0.5^{o}C warmer than the freezing point of the ice shelf base because of the greater hydrostatic pressure below the ice (Gill, 1973).

Unlike the previous hypotheses, this hypothesis can explain the geometry and internal layer characteristics of the syncline-layer boundaries. In addition, floatation (or near-floatation) can cause basal crevassing which provides an explanation for the deep diffractors (Van der Veen, 1998). Similar diffractors seen on ice shelves are also interpreted to be basal crevasses (Jezek and others, 1979; Jezek and Bentley, 1983; Uratsuka and others, 1996). Furthermore, the incursion of marine waters beneath the ice in the trunk of KIS may be responsible for the high bed reflectivity measured there (Bentley and others, 1998; Catania and others, 2003). Lower bed reflectivity within the flat-ice areas outside of the main body of KIS may be due to signal scattering within the bottom crevasses throughout these areas.

Other observations argue against floatation conditions in the mouth of KIS; (1) BEDMAP data indicate that the ice here is currently 40-80 m above floatation (Catania and others, 2005); (2) the pattern of basal melt beneath ice shelves is largely unknown. Modelled melt rates show that melting associated with thermohaline circulation is spread out over $\sim$20 km

from the grounding line (Joughin and Padman, 2003; Jenkins and Doake, 1991) however, interpretation of internal seismic reflectors suggests that much more focussed rates (up to 7 m a^{-1} over 4 km) may be possible Smith (1996); (3) the present grounding line is ∼100 km downstream of B1 and B2 implying rapid grounding line retreat and re-advance.

In lieu of a more acceptable hypothesis, we believe that the balance of evidence favors syncline formation through grounding line melt because this hypothesis can explain nearly all of the internal layer characteristics observed. Two separate lines of evidence indicate that floating conditions ended some time ago. First, we have not detected bottom crevasses in the main body of KIS (from radar profiles as close as 20 km to the grounding line). If streaming flow continued through this area after it stopped floating (over a distance of 140 km at velocities as high as ∼700 m a^{-1}) we estimate that all of the basal crevasses could be evacuated from the main body of KIS in ∼200 years and thus that floatation last occurred 350 years ago. Second, Catania and others (2005) demonstrate that the tilt of the syncline axis nearest to Siple Dome could be created through ∼170 years of flow from Siple Dome subsequent to the cessation of basal melting. On the south side of KIS, B2 and B3 are vertical implying recent grounding and/or very little accumulated flow off of Engelhardt Ridge (Figure 5.2A). However, the presence of two syncline-layer boundaries here implies two different grounding or coupling line positions in the past, both possibly short lived but representing a cumulative time in ungrounded conditions which matches that determined for the north side of KIS.

5.8 Elevation of KIS 350 Years Ago

We use the uppermost estimate of when floating conditions ended (350 years ago) to examine the likelihood that the ice in the mouth of KIS could have been floating at that time based on changes in mass balance and ice dynamics. We calculate the height above buoyancy H_{ab}, using a depth averaged ice density following Van der Veen (1998) to account for the variation in density within the firn layer

$$\bar{\rho} = \rho_i - \frac{\rho_i - \rho_s}{CH}[1 - e^{-CH}] \tag{5.19}$$

where $\rho_i = 910$ kg m^{-3} and $\rho_s = 350$ kg m^{-3} are ice and snow density respectively, H is ice thickness and C is a constant that ranges from 0.0165 to 0.0314 m^{-1} (Paterson, 1994, pg. 16) depending on accumulation and the rate of snow densification. We choose C =0.0238, its value at Siple Dome (Hawley and others, in press). Height above buoyancy is then expressed as

$$H_{ab} = S - (1 - \frac{\bar{\rho}}{\rho_w})H \tag{5.20}$$

where S is the surface elevation above sea level and ρ_w is the density of sea water (1027.5 kg m^{-3}). We use ice thickness and surface elevation measurements from ice-penetrating radar and GPS data (corrected from the WGS84 ellipsoid to sea-level) to define a more accurate range of modern H_{ab} (Table 5.1). The coverage of our data indicate that the flat-ice terrains are currently 50-100 m above buoyancy with maximum H_{ab} at the edges of the terrains (B1 and B2). Measurements on the Ross Ice Shelf shows that $\bar{\rho}$ can vary by $\pm$5% (Shabtaie and Bentley, 1982). If $\bar{\rho}$ is just 5% lower (due to changes in the salinity content, presence of basal crevasses, ice thickness, and changes in the depth of the firn, etc.), modern H_{ab} would be 25-70 m illustrating the sensitivity of H_{ab} to subtle changes in density.

Assuming that outflow from the flat-ice terrains is negligible (due to low surface slopes), several processes have affected buoyancy in this area over the last 350 years:

1. Relative sea-level drop is estimated at 1 m over the last 350 years from isostatic rebound at a rate of 5 mm a^{-1} (James and Ivins, 1998) and global sea level rise at 2 mm a^{-1} (Miller and Douglas, 2004).

2. Measured and calculated accumulation rates from several locations in the grounding zone (Giovinetto and Zwally, 2000; Nereson and others, 2000) give an estimate of 18-25 m of ice equivalent thickness change in the last 350 years.

3. Current rates of basal freeze-on for KIS estimated by Joughin and others (2003a) are roughly 8 mm a^{-1} in the grounding zone, or ∼3 m in 350 years.

4. Expansion of the inter-ice stream ridges after margin shutdown, described by Nereson (2000) is estimated to be as high as 31 m in locations where B1 and B2 are close to the relict margins of KIS and only 1 m at larger distances (∼20 km) from the margins.

From these four processes, we estimate a minimum total thickness change of ∼20 m (in the middle of the flat-ice terrains) and a maximum total thickness change of ∼60 m (for areas close to the junction between relict margins and inter-ice stream ridges). We predict that 350 years ago, ice in the lower end of KIS was 25-55 m above floatation.

It is still possible that an ice shelf existed in the mouth of KIS, and we argue that additional ice thickness changes here could be related to longitudinal compression similar to the thickness changes observed in the central portion of KIS (Price and others, 2001; Joughin and others, 2003b). It is thought that grounding of the Steershead Ice Rise (∼90 km downstream of Siple Dome) occurred ∼350 years ago because of thickening from the expansion of WIS (Fahnestock and others, 2000). In addition, the inward migration of the northern KIS margin between 300-500 years ago (Nereson, 2000) likely also caused thickening in the mouth of KIS. We estimate that if KIS flux decreased by as little as 5 km^3 a^{-1}, 200 years prior to its shutdown that ice in the mouth of KIS (an area of 20,000 km^2) could thicken by as much as 50 m. Local blocking of the outflow might leave topographic bumps in the flat-ice terrains and satellite images do show rougher topography in these areas compared to the ridges.

Table 5.1: Latitude, Longitude, Surface Elevation (m above WGS84), Ice Thickness (m), local WGS84 geoid correction (m), Height above buoyancy H_{ab} and estimated H_{ab350} for conditions ∼350 years ago in the flat-ice terrains on both sides of Kamb Ice Stream.

Location	Lat.	Long.	S	H	WGS84$_{cor}$	H_{ab}	H_{ab350}
Duckfoot min.	-82.22	-150.05	120	633	-46.17	67.1	49.4
Duckfoot max.	-82.17	-149.93	147	602	-46.2	96.9	53.6
Goosefoot min.	-83.23	-151.19	21	505	-44.54	50.1	27.1
Goosefoot max.	-83.39	-150.30	119	562	-44.31	71.7	48.7

5.9 Synthesis

Our model results indicate that not all processes causing local layer downwarping produce similar-looking internal layer patterns; both a local peak in accumulation and basal sliding produce layers that show changes in thickness across the model domain that are not qualitatively consistent with the observed layer structure. In contrast, localized basal melting produces downwarped layers that maintain constant thickness, show increasing amplitude with depth and can explain truncation of basal layers. From this, we conclude that the processes responsible for the syncline-layer boundaries must contain some component of basal melting, with less important contributions from sliding and/or local accumulation gradients still possible. While we propose several mechanisms that involve basal melting none can explain all of the observed layer and topographic characteristics. Fewer still, (arguably none) can explain the transient nature of the melting and its narrowly focussed spatial pattern. Because it can explain the most modelled and observed characteristics, we put forth an hypothesis that the synclines mark the edge of a relict ice shelf or grounding zone in the mouth of KIS with numerous diffractors here caused by basal crevassing as is typical in ice shelves.

Joughin and others (2003b) suggest that rapid thinning in an ice stream could cause it to become afloat. Numerical ice stream modelling by (Bougamont and others, 2003) shows that width is a key factor in determining the longevity of streaming flow. They argue that the stoppage of KIS is unavoidable if its width grows beyond ∼80 km. This is smaller than the estimated pre-shutdown width of 100-120 km discussed by Catania and others (2005) and indicates that progressive thinning in the mouth region could have caused this region to go afloat.

The boundaries of a grounding zone move in response to changes in ice thickness and sea level with increases in ice thickness or decreases in sea level leading to advance, and the opposite for retreat. Since sea-level changes were small over the estimated time of grounding line fluctuation, any variability in the buoyant condition requires regional changes in ice

thickness over relatively short time scales (i.e. century scale). Short time-scale variations in grounding line position are observed for Pine Island Glacier (Rignot, 1998) and have raised concern about the collapse of the ice sheet through continued grounding line retreat over inwardly sloping bed topography (Weertman, 1974). In contrast, we see that grounding line retreat, at least for KIS, is limited (possibly by the presence of the stable inter-ice stream ridges) and ice streams are eventually forced to slow when they become too thin. As a result, grounding zones are likely to be transient features in the lifetime of an ice stream.

Chapter 6

RECENT FLOW HISTORY OF THE KAMB ICE STREAM AREA, WEST ANTARCTICA

6.1 Summary

Ice-penetrating radar profiles across several buried margins in the Kamb Ice Stream (KIS) area, West Antarctica, are used to reveal the time of margin burial. These times are combined with satellite data and other sources of information to deduce a 700 year ice flow history for the KIS area including details about its recent shutdown. This history is dominated by short-term (century scale) variability in ice stream margin positions and discharge that is likely linked to changes in subglacial conditions and ice thickness. We argue for the existence of a wide, thin, ungrounded region in the lower trunk of KIS until at least 350 years ago. Lagged development of the subglacial drainage system after grounding may have slowed the transport of meltwater generated in the tributaries to the freezing trunk region. Shutdown of the ice stream would result from basal freezing before this drainage system could be re-established. We believe that the short-term variability observed in this area is indicative of an ice stream system that is constantly responding to shifts in basal resistance, sea level, and flux of tributary streams, but which is stable over large temporal and spatial scales.

6.2 Introduction

Since the end of the last glacial maximum (LGM) ∼14,000 years ago, losses of ice volume and grounding line retreat in Antarctica have been greatest in the West Antarctic Ice Sheet (WAIS) (Conway and others, 1999; Bindschadler, 1998) where outflow is largely through fast flowing ice streams. This has led to concern over the future stability of the WAIS in

a changing climate. Ice streams appear to exhibit short-term (century scale) changes in discharge, position and flow direction (Rignot, 1998; Jacobel and others, 2000; Fahnestock and others, 2000). Such variability may in part, be related to sea level and climatic changes such as the end of the LGM; however, the exact response of the ice streams to forcing remains unclear. It is equally likely that these short-term changes are instead indicative of natural adjustments that are driven by feedbacks that are entirely internal to the ice stream system.

Kamb Ice Stream (KIS) illustrates the uniqueness of the Siple Coast ice stream system. No where else do we see an ice stream that, despite a large and active catchment, has little or no flow in its lower region (here called the "trunk"). There are several contrasting views regarding the cause and pattern of the KIS shutdown ∼150 years ago (Retzlaff and Bentley, 1993). Two competing hypotheses have emerged; (1) the ice stream suffered from "water piracy": a diversion of basal water (and latent heat) away from the trunk of the ice stream causing a reduction in speed due to insufficient basal lubrication (Anandakrishnan and Alley, 1997; Alley and others, 1994). Maps of hydraulic potential indicate that piracy likely occurred near the upstream end of Engelhardt Ridge implying that stagnation initiated there and migrated toward the grounding line; (2) the ice stream stopped when the basal thermal regime in the trunk switched from melting to freezing following ice stream thinning (Bougamont and others, 2003). A small reduction in the water content of underlying till through basal freezing can lead to significant strengthening (Tulaczyk and others, 2000b) and the ice stream will slow as basal resistance increases at a rate faster than can be compensated for through increased driving stress. In this hypothesis stagnation initiates near the grounding line with ice stream shutdown in roughly ∼100 years (Bougamont and others, 2003).

These are not the only hypotheses for ice stream shutdown (for a review see Anandakrishnan and others (2001)) and it is possible to imagine that ice streams could shutdown for different reasons. For example, "ice piracy" can cause discharge to be re-routed due to regional changes in topography (Rose, 1979) and is thought to be the cause behind the

shutdown of a tributary to KIS (Conway and others, 2002). Here we present a history of the rapid (century scale) changes that KIS and to some degree Whillans Ice Stream (WIS) underwent in the past several hundred years prior to the shutdown of KIS. This reconstruction is based on ice-penetrating radar data presented in Chapter 4 and constrained by additional published and unpublished data. Our ability to predict the outcome of the WAIS amidst a changing climate is limited by our ability to understand the mechanics that control the behavior of the ice stream system. Our aim is to illuminate the changes in activity of KIS prior to shutdown in context of the behavior of the ice stream system as a whole.

6.2.1 Results from Other Studies

We examine the ice flow history in the KIS area constrained with observations from several other published sources. Ice-penetrating radar has been used to obtain ages of buried margins (Clarke and others, 2000; Retzlaff and Bentley, 1993; Smith and others, 2002; Conway and others, 2002; Catania and others, 2003) and has also been used to map the spatial pattern of bed echo strength to infer ice flow history (Catania and others, 2003; Gades and others, 2000; Bentley and others, 1998; Jezek, 1984). Modern rates of ice stream boundary migration have been measured through repeat GPS surveys (Echelmeyer and Harrison, 1999; Thomas and others, 1988). Satellite images also show many flow features (flowlines and crevasse traces) preserved on the ice sheet surface that reveal ice stream variability over time (Fahnestock and others, 2000). Finally, ice flow models can be used to test different scenarios that give rise to observations helping to set limits on past ice sheet behavior (Chapter 5 and Nereson, 2000; Nereson and Raymond, 2001; Hulbe and Fahnestock, in press).

The aim of this paper is to synthesize results from these previous publications and results from data presented here and in Chapter 5. We assume that the timing of an event (e.g. grounding of the Steershead) provided by outside sources is correct and leave the burden of proof on the authors providing such information. Part of our goal here is to see where our results are consistent with other sources of information and what the implications are

of this combined ice flow history. We specifically compare our results to that of Fahnestock and others (2000) who have provided a highly detailed ice flow history for this area over the last millennia through the interpretation of flow features on the Ross Ice Shelf. Their dates are obtained by examining ice provenance using the modern-day flow field. Likely errors in their age estimates arise from the assumption that this flow field has remained constant through time.

In Chapter 5, I propose that a grounding zone existed in the trunk of KIS, the extent of which aligns with features C1 and C2 (Figure 6.1 and 6.2A). Grounding zones (or "ice plains") are regions at the downstream end of ice streams where grounding is ephemeral and/or patchy over large areas and where large, short-term velocity variations are possible due to tidal cycles (Bindschadler and others, 2003; Schmeltz and others, 2001). Grounding zones are delimited at their upstream ends by a "coupling line" (Corr and others, 2001) which separates fully grounded from lightly grounded conditions, and at their downstream ends by a grounding line where the transition to constantly floating conditions occurs. Results from Chapter 5 suggest that a grounding zone in the trunk of KIS could have been active for as long as 300 years and grounded as early as ∼350 years ago. Retreat of the coupling line into the upper reaches of KIS likely occurred over short time scales in two stages as evidenced by two possible coupling line positions in the Goosefoot (Chapter 5).

Hulbe and Fahnestock (in press) lend further evidence for the existence of a grounding zone in the trunk region of KIS. Their examination of flow features on the Ross Ice Shelf near the Steershead reveal flow traces that are not oriented with present-day flow directions. They argue that this pattern of flow traces can be explained if the flow direction was significantly different in the past and/or if the area was once lightly grounded.

6.3 Methodology

Figure 6.1 shows our field area including the flat-ice terrains on either side of KIS that have been nicknamed the Duckfoot (south of Siple Dome) and the Goosefoot (north of Engelhardt Ridge). Surface lineations sub-parallel to the ice flow direction have been

distinguished using ice-penetrating radar and satellite images (Chapter 4). Regions with a similar origin are identified based on their internal layer characteristics. Relict grounding zone terrain contains numerous, deep line-diffractors interpreted to be due to basal crevassing, and is bounded by a surface lineation beneath which internal layers strongly downwarp into a syncline shape (C1 in Figure 6.2A). Relict ice stream terrain is characterized by deep warped layers and bounded by buried shear margins where deep layers are highly-disturbed by high strain and near-surface ($\leqslant$100 m) crevasses are present (M1 and M2 in Figure 6.2).

We use the two-way travel time to the deepest continuous layer (averaged over a few kilometers) with locally determined accumulation rates to date the time of crevasse burial in margins M1-M4 (Figure 6.1). To convert travel time to depth we use a correction for the density variation within the firn layer based on ice core analysis from Alley and Bentley (1988) at the upstream end of Engelhardt Ridge. The standard deviation of layer depth picked in this way is $\sim$4%. Additional error comes from uncertainty in the measured accumulation rate. We use several sources for the accumulation rate and adopt the error associated with these sources; 6% for the Duckfoot (Smith and others, 2002; Nereson and others, 2000) and 15% for the Goosefoot (Venteris and Whillans, 1998).

Nath and Vaughan (2003) show that it is possible for crevasses to form at depth (up to 30 m below the surface) which give the appearance of crevasses buried by many years of accumulation. We believe that the crevasses observed in our data originated at the surface because modern strain rates in these areas are too small to permit crevassing at present. Further, the morphology of M1-M4 on the surface; buried crevasses that span several hundred kilometers in the paleo-flow direction is similar to the morphology of active margins. At worst, the dates estimated here are useful in a relative sense (i.e. they allow us to identify margins that are older or younger than others).

The ages given for margins reflect the time of margin burial by accumulation. However, velocities can still remain high even after crevassing is no longer active. Smith and others (2002) argue that marginal crevasses can only develop when the center-line speed of an ice stream exceeds $\sim$130 m a^{-1}. As a result we expect that the ages of margins presented here

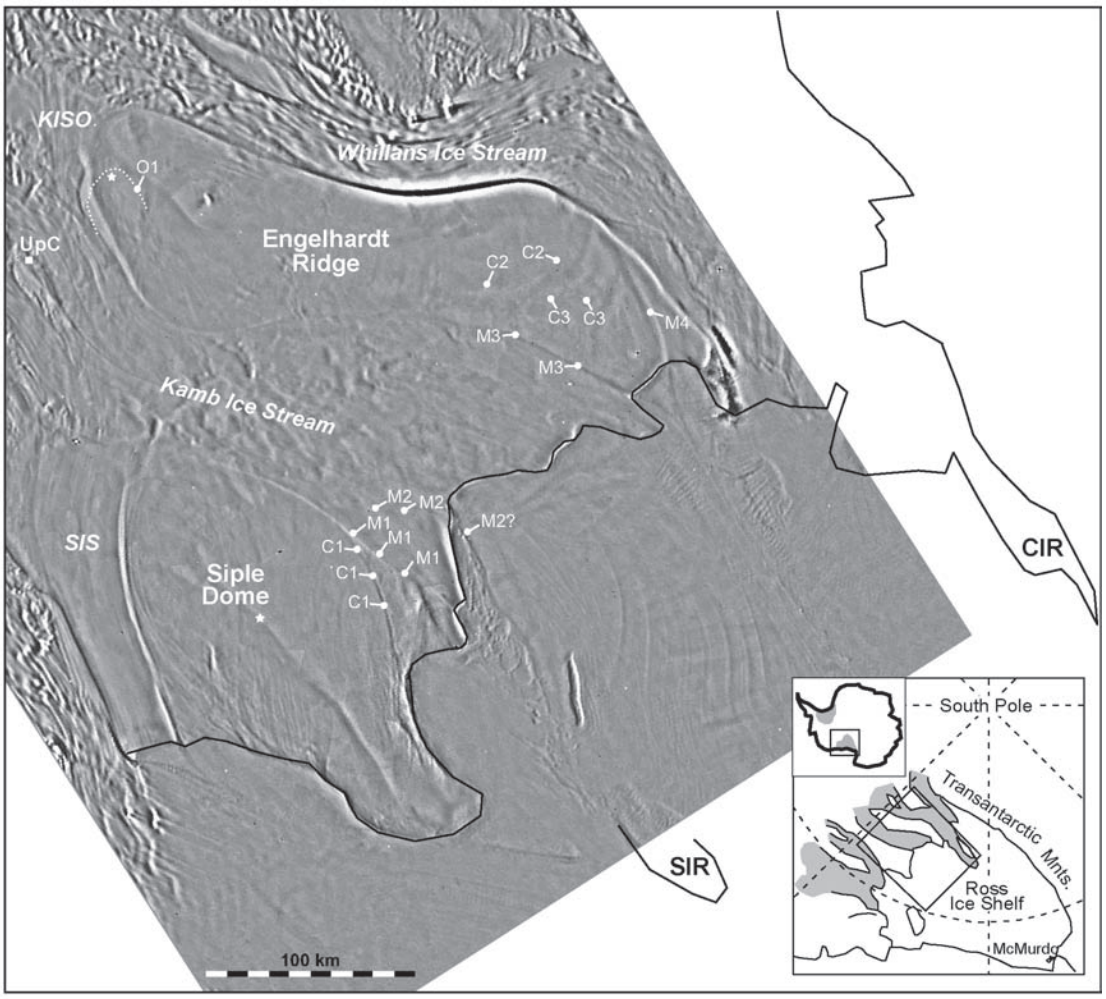

Figure 6.1: AVHRR image of the KIS area. The grounding line is shown in black and outlines the locations of Crary and Steershead Ice Rises not covered by the AVHRR image. Labelled features correspond to boundaries observed with ice-penetrating radar as described in Chapter 4; M1-M4 are relict ice stream margins, C1-C3 are relict coupling lines (limits to ephemeral grounding) and O1 (white dotted line) marks the boundary of shallowly buried crevasses. Sites of ice cores (described in text) are marked by stars. Siple Ice Stream and tributary KIS0 are labelled as SIS and KIS0 respectively. Inset shows the Siple Coast ice streams in context of West Antarctica.

represent the initiation of ice stream slowdown. We report margin ages from the time of our 2002 field season. All ages from previous studies (including Retzlaff and Bentley (1993)) have been adjusted to match this for ease of comparison.

6.4 Observations

6.4.1 Dating of Relict Margins

A total of four relict margins are identified in Chapter 4 in the flat-ice terrains on both sides of Kamb Ice Stream (KIS). Two margins surveyed in the Goosefoot have been discussed previously; M4 is a relict northern WIS margin dated to be 150±23 years old (Catania and others, 2003) and M3 is a southern KIS margin dated to be 146±25 years old (Retzlaff and Bentley, 1993). High frequency radar data across M3 shows buried crevasses at 21 m depth that continue in the direction of KIS. No near-surface crevasses are found south of M3 in the Goosefoot and so we believe M3 is the southernmost margin of KIS. Using a nearby accumulation rate of 0.073 m a^{-1} (Venteris and Whillans, 1998) we estimate that M3 shutdown 145±22 years ago in agreement with Retzlaff and Bentley (1993).

Two relict margins of KIS are identified in the Duckfoot (Figure 6.2A). We believe that M2 is the youngest northern margin of KIS because the depth to crevasses at M2 (∼18 m) remains constant for at least 14 km into the main body of KIS (Figure 6.2B). To obtain a local rate of accumulation we assume (based on satellite image maps) that a relict KIS margin located further upstream (82 ^{o} S, 142.83 ^{o} W) is the same margin as M2. This margin is dated to be 150±18 years old (Smith and others, 2002) and we use this age along with the depth to crevasses at M2 to obtain a local accumulation rate of 0.058 m a^{-1} for M2. By tracing internal layers from Siple Dome summit toward the Duckfoot, Nereson and others (2000) obtained an accumulation rate of ∼0.044 m a^{-1} at 50 km from the Siple Dome summit (26 km from M2). Interpolating between these two rates we estimate an accumulation rate of 0.049 m a^{-1} for M1 (60 km from the summit).

A high-frequency radar profile across M1 shows crevasses buried ∼30 m below the surface that begin at M1 and remain at a constant height until roughly 1.5 km from M2 where

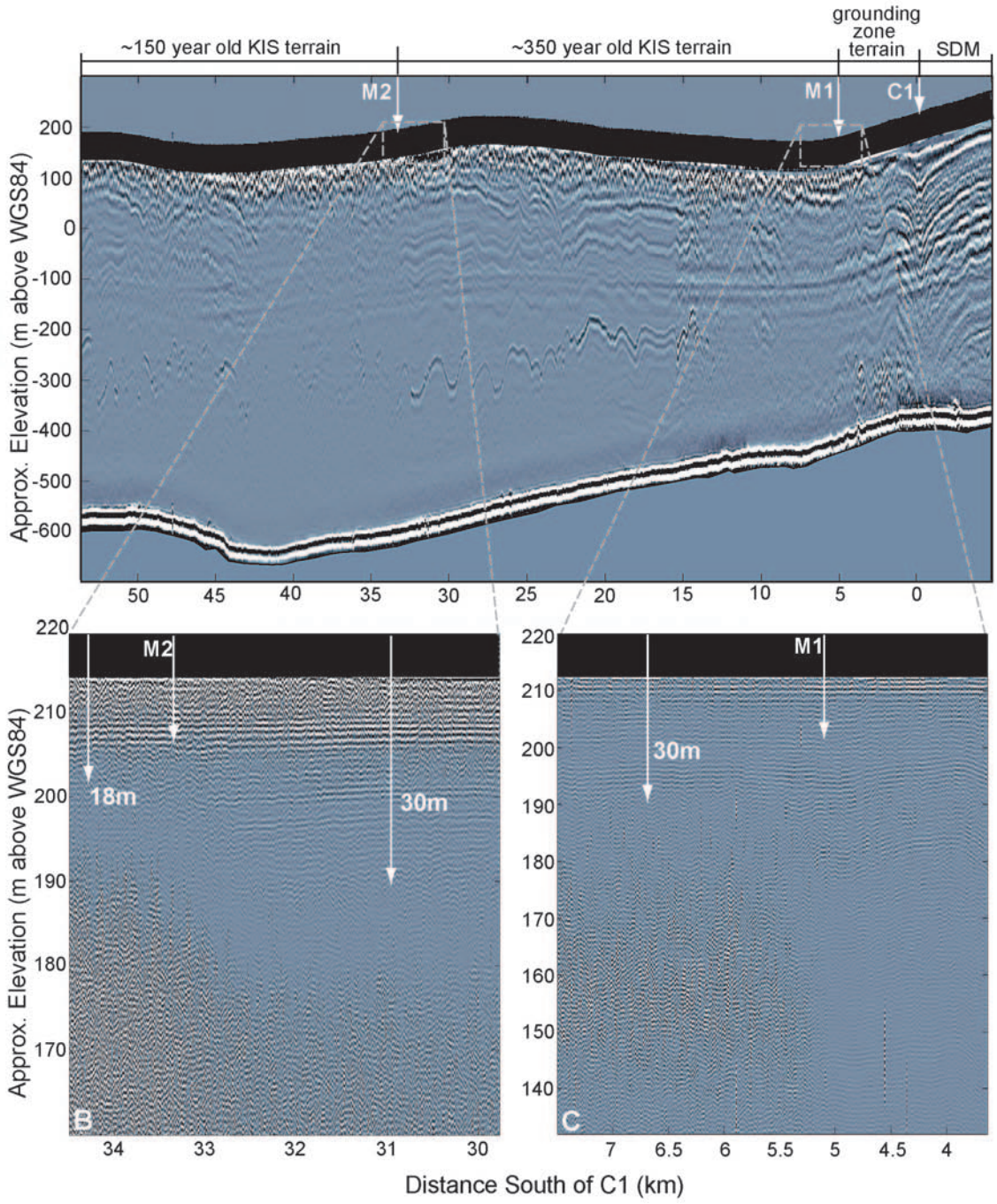

Figure 6.2: A. 2 MHz ice-penetrating radar profile across C1, M1 and M2 in the Duckfoot. The prominent return at ∼-100 m depth is a glitch in the transmitter. Data in the upper ∼80 m (shown as a black band) are not resolved by the radar system. B. 100 MHz radar profile across M2. Data in the upper ∼8 m (shown as a black band) are not resolved by the radar system. Arrows indicate the depth to the deepest continuous layer. C. 100 MHz radar profile across M1. Continuous layers are visible as deep as 140 m north of km 5.

they climb steeply to ∼18 m below the surface (Figure 6.2B). We believe that M1 is the northernmost margin of KIS because no buried crevasses exist to the north (toward Siple Dome). Using the accumulation rate from above we estimate that the M1 margin shutdown 340±20 years ago (∼200 years prior to the shutdown of the KIS trunk). We obtain independent confirmation of these ages by tracing layers of known ages from the Siple Dome core site (Taylor and others, 2004) to the Duckfoot. Interpolation of this age-depth scale indicates that layers at 18 and 30 m depth in the Duckfoot are ∼165 and ∼350 years old respectively.

Buried crevasses of a different origin are found on the upstream end of Engelhardt Ridge ("O1" in Figure 6.1). Radar data from this area show crevasses at ∼54 m depth overtop of relatively undisturbed deeper layers (Figure 6.3). These crevasses extend across a large portion of this end of the ridge including the site of an ice core established by Alley and Bentley (1988) providing excellent control on the time of burial (∼450 years ago). Because of the lack of deep disturbed layers, and the spatial pattern of crevasses on the surface (Figure 6.1) we believe that these crevasses were not created in a classic ice stream margin. More likely, they represent an area of quasi-ice stream behavior (akin to onset regions) where strain rates increase gradually and/or were not large for long enough to intensely distort deeper internal layers.

6.4.2 Observed Margin Migration

The existence of two northern KIS margins (M1 and M2) implies a jump in position occurred ∼340 years ago. We believe that migration occurred quickly because slow, gradual migration would destroy the deep, continuous layers that exist between M1 and M2 (between km 15 and 32 in Figure 6.2A) and because high-frequency radar profiles between M1 and M2 show no change in crevasse depth until only 1.5 km from M2 where they climb steeply from 30 to 18 m below the surface (Figure 6.2B).

Continuous but warped internal layering, often seen in the central portions of ice streams (Catania and others, 2003; Ng and Conway, 2004) likely indicates low strain rates and "plug

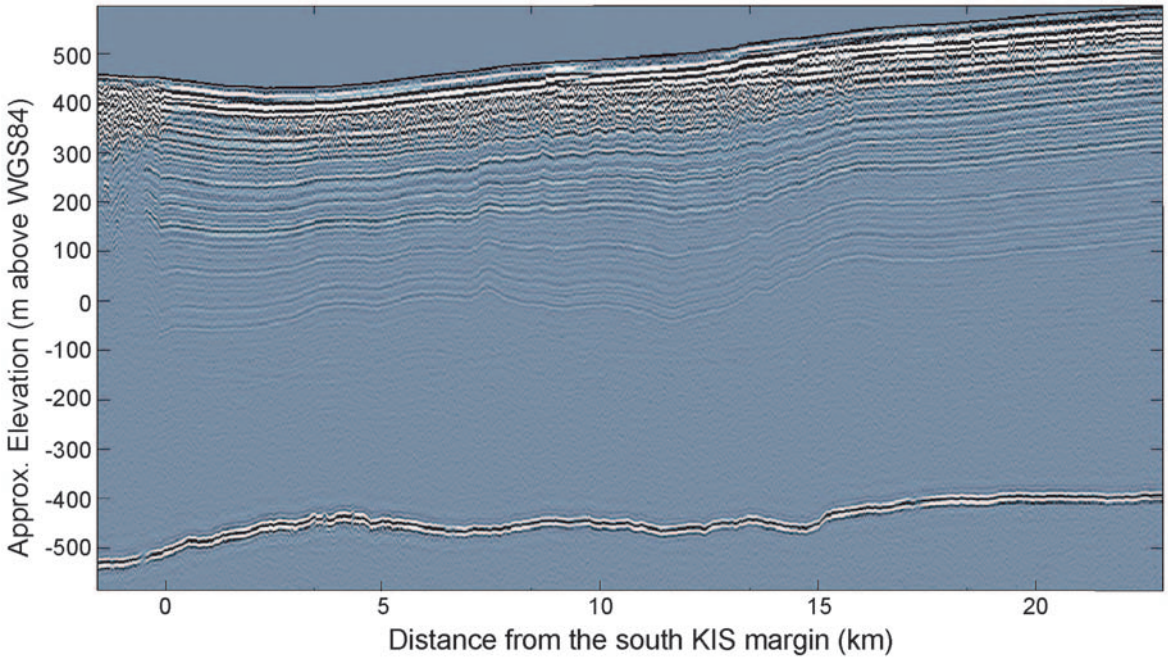

Figure 6.3: 5 MHz radar profile in the crevassed area on the upstream flank of Engelhardt Ridge. No crevasses are present for roughly 2 km between the southern KIS margin and the onset of these ∼450 year old crevasses.

flow" type ice motion. The small dome containing continuous layers within the Duckfoot could represent a section of relict KIS when the northernmost margin (M1) was active. Preservation of the layers beneath this dome indicate that the outer KIS margin (and part of the ice stream) stagnated suddenly, forcing the ice stream to abandon the outer margin and establish a new one further inboard. The consistency of crevasse depth between M1 and M2 indicates that the margin changed position rapidly. We are not able to resolve changes in the depth of radar-detected layers $\leqslant$5 m but we estimate that it would have taken less than 50 years for the switch in margin position, suggesting a migration rate of over 500 m a^{-1}or a sudden "jump" in position. Current migration rates for other margins range from 10-100 m a^{-1}(Echelmeyer and Harrison, 1999; Clarke and others, 2000). The change in crevasse depth that occurs over 1.5 km near M2 may represent a more gradual adjustment ($\sim$10 m a^{-1}) in margin position after the jump or fast migration occurred.

6.5 Chronology of Variability in the KIS Area

Our radar data revealing ice flow history lacks detailed information regarding the longevity of streaming activity. Longevity of streaming flow can be measured by examining the continuity of flow traces preserved on the surface of the Ross Ice Shelf (Fahnestock and others, 2000). Continuous flow traces emanating from Bindschadler Ice Stream (formerly Ice Stream D) and East Antarctic outlet glaciers draining to the Ross Sea show little distortion compared to the modern-day flow field indicating relatively steady, streaming flow from these regions for the last $\sim$1000 years. In contrast, flow traces from KIS are highly distorted relative to the modern flow field and thus indicate a more complex history (Hulbe and Fahnestock, in press). We also lack detailed knowledge regarding changes occurring in ice streams adjacent to KIS; for simplicity, our illustrated history (Figure 6.4) assumes no changes in these ice streams over time.

The specific positions of the KIS coupling line and grounding line in the past are not known. We infer their past locations using several lines of evidence; (1) Jezek (1984) mapped the spatial pattern of basal reflectance downstream of Crary Ice Rise (Figure 6.1) and

found that bands of low signal strength downstream from Crary do not correlate with the modern flow direction from which he inferred that the grounding line retreated past Crary within the last 1000 years; (2) crevasses in the tracks downstream from Crary Ice Rise have characteristics similar to rifts formed in floating ice in the recent past, but have character of shear margin crevasses formed in grounded ice further downstream. The time for the switch from shear to rift crevasses occurred ∼550 years ago (Fahnestock and others, 2000) implying that the grounding line was just downstream of Crary at this time. This is roughly coincident with the estimate of initial grounding of the north side of Crary based on vertical temperature profiles (Bindschadler and others, 1990); (3) MacAyeal (1989) suggests that extensional flow would occur downstream of a grounding line after ice stream stagnation but Fahnestock and others (2000) show that for KIS extension occurred downstream of the Steershead. They argue that this offset was due to the presence of a grounding zone between the modern grounding line and the Steershead prior to stagnation; (4) Thomas and others (1988) measure modern grounding line retreat of 30 m a^{-1} for KIS but argue that low bed slopes downstream of the modern grounding line could have allowed retreat rates of up to 20 times faster in the past. Substantiating this are crevasse patterns downstream from the current grounding line which imply a much faster rate of retreat in the past (Hulbe and Fahnestock, in press).

On the basis of the results described earlier and the constraints placed by past research, we outline an ice flow history for the KIS area beginning when the ice stream was active over a large area (Figure 6.4).

- **>700 years ago**(Figure 6.4A)
    - Southern end of Crary Ice Rise grounds ∼1100 years ago (Bindschadler and others, 1990).
    - KIS is 120 km wide in its trunk, SIS and KIS0 are both active and until ∼700 years ago, the KIS southern margin runs alongside of Crary Ice Rise. Flow was more southerly (Fahnestock and others, 2000).
    - KIS grounding zone includes Steershead and Crary Ice Rises ∼700 years ago (Hulbe and Fahnestock, in press; Fahnestock and others, 2000).

  - Northward shift in the southern KIS margin (forming the ice of "unknown origin" discussed by Fahnestock and others (2000)) ∼700 years ago.

- **550-400 years ago**(Figure 6.4B-D)

  - Expansion of WIS around the north side of Crary ∼550 years ago pushes the ice of "unknown origin" further downstream (Fahnestock and others, 2000).
  - Ice rumple forms at the location of Steershead ∼550 years ago (Fahnestock and others, 2000).
  - Possible retreat of the coupling line to C1 and C2 (Chapter 5).
  - Siple Ice Stream (SIS) and the crevasses on the upper end of Engelhardt Ridge become inactive ∼450 years ago.

- **350 years ago**(Figure 6.5E)

  - Grounding of the Steershead ∼350 years ago (Fahnestock and others, 2000).
  - Inward migration of the northern margin of KIS ∼340 years ago.
  - Grounding throughout the trunk of KIS between ∼200-350 years ago (Chapter 5).

- **250 years ago - Present**(Figure 6.5F-H)

  - Tributary to KIS, KIS0 shuts down ∼250 years ago (Conway and others, 2002).
  - Inward migration of the southern margin of the WIS north tributary (the Dragon) ∼190 years ago (Clarke and others, 2000).
  - Shutdown of KIS trunk ∼145 years ago (Retzlaff and Bentley, 1993).
  - Southward migration of the north WIS margin in the Goosefoot ∼150 years ago (Catania and others, 2003).
  - Upstream end of WIS margin (the Dragon) is currently migrating outwards at 10 m a^{-1}Echelmeyer and Harrison (1999).
  - Modern KIS grounding line retreat of 30 m a^{-1}(Thomas and others, 1988).
  - Ice surface of KIS near old UpC camp has risen ∼50 m since the KIS shutdown (Joughin and others, 1999; Price and others, 2001).

6.6 Discussion: Patterns of Ice Stream Variability

Our reconstruction of ice flow in the KIS area reveals a complex sequence of interconnected events. We believe that KIS switched from a thinning ice stream to a thickening ice stream at some point in the last ∼700 years, a switch that possibly led to the shutdown of the ice stream. In context with the history outlined above we describe possible phases in the life-cycle of an ice stream.

6.6.1 Phase I: Thinning and Grounding Zone Expansion

Prior to 700 years ago, KIS was actively streaming through a wide (∼120 km) trunk, distributary Siple Ice Stream was active, and the grounding line was likely located downstream of Crary Ice Rise. If the bed was well lubricated, large widths here would permit increased speeds and thinning of ice (Raymond, 2000). A thinning ice stream combined with flat bed topography in the area downstream of the present KIS grounding line promotes the formation of a grounding zone. Results from Chapter 5 indicate that ungrounded conditions at the maximum upstream extent of the grounding zone (at C1 and C2) initiated between 360-650 years ago depending on the rate of basal melt and the amount of basal sliding. While we are unable to determine when ungrounded conditions occurred with a high degree of accuracy, we believe that the wide mouth of KIS between 700-550 years ago would promote extension and thinning of ice. These conditions are favorable to the formation of a grounding zone and so we tentatively estimate grounding zone extension to C1 and C2 ∼550 years ago (Figure 6.4).

Fahnestock and others (2000) suggest that the southern KIS margin migrated northward ∼700 years ago altering the flow direction and isolating a section of ice between KIS and WIS which they term the ice of "unknown origin". We believe that this switch in margin position took place in the grounding zone of KIS downstream from the Goosefoot (Figure 6.4A) because near-surface crevasses are not found south of M3 in the Goosefoot and because it is likely that the grounding line was downstream of Crary Ice Rise at this time (see above discussion).

Thinning in the trunk of KIS relative to Siple Ice Stream may have resulted in water and/or ice piracy from Siple Ice Stream causing it to stagnate ∼420 years ago (personal communication B.Smith, 1999).

6.6.2 Phase II: Regional Thickening and Grounding of the KIS Trunk

Sometime between 550-400 years ago, the downstream end of KIS began to thicken due to; (1) the expansion of WIS toward KIS around the northern side of Crary Ice Rise ∼550 years ago (Fahnestock and others, 2000) and (2) the shutdown of SIS diverting ice that once flowed through SIS into the trunk region of KIS. This thickening is likely responsible for the creation of an "ice rumple" at the current location of the Steershead (Fahnestock and others, 2000).

Grounding through the grounding zone ∼350 years ago (Chapter 5) would likely be another consequence of thickening. Grounding in the trunk of KIS is simultaneous with fully grounded conditions at the Steershead (Fahnestock and others, 2000) and the inward migration of the northern KIS margin described earlier. Jacobson and Raymond (1998) and Raymond (2000) argue that inward margin migration could occur very fast through a switch of the basal heat balance from melting to freezing driven by feedbacks associated with stress redistribution in the margin. No relict margins exist within the Goosefoot south of M3 and based on the length of the crevasse track emanating downstream of M3, Fahnestock and others (2000) presume that this margin was stationary for ∼550 years. The jump in position of the northern KIS margin from M1 to M2 therefore represents a narrowing in the trunk of KIS by ∼25% (Figure 6.5E).

Conway and others (2002) believe that the shutdown of KIS0 (tributary to KIS) ∼250 years ago occurred when the northern limb of WIS migrated upstream effectively "beheading" KIS0 and caused ice and/or subglacial water to divert into WIS. Currently, ice flow is from KIS through KIS0 to WIS (Price and others, 2001; Conway and others, 2002). We believe that increased thickness in the trunk region of KIS could also contribute to the ice thickness imbalance between KIS and WIS further driving KIS0 toward shutdown and flow

reversal.

6.6.3 Phase III: Stagnation

We speculate that the shutdown of KIS began because of widespread grounding in the trunk region. If the ice in the grounding zone was thin enough at the time of grounding, the basal temperature gradient may have been too steep to maintain melting conditions at the bed (Raymond, 2000). Over time, successive de-watering of the till through freeze-on could lead to till consolidation and increased basal resistance (Tulaczyk and others, 2000b). Without the import of water from upstream ice stream shutdown would be inevitable (Bougamont and others, 2003). However, both Joughin and others (2003a) and Parizek and others (2003) argue that there was enough basal melt from beneath the KIS tributaries to offset freezing in the trunk if the excess water from upstream could be redistributed over the bed. Furthermore, floatation beneath the trunk would allow for the infiltration of sea water throughout this area. Despite the availability of water at the bed, KIS continued to shutdown over the next 200 years. One possible explanation for this discrepancy is pointed out by Joughin and others (2003a) who suggest that a subglacial drainage system is necessary to facilitate the movement of basal meltwater from the tributaries to the trunk. Ephemeral ungrounding in the trunk of KIS may have destroyed any through-going subglacial drainage system and the lag time between re-establishing this system compared to initiating freeze-on could be large. As a result, localized freezing could begin and may have initiated a positive feedback between loss of shear heating and increased basal freezing leading to a runaway increase in resistance and decreased ice velocity (Bougamont and others, 2003).

6.6.4 Phase IV: Post-Stagnation Adjustment and Reactivation

For the next 200 years KIS continued to flow through its narrower, grounded trunk region. Localized freezing at the bed in the trunk and thickening over this time caused reduced velocity and the eventual stagnation of KIS $\sim$150 years ago (Retzlaff and Bentley, 1993). Shutdown in the trunk of KIS is concurrent with the switch in position of the

northern WIS margin from M4 to its present active location suggesting some degree of interconnectedness between ice streams. It is possible that the position of M4 could not be maintained due to increased resistance in the confluence where these two margins meet on the ice shelf once M3 shutdown (Figure 6.1).

Since the shutdown of KIS, active tributaries have continued to feed into the stagnant trunk causing a "bulge" on the ice sheet surface to develop in the transition region between active and stagnant flow (near the old UpC camp, Figure 6.1). Thickening here at an average rate of 0.5 m a^{-1}has altered the hydraulic gradient and diverted water away from the trunk of KIS toward WIS leading some to speculate that "water piracy" is a consequence of stagnation and not the cause (Price and others, 2001). Increased basal meltwater beneath the stagnant trunk may be possible in the future with continued thickening due to both accumulation and the downstream migration of the surface bulge (Price and others, 2001; Bougamont and others, 2003). Using ice-penetrating radar Bentley and others (1998) find high basal reflectivity beneath the trunk of KIS indicating a wet bed possibly with high salinity associated with earlier floatation and stagnant water drainage. It is currently freezing in the trunk region of KIS (Joughin and others, 2003a). If we believe the method of shutdown proposed by Tulaczyk and others (2000b) and assume that the till in the mouth of KIS is not sufficiently lubricated for streaming flow, an effective subglacial drainage system must be established in order to transfer meltwater from the tributaries to the trunk in order for streaming to be re-activated.

6.7 Conclusions

Field studies in the Siple Coast area highlight the high degree of variability found in ice stream activity over time scales as short as 100 years. On a spatially small scale (i.e. looking at one ice stream in isolation), the observed behavior for KIS appears unstable and dominated by short-term variability. On a more regional scale (i.e. looking at the Siple Coast ice streams together), this short-term variability may occur everywhere making the stoppage of KIS less significant. In this sense, the shutdown of tributaries and migration

of ice stream margins simply force topographic readjustment of the ice stream system and ice flow is diverted elsewhere. Similar dynamics are inherent to braided channel systems, which exhibit channel migration and unpredictable flow switching on short time scales but maintain a relatively stable channel pattern over the long term. In this respect, the short-term variability that we observe for KIS does not influence the long-term mass balance of the ice sheet.

From this, we stress the interconnectedness of the ice stream system and the ability of one ice stream to adjust to changes in adjacent ice streams as is observed between WIS and KIS. While geologic and thermal properties may ultimately control the positions of ice streams and the direction of flow, fluctuations in ice stream discharge and boundaries can cause regional changes in ice thickness and surface gradients to which adjacent ice streams must constantly adjust.

The history of ice flow in the KIS area over the last several hundred years reveals the many changes taking place in the trunk region that could have ultimately led to ice stream shutdown. We believe that ice stream activity is driven by changes in thickness that cause fluctuations between grounded and ungrounded conditions that can impede streaming flow by destroying sub-glacial drainage systems. In the end, we believe that the shutdown of KIS cannot be attributed to one particular event but a series of events that simply represent the natural variability of the ice stream system as a whole.

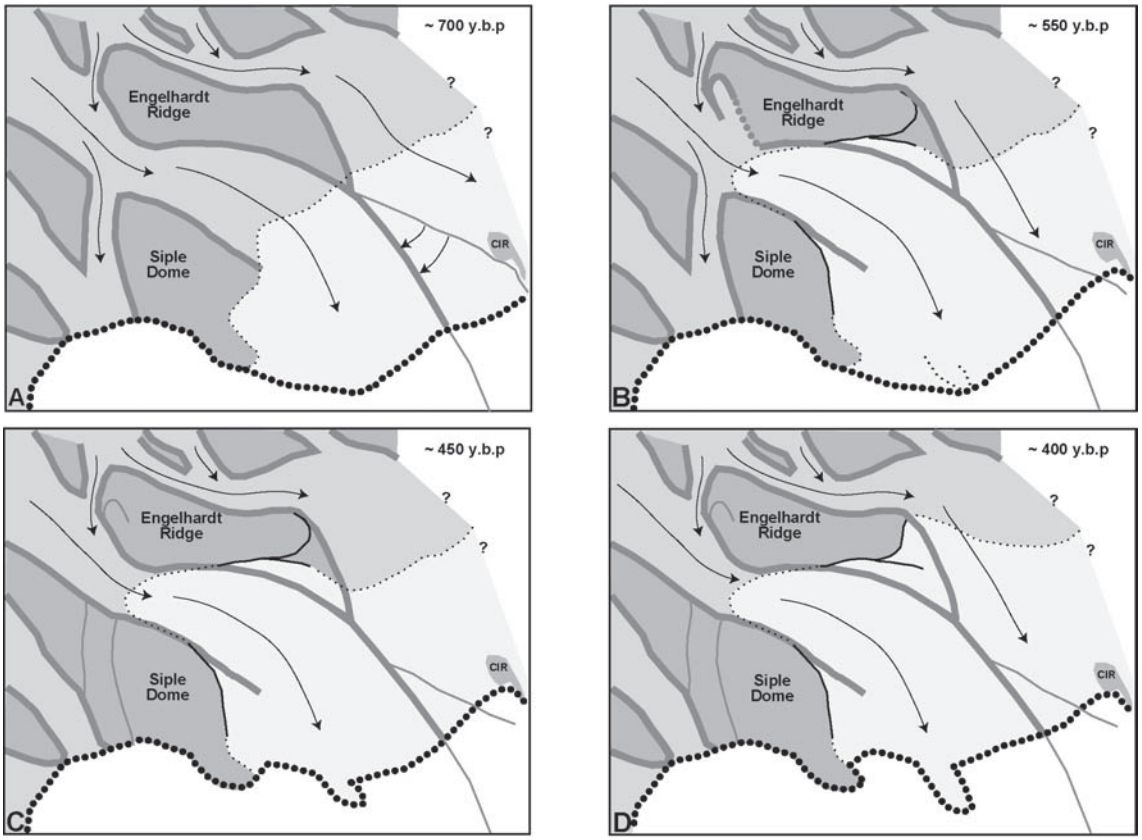

Figure 6.4: Panels A-D show the positions of ice stream configuration from 700-400 years ago. Ice stream margins are indicated by the dark grey lines (active margins are thicker than relict margins). The grounding line is indicated by a thick black line (unknown position is given as dotted thick black line, known position is solid). Coupling lines are indicated as thin black lines (unknown position given as dotted, known given as solid). Areas colored with dark grey indicate non-streaming grounded areas, those with light grey are grounding zones (ephemerally grounded), middle-grey areas are streaming grounded areas and white indicates the ice shelf (fully floating). Arrows indicate flow direction and migration direction of margins.

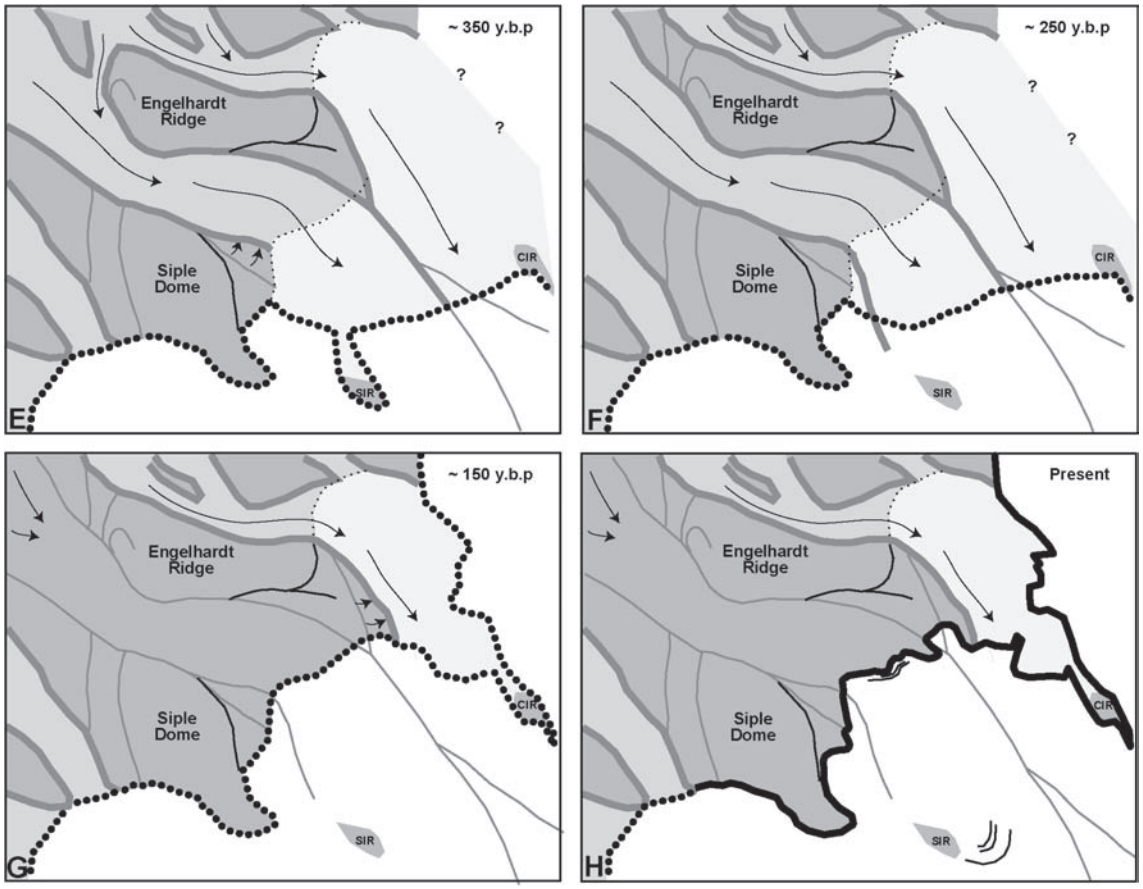

Figure 6.5: Panels E-H show the positions of ice stream boundaries from 350 years ago through to the present configuration. Ice stream margins are indicated by the dark grey lines (active margins are thicker than relict margins). The grounding line is indicated by a thick black line (unknown position is given as dotted thick black line, known position is solid). Coupling lines are indicated as thin black lines (unknown position given as dotted, known given as solid). Areas colored with dark grey indicate non-streaming grounded areas, those with light grey are grounding zones (ephemerally grounded), middle-grey areas are streaming grounded areas and white indicates the ice shelf (fully floating). Arrows indicate flow direction and migration direction of margins. Modern grounding line position is given by Gray and others (2002); Shabtaie and Bentley (1987).

Chapter 7

SYNTHESIS

While the work presented in this dissertation focusses on the specific details of the Kamb Ice Stream (KIS) system it is also part of a larger question regarding the processes involved in ice stream shutdown. The observed and modelled short-term variability embodied in KIS, and described here, aims to improve the general understanding of ice stream dynamics and the influences that ice streams have on the deglaciation and mass balance of the ice sheet. Here I present the main conclusions from the work described in the previous chapters and outline some directions for future research.

7.1 Characterization of Ice Stream Margins

The data presented in Chapters 2 and 4 demonstrate that margins are distinct, relatively narrow ($\sim$10 km) zones that separate ice streams from other ice terrains. When ice streams are active, margins mark the location where shear stress is concentrated. Large strain rates here causes crevassing on the surface which is the reason why margins are easily seen in satellite images. Relict margins are less distinct because crevasses have become buried by several years of accumulation. On the surface, relict margins are associated with broad (3-10 km), shallow (<50 m) troughs in topography. These troughs make relict margins visible in satellite images but differentiating between margins and other features remains difficult.

Ground-based ice-penetrating radar is an effective way to distinguish internal layer characteristics which can be diagnostic of once-active processes. Radar data indicate that relict margins are characterized by the onset-of or change-in-depth-of near-surface crevasses. Deeper layers become discontinuous and/or grossly distorted just inboard of the outermost crevasses (toward the ice stream interior) and regain continuity after roughly 10 km. In

the main body of the ice stream internal layers are distorted but generally continuous since strain is decreased here and the ice moves as plug flow. The loss of deep layer continuity within the margin is due to a combination of processes; large strain distorts the layers and the incoming radar signal is scattered within the chaotically oriented crevasses above. A large increase in bed reflectivity occurs across relict margins but this increase is offset from the outermost crevasses by about 4-10 km (toward the ice stream interior). High bed reflectivity here corresponds to wet conditions and indicates that the beds of ice streams remain thawed for several hundred years after shutdown. The offset in reflectivity may be due to the loss of signal within the more deeply distorted internal layers of the ice stream margin.

High-frequency radar profiles across several relict margins in the Duckfoot region combined with estimates of accumulation, permit accurate dating of buried crevasses and a revision of the ice flow history described by Jacobel and others (2000). Margin migration rates are estimated for the northern margin of KIS and indicate a sudden stagnation of streaming flow in the Duckfoot which forced the margin to jump (up to 20 km) inward very quickly (less than 50 years). Migration of this margin is much faster than rates measured elsewhere which may demonstrate the high degree of sensitivity of the strength of the underlying till to its water content (Tulaczyk and others, 2000a,b).

7.2 Characterization of Ice Stream Grounding Zones

Our field investigations led to the identification of distinctive flat-ice terrains that bound the downstream end of KIS. Within the terrains, internal layers are lightly disturbed in the upper half of the ice and contain numerous diffractors of constant height in the lower half of the ice. At the edge of these terrains (where they meet the inter-ice stream ridges) layers become strongly downwarped ($\sim$100 m) over a narrow region ($\sim$2 km). The similarity of internal structure within these terrains suggests that similar processes occurred in both regions despite the fact that they are separated by roughly 100 km of ice stream terrain.

A kinematic ice-flow model, developed in Chapter 5, is used to test several scenarios that lead to localized layer downwarping. Results indicate that the downwarped layers are best

matched through focused basal melting that occurred for as long as 300 years in the current flow regime or as little as 130 years if a jump in basal sliding of up to 6 m a^{-1}perpendicular to the boundary is allowed.

I explore the hypothesis that these flat-ice terrains formed in the past when they were once floating; deep diffractors indicate basal crevasses which are common features on ice shelves, and downwarped-layer boundaries mark the past position of the grounding line where melting can be focused due to sub-ice shelf circulation patterns. Some problems with this hypothesis are that these areas are not floating today (they are ∼50-100 m above buoyancy), and that the melting appears more focussed than is generally expected beneath ice shelves.

If these regions do represent relict ice shelf terrain the evidence presented in Chapters 4 and 5 indicate retreat and re-advance of the grounding zone on relatively short time scales. Sudden floatation may be a response of the ice stream to progressive thinning in the mouth of KIS (which prior to shutdown, was over 100 km wide). Our interpretation of grounding line dynamics in the mouth of KIS argues that the theory put forth by Weertman (1974) is incomplete. Weertman (1974) argued that grounding line retreat would continue unstably in the presence of inward sloping bed topography. We observe short-term grounding line retreat that appears to be limited by the presence of inter-ice stream ridges in the KIS region followed by re-advance of the grounding line due to regional thickening (from the expansion of WIS). A decrease in ice velocity and eventual shutdown of the ice stream would be expected subsequent to re-grounding since the ice here is very thin and the subglacial water system that supplies water (and latent heat) from far upstream was likely destroyed during grounding line advance.

7.3 Ice Flow History of KIS

Identifying the limits to streaming flow, both spatially and temporally is crucial to reconstructing past ice stream configurations. Results from Chapters 2 through 5 provide background for interpreting KIS ice flow history over the past 700 years (Chapter 6). This

history reveals numerous short-term (century scale) fluctuations in ice stream velocity, flow-direction, and position that result from changes in thickness and bed conditions. Such fluctuations appear to be inherent to the ice stream system and highlight the high degree of interconnection between neighboring ice streams.

Amongst this ongoing variability a possible pattern of ice stream flow and shutdown emerges; (1) ice stream widening, extension and thinning; (2) extreme thinning in the mouth causing floatation which supplies enough water to the basal area to temporarily offset freezing at the bed; (3) grounding due to regional changes in ice thickness which may make the re-establishment of a through going drainage system difficult; (4) localized freezing causes unstable behavior of the ice stream -narrowing and decreased velocity; (5) eventual shutdown in the trunk region but active flow continues in the tributaries; (6) possible reactivation through reestablishment of a subglacial drainage network and increased driving stress.

7.4 Implications for Future Research

The identification of the flat-ice terrains in the trunk region of KIS opens several new avenues of investigation. Certainly, more information is required to understand the influence of grounding line processes on streaming behavior. In particular, important future questions include:

1. Are the identified features really relict grounding lines?

2. What processes operate at grounding lines? How can these be characterized?

3. Does grounding line retreat signal the onset of ice stream stagnation?

4. What are the characteristics of flowstripes and basal crevasses that might require a new interpretation of this work?

The most uncertain part of my work is the assumption that the downwarped layers mark the limits of ungrounded conditions in the mouth of KIS in the past. More field data could shed further evidence on this issue to either prove or disprove this ice-shelf hypothesis. An ice core in the flat-ice terrains, could provide more accurate average density measurements for buoyancy analysis. Coupled with high-resolution topographic and ice thickness measurements through these regions using GPS and radar sounding, an improved estimate of the height above buoyancy can be made. Other proof of ungrounded conditions could come from borehole observations in the mouth of KIS which could sample the underlying sediment to determine salinity and water content to explain the high bed reflectivity measured here and the amount of through-flow in the subglacial drainage system.

In addition, corroboration of these ideas can come from the identification of similar features where processes are currently active. Possible locations for future radar investigations in the Siple Coast region include the modern grounding zone of Whillans Ice Stream, the small modern grounding zone in the mouth of Bindschadler Ice Stream and a possible relict grounding zone between the north side of Siple Dome and Bindschadler Ice Stream. Any differences and similarities in layer geometry between these regions will facilitate our understanding of the possible processes that affect grounding line position and provide a range of internal structures that can define the grounding line position.

Grounding line processes are poorly understood largely because of a lack of high-resolution field data. Melting at the bottom of the ice shelf appears to be important but little is known about the pattern and magnitude of melt. While radar profiles across grounding lines could improve estimates of melt rates, more accurate information comes from in situ measurements through borehole observations. A series of borehole and sub-ice water column temperature and salinity measurements at and across a grounding line could help constrain the amount and pattern of melt.

Other areas in the Siple Coast might provide additional information to help constrain the regional ice flow history. Some possible areas to explore with radar include Crary Ice Rise where layer stratigraphy could confirm if it has ever been over-run by streaming flow,

and the terrain to the south of Mercer Ice Stream where numerous surface flow features exist. In addition, the interpretation of internal layer data from Conway Ridge will add important information about the ice flow history from an area where little is known.

Several features identified in satellite images and radar layers in this study should be substantiated with further data. Flow-related features are commonly used as diagnostic indicators of past flow variability (Fahnestock and others, 2000) however, the origin of these flow features is unknown. Ground-based radar data acquired across these features is needed to improve understanding of their origin.

Finally, the ambiguity surrounding the presence of bottom crevasses could be reduced with additional radar data on modern ice shelves where bottom crevasses are known to exist. Previous studies of the ice shelf internal layer characteristics used airborne radar data (Jezek and Bentley, 1983; Jezek and others, 1979) which lacks the resolution that ground-based radar data can provide to accurately characterize the geometry and reflectivity of internal layers. This would improve our understanding of the characteristics of bottom crevasses and the mechanisms that lead to their formation.

BIBLIOGRAPHY

Alley, R. B. and C. R. Bentley. 1988. Ice-core analysis on the Siple Coast of West Antarctica. *Annals of Glaciology*, **11**, 1–7.

Alley, R. B., S. Anandakrishnan, C. R. Bentley and N. Lord. 1994. A water-piracy hypothesis for the stagnation of Ice Stream C, Antarctica. *Annals of Glaciology*, **20**, 187–194.

Anandakrishnan, S. and R. B. Alley. 1997. Stagnation of Ice Stream C, West Antarctica by water piracy. *Geophysical Research Letters*, **24**(3), 265–268.

Anandakrishnan, S., R. Alley, R. Jacobel and H. Conway. 2001. The flow regime of Ice Stream C and hypotheses concerning its recent stagnation. *In* R. B. Alley and R. A. Bindschadler, *eds*, *The West Antarctic Ice Sheet: Behavior and Environment*, volume 77 of *Antarctic Research Series*. American Geophysical Union, 283–294.

Barcilon, V. and D. R. MacAyeal. 1993. Steady flow of a viscous ice stream across a no-slip/free-slip transition at the bed. *Journal of Glaciology*, **39**(131), 167–185.

Behrendt, J. C., D. D. Blankenship, D. L. Morse and R. E. Bell. 2004. Shallow-source aeromagnetic anomalies observed over the West Antarctic Ice Sheet compared with coincident bed topography from radar ice sounding. *Global and Planetary Change*, **42**, 177–193.

Bentley, C. R., N. Lord and C. Liu. 1998. Radar reflections reveal a wet bed beneath stagnant Ice Stream C and a frozen bed beneath Ridge BC, West Antarctica. *Journal of Glaciology*, **44**(146), 149–156.

Bindschadler, R. 1998. Future of the West Antarctic Ice Sheet. *Science*, **282**, 428–429.

Bindschadler, R. and P. Vornberger. 1998. Changes in the West Antarctic Ice Sheet since 1963 from declassified satellite photography. *Science*, **279**(5351), 689–692.

Bindschadler, R., E. Roberts and A. Iken. 1990. Age of Crary Ice Rise, Antarctica, determined from temperature-depth profiles. *Annals of Glaciology*, **14**, 13–16.

Bindschadler, R., M. King, R. Alley, S. Anandakrishnan and L. Padman. 2003. Tidally controlled stick-slip discharge of a West Antarctic ice stream. *Science*, **301**, 1087–1089.

Bindschadler, R. A., J. Bamber and S. Anandakrishnan. 2001. Onset of streaming flow in the Siple Coast region, Antarctica. *In* R. B. Alley and R. A. Bindschadler, *eds*, *The West Antarctic Ice Sheet: Behavior and Environment*, volume 77 of *Antarctic Research Series*. American Geophysical Union, 123–136.

Bougamont, M., S. Tulaczyk and I. Joughin. 2003. Response of subglacial sediments to basal freeze-on 2. application in numerical modelling of the recent stoppage of Ice Stream C, West Antarctica. *Journal of Geophysical Research*, **108**(B4). Art. No. 2233.

Catania, G. and C. Paola. 2001. Braiding under glass. *Geology*, **29**(3), 259–262.

Catania, G., H. Conway, C. Raymond, A. Gades and H. Engelhardt. 2003. Bed reflectivity beneath inactive ice streams in West Antarctica. *Annals of Glaciology*, **36**, 287–291.

Catania, G., H. Conway, C. Raymond and T. Scambos. 2005. Surface morphology and internal layer stratigraphy in the downstream end of Kamb Ice Stream, West Antarctica. *Journal of Glaciology*. submitted.

Clarke, T. S., C. Liu, N. E. Lord and C. R. Bentley. 2000. Evidence for a recently abandoned shear margin adjacent to ice stream B2, Antarctica, from ice-penetrating radar measurements. *Journal of Geophysical Research*, **105**(B6), 13,409–13,422.

Conway, H., B. Hall, G. Denton, A. Gades and E. Waddington. 1999. Past and future grounding-line retreat of the West Antarctic ice sheet. *Science*, **286**, 280–283.

Conway, H., G. Catania, C. Raymond, A. Gades, T. Scambos and H. Engelhardt. 2002. Switch of flow in an Antarctic ice stream. *Nature*, **419**, 465–467.

Copeland, L. and M. Sharp. 2001. Mapping thermal and hydrological conditions beneath a polythermal glacier with radio-echo sounding. *Journal of Glaciology*, **47**(157), 232–242.

Corr, H., C. Doake, A. Jenkins and D. Vaughan. 2001. Investigations of an "ice plain" in the mouth of Pine Island Glacier, Antarctica. *Journal of Glaciology*, **47**(156), 51–57.

Dansgaard, W. and S. J. Johnsen. 1969. A flow model and a time scale for the ice core from Camp Century, Greenland. *Journal of Glaciology*, **8**(53), 215–223.

Echelmeyer, K. and W. D. Harrison. 1999. Ongoing margin migration of Ice Stream B, Antarctica. *Journal of Glaciology*, **45**(150), 361–369.

Echelmeyer, K. A., W. D. Harrison, C. Larsen and J. E. Mitchell. 1994. The role of the margins in the dynamics of an active ice stream. *Journal of Glaciology*, **40**(136), 527–538.

Engelhardt, H. and B. Kamb. 1997. Basal hydraulic system of a West Antarctic ice stream: constraints from borehole observations. *Journal of Glaciology*, **43**(144), 207–231.

Engelhardt, H., N. Humphrey and B. Kamb. 1990a. Borehole geophysical observations on Ice Stream B, Antarctica. *Antarctic Journal of the U.S.*, **25**(5), 80–82.

Engelhardt, H., N. Humphrey, B. Kamb and M. Fahnestock. 1990b. Physical conditions at the base of a fast moving Antarctic ice stream. *Science*, **248**, 57–59.

Fahnestock, M., T. Scambos, R. Bindschadler and G. Kvaran. 2000. A milennium of variable ice flow recorded by the Ross Ice Shelf, Antarctica. *Journal of Glaciology*, **46**(155), 652–664.

Fahnestock, M., W. Abdalati, I. Joughin, J. Brozena and P. Gogineni. 2001. High geothermal heat flow, basal melt, and the origin of rapid ice flow in central Greenland. *Science*, **294**, 2338–2342.

Fialko, Y. 2004. Temperature fields generated by the elastodynamic propagation of shear cracks in the Earth. *Journal of Geophysical Research*, **109**(doi:10.1029/2003JB0024972004).

Gades, A., C. Raymond, H. Conway and R. Jacobel. 2000. Bed properties of Siple Dome and adjacent ice streams, West Antarctica, inferred from radio-echo sounding measurements. *Journal of Glaciology*, **46**(152), 88–94.

Gades, A. M. 1998. *Spatial and Temporal Variations of Basal Conditions Beneath Glaciers and Ice Sheets Inferred From Radio Echo-Sounding Measurements*. (Ph.D. thesis, University of Washington, Seattle.)

Gill, A. 1973. Circulation and bottom water production in the Weddell Sea. *Deep Sea Research*, **20**, 111–140.

Giovinetto, M. and H. Zwally. 2000. Spacial distribution of net surface accumulation on the Antarctic Ice Sheet. *Annals of Glaciology*, **31**, 171–178.

Glen, J. W. 1958. The flow law of ice. A discussion of the assumptions made in glacier theory, their experimental foundations and consequences. *International Association of Scientific Hydrology*, **47**, 171–183.

Gray, L., N. Short, R. Bindschadler, I. Joughin, L. Padman, P. Vornberger and A. Khananian. 2002. RADARSAT interferometry for Antarctic grounding-zone mapping. *Annals of Glaciology*, **34**, 269–276.

Gudmundsson, G. H., C. F. Raymond and R. Bindschadler. 1998. The origin and longevity of flow-stripes on Antarctic ice streams. *Annals of Glaciology*, **27**, 145–152.

Harrison, W., K. Echelmeyer and C. Larsen. 1998. Measurement of termperature in a margin of Ice Stream B, Antarctica: implications for margin migration and lateral drag. *Journal of Glaciology*, **44**(148), 615–624.

Hawley, R., E. Waddington, G. Lamorey and K. Taylor. in press. Vertical-strain measurements in firn at Siple Dome, Antarctica. *Journal of Glaciology*.

Hulbe, C. L. and M. Fahnestock. in press. West Antarctic ice stream discharge variability: mechanism, controls, and pattern of grounding line retreat. *Journal of Glaciology*.

Jacobel, R., T. Scambos, N. Nereson and C. Raymond. 2000. Changes in the margin of Ice Stream C, Antarctica. *Journal of Glaciology*, **46**(152), 102–110.

Jacobson, H. P. and C. F. Raymond. 1998. Thermal effects on the location of ice stream margins. *Journal of Geophysical Research*, **103**(B6), 12,111–12,122.

James, T. and E. Ivins. 1998. Predictions of Antarctic crustal motions driven by present-day ice sheet evolution and by isostatic memory of the Last Glacial Maximum. *Journal of Geophysical Research*, **103**(B3), 4993–5017.

Jenkins, A. and C. Doake. 1991. Ice-ocean interaction on Ronne Ice Shelf, Antarctica. *Journal of Geophysical Research*, **96**(C1), 791–813.

Jezek, K. 1984. Recent changes in the dynamic condition of the Ross Ice Shelf, Antarctica. *Journal of Geophysical Research*, **B89**(1), 409–416.

Jezek, K. and C. Bentley. 1983. Field studies of bottom crevasses in the Ross Ice Shelf, Antarctica. *Journal of Glaciology*, **29**(101), 118–126.

Jezek, K., C. Bentley and J. Clough. 1979. Electromagnetic sounding of bottom crevasses on the Ross Ice Shelf, Antarctica. *Journal of Glaciology*, **24**(90), 321–330.

Joughin, I. and L. Padman. 2003. Melting and freezing beneath Filchner-Ronne Ice Shelf, Antarctica. *Geophysical Research Letters*, **30**(9). Art. No. 1477.

Joughin, I. and S. Tulaczyk. 2002. Positive mass balance of the Ross ice streams, West Antarctica. *Science*, **295**, 476–480.

Joughin, I., L. Gray, R. Bindshadler, S. Price, D. Morse, C. Hulbe, K. Mattar and C. Werner. 1999. Tributaries of the West Antarctic ice streams revealed by RADARSAT interferometry. *Science*, **286**, 283–286.

Joughin, I., S. Tulaczyk and H. Engelhardt. 2003a. Basal melt beneath Whillans Ice Stream and Ice Streams A and C, West Antarctica. *Annals of Glaciology*, **36**, 257–262.

Joughin, I., S. Tulaczyk, R. Bindschadler and S. Price. 2003b. Changes in West Antarctic ice stream velocities: Observation and analysis. *Journal of Geophysical Research*, **107**(B11), 2289–2311.

Kamb, B. 2001. Basal zone of the West Antarctic ice streams and its role in lubrication of their rapid motion. *In* R. B. Alley and R. A. Bindschadler, *eds*, *The West Antarctic Ice Sheet: Behavior and Environment*, volume 77 of *Antarctic Research Series*, 157–199. American Geophysical Union.

Lawson, D. E., J. Strasser, E. B. Evenson, R. B. Alley, G. J. Larson and S. A. Arcone. 1998. Glaciohydraulic supercooling: a freeze-on mechanism to create stratified, debris-rich basal ice: I. Field evidence. *Journal of Glaciology*, **44**(148), 547–562.

Lythe, M., D. Vaughan and BEDMAP Consortium. 2001. BEDMAP: a new ice thickness and subglacial topographic model of Antarctica. *Journal of Geophysical Research*, **106**(B6), 11335–11352.

MacAyeal, D. R. 1984. Thermohaline circulation below the Ross Ice Shelf: A consequence of tidally induced vertical mixing and basal melting. *Journal of Geophysical Research*, **89**(C1), 597–606.

MacAyeal, D. R. 1985. Tidal rectification below the Ross Ice Shelf. *In* S. Jacobs, *ed*, *Oceanology of the Antarctic Continental Shelf*, volume 43 of *Antarctic Research Series*. American Geophysical Union, 109–132.

MacAyeal, D. R. 1989. Ice-shelf response to ice-stream discharge fluctuations: Iii. The effects of ice-stream imbalance on the Ross Ice Shelf, Antarctica. *Journal of Glaciology*, **35**(119), 38–42.

Merry, C. J. and I. M. Whillans. 1993. Ice-flow features on Ice Stream B, Antarctica, revealed by SPOT HRV imagery. *Journal of Glaciology*, **39**(133), 515–552.

Miller, L. and B. Douglas. 2004. Mass and volume contributions to twentieth-century global sea level rise. *Nature*, **428**(6981), 406–409.

Nath, P. and D. Vaughan. 2003. Subsurface crevasse formation in glaciers and ice sheets. *Journal of Geophysical Research*, **108**(B1), 527–530.

Nereson, N. A. 2000. Elevation of ice-stream margin scars after stagnation. *Journal of Glaciology*, **46**(152), 111–118.

Nereson, N. A. and C. F. Raymond. 2001. The elevation history of ice streams and the spatial accumulation pattern along the Siple Coast of West Antarctica inferred from ground-based radar data from three inter-ice-stream ridges. *Journal of Glaciology*, **47**(157).

Nereson, N. A., C. F. Raymond, E. D. Waddington and R. W. Jacobel. 1998. Recent migration of the Siple Dome ice divide, West Antarctica. *Journal of Glaciology*, **44**(148), 643–652.

Nereson, N. A., C. F. Raymond, R. W. Jacobel and E. D. Waddington. 2000. The accumulation pattern across Siple Dome, West Antarctica, inferred from radar-detected internal layers. *Journal of Glaciology*, **46**(152), 75–87.

Ng, F. and H. Conway. 2004. Fast-flow signature in the stagnated Kamb Ice Stream, West Antarctica. *Geology*, **32**(6), 481–484.

Parizek, B., R. Alley and C. Hulbe. 2003. Subglacial thermal balance permits ongoing grounding-line retreat along the Siple Coast of West Antarctica. *Annals of Glaciology*, **36**, 251–256.

Paterson, W. S. B. 1994. *The Physics of Glaciers*. Pergamon Press, Oxford, 3rd edition.

Price, S., R. Bindschadler, C. Hulbe and I. Joughin. 2001. Post-stagnation behavior in the upstream regions of Ice Stream C, West Antarctica. *Journal of Glaciology*, **47**(157), 283–294.

Raymond, C. F. 1996. Shear margins in glaciers and ice sheets. *Journal of Glaciology*, **42**(140), 90–102.

Raymond, C. F. 2000. Energy balance of ice streams. *Journal of Glaciology*, **46**(155), 665–676.

Raymond, C. F., K. A. Echelmeyer, I. M. Whillans and C. S. M. Doake. 2001. Ice stream shear margins. *In* R. B. Alley and R. A. Bindschadler, *eds*, *The West Antarctic Ice Sheet: Behavior and Environment*, volume 77 of *Antarctic Research Series*. American Geophysical Union, 137–155.

Reeh, N. 1988. A flow line model for calculating the surface profile and the velocity, strain rate, and stress field in an ice sheet. *Journal of Glaciology*, **34**(127), 46–54.

Retzlaff, R. and C. R. Bentley. 1993. Timing of stagnation of Ice Stream C, West Antarctica, from short-pulse radar studies of buried surface crevasses. *Journal of Glaciology*, **39**(133), 553–561.

Rignot, E. 1998. Fast recession of a West Antarctic glacier. *Science*, **281**, 549–551.

Rignot, E. and S. Jacobs. 2002. Rapid bottom melting widespread near Antarctic Ice Sheet grounding lines. *Science*, **296**, 2020–2023.

Rignot, E., K. Echelmeyer and W. Krabill. 2001. Penetration depth of interferometric synthetic-aperture radar signals in snow and ice. *Geophysical Research Letters*, **28**(18), 3501–3504.

Rose, K. E. 1979. Characteristics of ice flow in Marie Byrd Land, Antarctica. *Journal of Glaciology*, **24**(90), 63–75.

Scambos, T. A. and R. Bindschadler. 1993. Complex ice stream flow revealed by sequential satellite imagery. *Annals of Glaciology*, **17**, 177–182.

Schmeltz, M., E. Rignot and D. MacAyeal. 2001. Ephemeral grounding as a signal of ice-shelf change. *Journal of Glaciology*, **47**(156), 71–77.

Shabtaie, S. and C. R. Bentley. 1982. Tabular icebergs: Impications from geophysical studies of ice shelves. *Journal of Glaciology*, **28**(100), 413–430.

Shabtaie, S. and C. R. Bentley. 1987. West Antarctic Ice Streams draining into the Ross Ice Shelf: Configuration and mass balance. *Journal of Geophysical Research*, **92**(B2), 1311–1336.

Smith, A. 1996. Ice shelf basal melting at the grounding line, measured from seismic observations. *Journal of Geophysical Research*, **101**(C10), 22,749–22,755.

Smith, B. 2000. *Radar studies on Ice Stream C, West Antarctica*. (M.S. thesis, University of Wisconsin, Madison.)

Smith, B., N. Lord and C. Bentley. 2002. Crevasse ages on the northern margin of Ice Stream C, West Antarctica. *Annals of Glaciology*, **34**, 209–216.

Sweeney, R., C. Finn, D. Blankenship, R. Bell and J. Behrendt. 1999. Central West Antarctica aeromagnetic data; a web site for distribution of data and maps. Technical report, U.S. Geological Survey Open-File Report.

Taylor, K. and others. 2004. Dating the Siple Dome, Antarctica ice core by manual and computer interpretation of annual layering. *Journal of Glaciology*. submitted.

Thomas, R., S. Stephenson, R. Bindschadler, S. Shabtaie and C. Bentley. 1988. Thinning and grounding-line retreat on Ross Ice Shelf, Antarctica. *Annals of Glaciology*, **11**, 165–172.

Thorsteinsson, T., E. Waddington and R. Fletcher. 2003. Spatial and temporal scales of anisotropic effects in ice-sheet flow. *Annals of Glaciology*, **37**, 41–48.

Tulaczyk, S., B. Kamb and H. Engelhardt. 2000a. Basal mechanics of Ice Stream B, West Antarctica. I. Till mechanics. *Journal of Geophysical Research*, **105**(B1), 463–481.

Tulaczyk, S., B. Kamb and H. Engelhardt. 2000b. Basal mechanics of Ice Stream B, West Antarctica. II. Undrained-plastic-bed model. *Journal of Geophysical Research*, **105**(B1), 483–494.

Uratsuka, S., F. Nishio and S. Mae. 1996. Internal and basal ice changes near the grounding line derived from radio-echo sounding. *Journal of Glaciology*, **42**(140), 103–110.

Van der Veen, C. J. 1998. Fracture mechanics approach to penetration of bottom crevasses on glaciers. *Cold Regions Science and Technology*, **27**, 213–223.

Vaughan, D., H. Corr, C. Doake and E. Waddington. 1999. Distortion of isochronous layers in ice revealed by ground-penetrating radar. *Nature*, **398**, 323–326.

Venteris, E. and I. M. Whillans. 1998. Variability of accumulation rate in the catchements of Ice Streams B, C, D and E, Antarctica. *Annals of Glaciology*, **27**, 227–230.

Waddington, E., T. Neumann, M. Koutnik, H. Marshall and D. Morse. 2004. Inference of accumulation-rate pattern from deep radar layers. *Journal of Glaciology*. submitted.

Weertman, J. 1974. Stability of the junction of an ice sheet and ice shelf. *Journal of Glaciology*, **13**(67), 3–11.

Weertman, J. 1976. Sliding-no sliding zone effects and age determination of ice cores. *Quaternary Research*, **6**, 203–207.

Weertman, J. 1980. Bottom crevasses. *Journal of Glaciology*, **25**(91), 185–188.

Whillans, I., M. Jackson and Y.-H. Tseng. 1993. Velocity pattern in a transect across Ice Stream B, Antarctica. *Journal of Glaciology*, **39**(133), 562–572.

Whillans, I. M. and C. J. van der Veen. 1993. New and improved determinations of velocity of Ice Streams B and C, West Antarctica. *Journal of Glaciology*, **39**(133), 483–490.

Winebrenner, D., B. Smith, G. Catania, H. Conway and C. Raymond. 2003. Radio-frequency attenuation beneath Siple Dome, West Antarctica from wide-angle and profiling radar observations. *Annals of Glaciology*, **37**, 226–232.

Appendix A

RADAR DATA

Several data sets were used in this dissertation and have been made available on a cd (Catania_data) and through the National Snow and Ice Data Center website: http://nsidc.org/. Most of the data used here are from the 2000/01 and 2001/02 field season to the Kamb Ice Stream (Ice Stream C) area. Files pertaining to these field seasons are provided on this disk (GPS, high, and low frequency data). Other GPS and radar data used in this study come from previous field seasons. These data are archived elsewhere and are not duplicated here.

Line Name	Start Waypoint	End Waypoint	Raw Data Files
MID-BC1	S 83 11.848, W 145 23.684	S 83 21.922, W 144 41.595	0033201-03
MID-BC2	S 83 05 44, W 141 02 34	S 82 59 47, W 141 40 20	9834101
B UpBC	S 82 40.518, W 134 19.500	S 82 47.550, W 136 50.400	0033401-02
C UpBC	S 82 38.593, W 137 17.393	S 82 58.992, W 138 48.960	0033601-03
bumps	S 83 3.660, W 136 51.240	S 83 32.100, W 152 14.700	0202601-02
SIS	S 81 42.343, W 140 07.271	S 81 42.931, W 140 16.891	0033701-02
A DnBC	S 83 28.663, W 148 59.602	S 83 23.298, W 150 18.480	0032802-03
B DnBC	S 83 23.298, W 150 18.480	S 83 11.790, W 151 24.480	0032401-02
G GLBC	S 83 27.900, W 155 12.533	S 83 03.750, W 155 02.067	0201801-06
O GLBC	S 83 29.350, W 154 04.199	S 83 38.367, W 151 48.850	0201701-05
S GLBC	S 83 27.900, W 155 12.534	S 83 38.850, W 156 56.550	0201501-04
E GLBC	S 83 26.467, W 156 01.633	S 83 15.733, W 157 56.467	0201601-13
F GLBC	S 83 27.000, W 152 30.000	S 83 34.860, W 151 33.900	0202001-04
D Duck	S 82 00.000, W 151 06.600	S 82 07.871, W 151 45.575	0200701-05
U Duck	S 82 04.967, W 150 31.767	S 82 10.567, W 150 53.917	0201301-09
K Duck	S 82 07.700, W 149 29.900	S 82 12.900, W 149 40.200	0201201-02
RDE	S 80.217, W 140.850	S 80.762, W 139.800	9831801-02
ROO	S 79.53505, W 161.35113	S 79.29108, W 159.9775	9732801-02,04
MARGINE	S 83 17 37, W 139 02 40	S 83 16 00, W 138 28 35	9833401-02
MARGINW	S 83.288337, W 139.664898	S 83 17 18, W 139 39 39	9833602-07
MARGINC	S 83.243623, W 139.694108	S 83.308898, W 139.00262	9833101-03

Table A.1: Radar profiles used in this study. Profile name includes the closest camp.

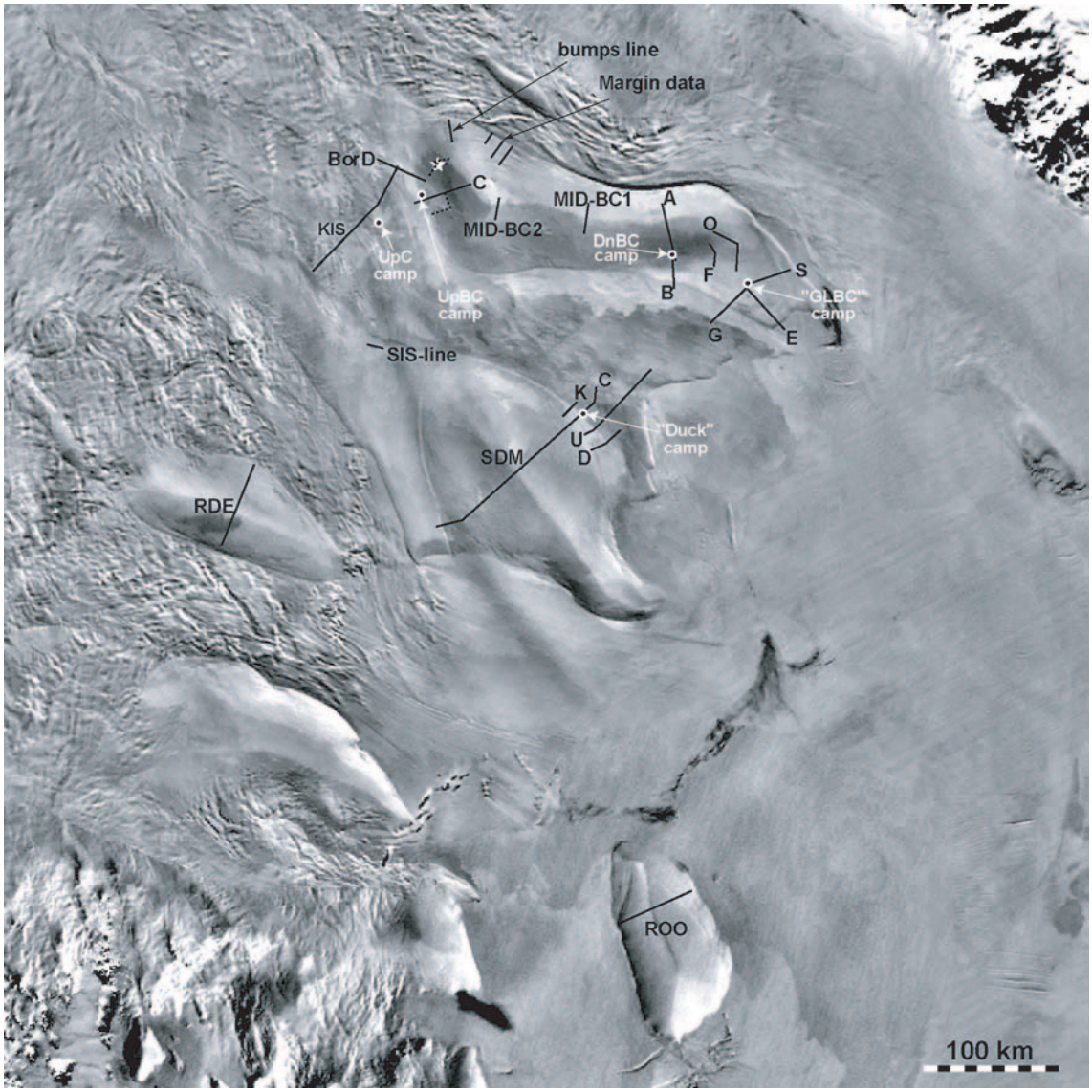

Figure A.1: Locations of all radar data from 2000-02 field seasons. Low frequency data were collected along all black lines. High-frequency data was collected along these lines in addition to the two black dotted lines in the "UpBC" area. The locations of camps are labelled as is the location of the Alley and Bentley (1988) core site (labelled as a white star). Data acquired during previous seasons (ROO, RDE, Margin data, SDM) are also shown.

VITA

GINNY CATANIA

Education

Ph.D. Geophysics, University of Washington, 2004

Dissertation Title: *The Dynamic History of Kamb Ice Stream: Controls on streaming behavior and ice stream shutdown*

M.S. Geology, University of Minnesota, 1998

Thesis Title: *A Physical Model of Pressurized Flow over an Unconsolidated Bed: Implications for Subglacial Braided Channels*

B.Sc. Geography, University of Western Ontario, 1994

Publications

D. Winebrenner, B. Smith, **G. Catania**, H. Conway and C. Raymond, 2003, Radio-frequency attenuation beneath Siple Dome, West Antarctica, from wide-angle and profiling radar observations, *Annals of Glaciology*, **37**, 226-232.

G. Catania, H. Conway, A. Gades, C. Raymond and H. Engelhardt, 2003, Bed reflectivity beneath inactive ice streams in West Antarctica, *Annals of Glaciology*, **36**, 287-291.

H. Conway, **G. Catania**, C. Raymond, A. Gades, T. Scambos, H. Engelhardt, 2002, Switch of flow direction of an Antarctic ice stream, *Nature*, **419**, p. 465-467.

G. Catania and C. Paola, 2001, Braiding under glass. *Geology*, **29**(3), 259-262.

Conference Abstracts

G. Catania, H. Conway, C. Raymond and T. Scambos, Flat ice terrain near the mouth of Kamb Ice Stream, *10th Annual WAIS Workshop*, 2003

G. Catania, H. Conway, C. Raymond and T. Scambos, Duckfoot and Goosefoot: What happened at the lower end of Ice Stream C, *9th Annual WAIS Workshop*, 2002

G. Catania, H. Conway, A. Gades, C. Raymond and H. Engelhardt, Bed-reflectivity beneath inactive ice streams in West Antarctica, *International Symposium on Fast Glacier Flow*, 2002

G. Catania, H. Conway, A. Gades, C. Raymond, T. Scambos, GPR and RES records of disturbed internal layers on Ridge BC, *8th Annual WAIS workshop*, 2001

G. Catania and C. Paola, A physical model of subglacial braided channels, *WAIS Chapman Conference*, 1998